U.S. Department of Energy
Energy Efficiency and Renewable Energy
Vehicle Technologies Program

Award: DE-EE0006442

CHRYSLER UPSET PROTRUSION JOINING TECHNIQUES FOR JOINING DISSIMILAR METALS

Final Report

Principal Investigator: Stephen D. Logan
stephen.logan@fcagroup.com
(248) 512-9485

Submitting Official: Stephen D. Logan
(see above)

Date of Submission: September 27, 2017
DUNS Number: 830966904
Recipient: FCA US LLC (fka Chrysler Group LLC)
800 Chrysler Drive
Auburn Hills, MI 48326-2757

Start Date: September 30, 2013; End Date: June 30, 2017

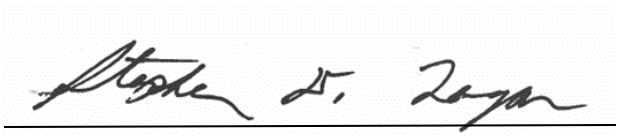

Stephen D. Logan
Principal Investigator

TABLE OF CONTENTS

ACKNOWLEDGEMENTS AND DISCLAIMER

Acknowledgment: This material is based upon work supported by the Department of Energy under Award Number(s) DE-EE0006442.

Disclaimer: This report was prepared as an account of work sponsored by an agency of the United States Government. Neither the United States Government nor any agency thereof, nor any of their employees, makes any warranty, express or implied, or assumes any legal liability or responsibility for the accuracy, completeness, or usefulness of any information, apparatus, product, or process disclosed, or represents that its use would not infringe privately owned rights. Reference herein to any specific commercial product, process, or service by trade name, trademark, manufacturer, or otherwise does not necessarily constitute or imply its endorsement, recommendation, or favoring by the United States Government or any agency thereof. The views and opinions of authors expressed herein do not necessarily state or reflect those of the United States Government or any agency thereof.

FCA US would like to acknowledge the support of William Joost and Sarah Ollila of the U.S. Department of Energy (DoE), as well as Richard Gerth and Martin McDonnell of the United States Army Tank Automotive Research, Development and Engineering Center (TARDEC) representing the U.S Department of Defense, (DoD) and Charles Alsup and John Terneus of the National Energy Technical Laboratory (NETL) for their ongoing support in the project's management. FCA would also like to acknowledge the outstanding work of Chonghua (Cindy) Jiang, Justin Hunt, and Yan (Jack) Sang of AET Integration, Inc. (AET), FCA's key partner in the project. AET consistently produced high quality work on a timely basis throughout the program and took on any additional work necessary to ensure the project was successful.

PARTICIPANTS / TEAMING MEMBERS

The organizations in Table 1 received funding assistance through DoD/DoE support of this project or donated materials to directly support the project. These organizations were essential to the success of the project.

Organization	Key personnel	Activities
FCA US LLC (Prime)	Stephen Logan (PI) Joseph Beckham Marites Gennette David Langer Florina Vartolas	Provided primary DoD/DoE interface for the program; managed and coordinated process development efforts and mechanical/testing/evaluation efforts; conducted corrosion testing/evaluation and provided all required reporting to DoD/DoE
• AET Integration, Inc.	Chonghau (Cindy) Jiang Justin Hunt Yan (Jack) Sang	Provided joining process development and optimization services; produced joined assemblies; conducted mechanical/structural testing and analysis; conducted forming simulation activities; and conducted corrosion testing to FCA specs
– ACT Test Panels LLC	Brad Kimpell Julie Piper	Provided commercial pre-treatment and coating services
– Agritek Industries, Inc.	Bill Maddox	Provided Armorgalv steel coating services
– Almond Products	Brian Hoeker	Provided commercial pre-treatment and coating services
– Dynacast	Eric Gates	Provided die-cast Upset Cast Rivets (UCR)
– Henkel	John Kukalis Jim Switzer	Provided adhesives and sealants as well as alternative experimental magnesium pre-treatment
– Henrob	David Coldwell Alex Trinick	Provided rivets and riveting equipment to AET for conducting benchmark SPR process evaluation
– Scientific Forming Technologies Corporation (SFTC)	Chris Fischer	Provided DEFORM software for forming simulation
– Upwind Technologies	Wen-Tzong Lee	Provided initial forming simulation services
• ArcelorMittal	Stefano Lepre	Provided steel with alternative Zagnelis coatings
• Meridian Lightweight Technologies	Joe Petrillo	Provided die-cast UPJ test coupons throughout the project
• Tata	Ravir Bhatnagar	Provided steel with alternative MagiZinc coatings
• TARDEC	Martin McDonnell	Provided steel coupons with alternative coatings

Table 1: Direct project participants and their roles in the project

The organizations listed in Table 2 were not involved directly with this project and were not supported by DoD/DoE funding. However, their indirect collaboration, funded by Automotive Partnership Canada (APC) played a significant complementary role in the overall success of this project.

Organization	Key personnel	Activities
McMaster University	Nicholas Andreae Dharmendra Chalasani Mukesh Jain Abbas Khalaf Sumanth Shankar	Conducted thermo-mechanical compression studies to characterize forging characteristics of AM60B and AZ91D materials at Canmet for inclusion in forming simulation efforts
Canmet Materials Laboratory	Kumar Sadayappan	Provided use of Gleeble thermo-mechanical compression test equipment and training to McMaster students to use equipment

Table 2: Organizations providing indirect project support

EXECUTIVE SUMMARY

The project goal was to develop and demonstrate a robust, cost effective, and versatile joining technique, known as Upset Protrusion Joining (UPJ), for joining challenging dissimilar metal combinations, especially those where one of the metals is a die cast magnesium (Mg) component. Since two of the key obstacles preventing more widespread use of light metals (especially in high volume automotive applications) are 1) a lack of robust joining techniques and 2) susceptibility to galvanic corrosion, and since the majority of the joint combinations evaluated in this project include die cast Mg (the lightest structural metal) as one of the two materials being joined, and since die casting is the most common and cost effective process for producing Mg components, then successful project completion provides a key enabler to high volume application of lightweight materials, thus potentially leading to reduced costs, and encouraging implementation of lightweight multi-material vehicles for significant reductions in energy consumption and reduced greenhouse gas emissions. Economic benefits to end-use consumers are achieved primarily via the reduction in fuel consumption.

Unlike currently available commercial processes, the UPJ process relies on a very robust mechanical joint rather than intermetallic bonding, so the more cathodic material can be coated prior to joining, thus creating a robust isolation against galvanic attack on the more anodic material. Additionally, since the UPJ protrusion is going through a hole that can be pre-drilled or pre-punched prior to coating, the UPJ process is less likely to damage the coating when the joint is being made. Furthermore, since there is no additional cathodic material (such as a steel fastener) used to create the joint, there is no joining induced galvanic activity beyond that of the two parent materials.

In accordance with its originally proposed plan, this project has successfully developed process variants of UPJ to enable joining of Mg die castings to aluminum (Al) and steel sheet components of various thicknesses, strengths and coating configurations. While most development focused on the simpler round boss version of the process, an additional phase of the work focused on development of an oval boss version to support applications with narrow flanges, while yet another variant of the process, known as Upset Cast Riveting (UCR), was developed and evaluated for joining mixed metals that may not necessarily include Mg or Al die cast components. Although each variation posed unique challenges described later in the report, all variations were successfully produced and evaluated, and each could be further developed for specific types of commercial applications.

In this project, UPJ performed favorably against the benchmark self-pierce riveting (SPR) process in Mg AM60B to Al 6013 combinations although significant corrosion challenges were observed in both processes, especially for the bare Mg to bare Al configurations. Additional challenges were observed in joining Mg to steel with the UPJ process (SPR was not evaluated for this combination as it was not considered viable). To pass FCA's specified corrosion tests with Mg/steel combinations, new steel treatments were evaluated, as well as adhesives and sealed edges. These showed significant improvement. In general, UPJ performed very well in Mg to Al 6016 combinations, even in corrosion evaluation of the bare Mg to bare Al configuration (again, SPR was not evaluated for this material combination as the 1.1 mm thick Al6016 sheet thickness was considered too thin for the SPR process). The improvement in corrosion performance of the Mg to Al 6016 combination over the Mg to Al 6013 combination was thought to be a result of the lower copper content in the Al 6016 alloy. Oval boss joints showed substantial improvement in all joint strength criteria compared to 8.0-mm diameter round boss joints but were not evaluated for corrosion performance. The improved joint strength is likely a result of larger shear area. Cosmetic corrosion performance of all test assemblies (UPJ, UCR and SPR) was a challenge due to exposed edges and crevices allowing undercutting of the coatings. In real world component applications, the exposed edges, so prevalent on the joining test coupons, would be less prevalent and easier to protect.

ACCOMPLISHMENTS

As mentioned in the Executive Summary, the overall project goal was to demonstrate a robust, cost effective and versatile technique for joining challenging dissimilar metal combinations, especially those where one of the metals is a die cast magnesium component. In accordance with the originally proposed plan, this project has developed UPJ process variants (round and oval boss configurations) to enable joining of Mg die castings to Al and steel sheet components of various thicknesses, strengths and coating configurations. The UCR variant of the process was developed and evaluated for joining mixed metals that do not necessarily include magnesium or aluminum die cast components.

Joints were evaluated through conventional microstructure and joining induced defect characterization, as well as through tensile lap shear and cross-tension testing, and fatigue and drop tower impact energy tests. The galvanic corrosion performance of the joints was evaluated through FCA's prescribed accelerated corrosion testing procedure, American Society for Testing Materials (ASTM) G85-A2, which has been shown to be aggressive for galvanic corrosion on dissimilar metal joints. At the end of the corrosion test, selected configurations were re-evaluated for fatigue and impact performance.

Table 3 below compares accomplishments to objectives for specific program tasks.

Statement of Objectives	Accomplishments
Task 0.0 - Develop and maintain the Project management Plan (PMP) and manage and report on activities in accordance with the plan.	The PMP was maintained and followed closely throughout the program. All technical reports were submitted on time and included budgetary reporting as well. The program maintained its original timeline until near the end, when the decision was made jointly between FCA and DOE to extend the program to allow for evaluation of additional corrosion treatments.
Task 1.0 – Process development and optimization	Conducted development/optimization preparation work for all joint configurations, including evaluating and characterizing Mg thermo-mechanical behavior to support computer simulations, obtaining and coating bulk materials, used computer simulations to optimize boss and electrode geometries and process parameters for all round boss UPJ configurations, oval boss configurations, and round rivet UCR configurations
Task 2.0 - Produce joined assemblies for testing and evaluation	Produced and coated (as appropriate) benchmark SPR joints, round boss UPJ joints, oval boss UPJ joints, and round rivet UCR joints
Task 3.0 – Initial (pre-corrosion) mechanical/structural testing and evaluation	Conducted initial mechanical/structural testing/evaluation, including microstructure evaluations, joining induced defect characterization, quasi-static lap shear tension testing and cross-tension testing, impact lap shear tension and cross-tension testing, and fatigue lap shear tension and cross-tension testing for benchmark SPR joints, round boss UPJ joints, oval boss UPJ joints, and round rivet UCR joints.
Task 4.0 – Accelerated corrosion testing and evaluation	Conducted 12 week accelerated corrosion exposure and evaluation of benchmark SPR joints, round boss UPJ joints, and round rivet UCR joints, including periodic visual examinations, followed by removal of 3 joined samples of each configuration from corrosion chambers to evaluate mechanical/structural performance as well as removal of any samples that were corroding excessively such that there would be no structural joint left before the next scheduled review, and final quasi-static, impact, and durability testing of select configurations after completion of the corrosion testing. Also performed corrosion evaluations of alternative corrosion treatments in addition to the original project scope.

Table 3: Comparison of actual accomplishments to project goals

ACTIVITIES

PROJECT APPROACH

The project technical approach is summarized as follows:

1. Establish the benchmark performance of Mg to Al joints produced with SPR, a currently available commercial process, for comparison purposes only. This evaluation includes:
    - For each coating configuration, produce shear-tension (ST) and cross-tension (CT) test coupons as shown in Figure 1.
    - Apply additional coating layers to select joint configurations prior to the mechanical/structural and corrosion evaluations.
    - Validate the joint performance through:
        - Characterization of material microstructure and joining induced defects in the joint region
        - Quasi-static lap shear tension (ST) and cross-tension (CT) tests
        - Drop tower impact tests of select tensile shear and cross-tension configurations
        - Cyclic fatigue testing of select tensile shear and cross-tension configurations
        - Subject select configurations to FCA's aggressive 12-week accelerated corrosion test (ASTM G85-A2) with quasi-static lap shear failure and cross-tension failure being evaluated after each 4-week increment, and fatigue testing and impact testing to be re-evaluated on select samples at the end of corrosion exposure
        - Characterization of failure mechanisms for each of the mechanical tests described above.
2. Conduct thermo-mechanical compression testing to obtain additional knowledge and understanding of thermo-mechanical behavior of Mg alloys to support development/optimization of the UPJ process.
3. Supplement existing UPJ process knowledge with computer-aided engineering forming simulation results based on knowledge gained through the thermo-mechanical compression testing.
4. Use this information to develop optimized cast protrusion and welding electrode shapes to reduce electrical current requirements and provide more robust, repeatable forming performance for each of the joint configurations being considered.
5. Produce sufficient quantities of each joint configuration to support prescribed evaluation matrices.
6. Evaluate all material configurations (e.g., MgAM60B to Al6022, Al6013, and high-strength steel [HSS] DP-590 materials in bare, pretreated, and coated conditions for round and oval shaped joints). For each configuration, produce tensile shear and cross-tension test coupons as shown in Figure 1. Apply additional coating layers to select joint configurations prior to the mechanical/structural and corrosion evaluations. Evaluate using the same procedure described above for the benchmark SPR joints.
7. Subject five samples of each configuration to the initial mechanical/structural tests described above.
8. Subject a substantial number of samples to FCA's accelerated corrosion tests, reviewing visually every two weeks and removing three samples of each configuration at four week intervals for quasi-static testing.
9. At the end of the 12-week accelerated corrosion exposure, subject select configurations to fatigue and impact testing for comparison to pre-corrosion performance.
10. Develop joining process parameters and evaluate performance of oval boss UPJ and round boss UCR joining processes and evaluate as described above for the benchmark SPR joints.

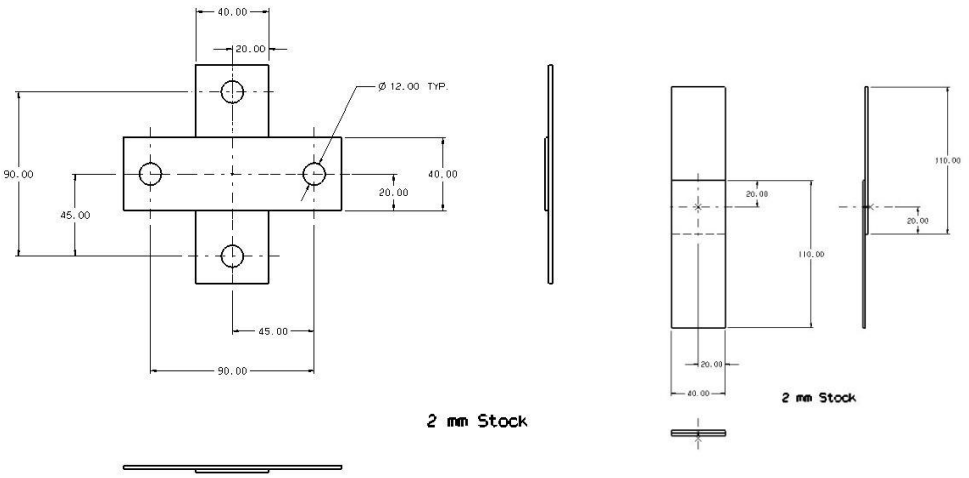

Figure 1: Schematic showing cross tension (CT) joint configuration on the left and shear tension (ST) joint configuration on the right

PROBLEMS ENCOUNTERED / CHANGES IN APPROACH

- The corrosion testing protocol was revised from 30-wks to 12-wks prior to start of the project due to testing at FCA that indicated Mg could not survive 30-wks of exposure to the new FCA test even without being joined to dissimilar materials. The project scope described above reflects this change.
- Excessive porosity was observed in the first die-cast Mg bosses received. This delayed completion of thermo-mechanical compression testing, but did not delay completion of the project as additional physical optimization was substituted to keep the project on time. Ultimately, the UPJ process seemed to be relatively insensitive to casting porosity.
- Numerical simulations were unable to predict cracking during head formation. Discussions with SFTC identified that several hundred test samples and associated physical testing would be required to develop a correlation with the software to accurately and consistently predict cracking. This level of testing was beyond the scope of the project and would have resulted in substantial timing delays. Ultimately, a combination of some simulation combined with experience, engineering judgement, and physical testing was used to identify process parameters with the lowest propensity to form cracks.
- Galvanic corrosion in certain material combinations turned out to be more challenging than expected with commercially available coatings. This caused shortages of post-corrosion test coupons in some configurations. Additional alternative coatings were added to the project in BP3 to determine if they could provide improved corrosion protection beyond that of the commercial leaders previously evaluated in the project. Due to this increase in project scope, combined with delays in the coating process, the project requested and received a no-cost extension to finalize corrosion testing of the added assemblies with alternative coatings.

BENCHMARK PERFORMANCE

During development of the initial project proposal, it was determined that the performance of the UPJ process would need to be validated against a current state of the art process for joining dissimilar metals. While there was very little in the way of commercially proven methods to join Mg to dissimilar metals beyond bolted joints and break-stem riveting (neither of which were considered commercially viable in high volume applications, due primarily to cost), some development work had been conducted with SPR. Consequently, this process was selected to serve as a benchmark for the new UPJ process, and the earliest work in the project focused on developing optimized SPR joints of the specified Mg to Al coupons.

SPR Joint Development

While much of the previous development work in joining Mg to Al with SPR had focused on heating the joint area prior to joining to eliminate cracking of the Mg sheet (which does not possess sufficient ductility at room temperature to support the SPR process), recent work through the DOE funded USAMP Magnesium Front End Project had indicated that Mg to Al SPR joints could be produced with minimal cracking by punching the rivet through the Mg and into the Al. The small amount of cracking that resulted during this process did not appear to adversely affect the structural performance (including fatigue) of the joint.

Using equipment provided by Henrob, AET evaluated a total of 17 different SPR rivet and process parameters in determining the most promising options to minimize the propensity for cracking in this joint. Figure 2 shows the 4 best joint configurations that resulted in maximum rivet engagement with minimal cracking. Joint 17 was selected as displaying the best combination of minimal cracking and consistently high joint strength results.

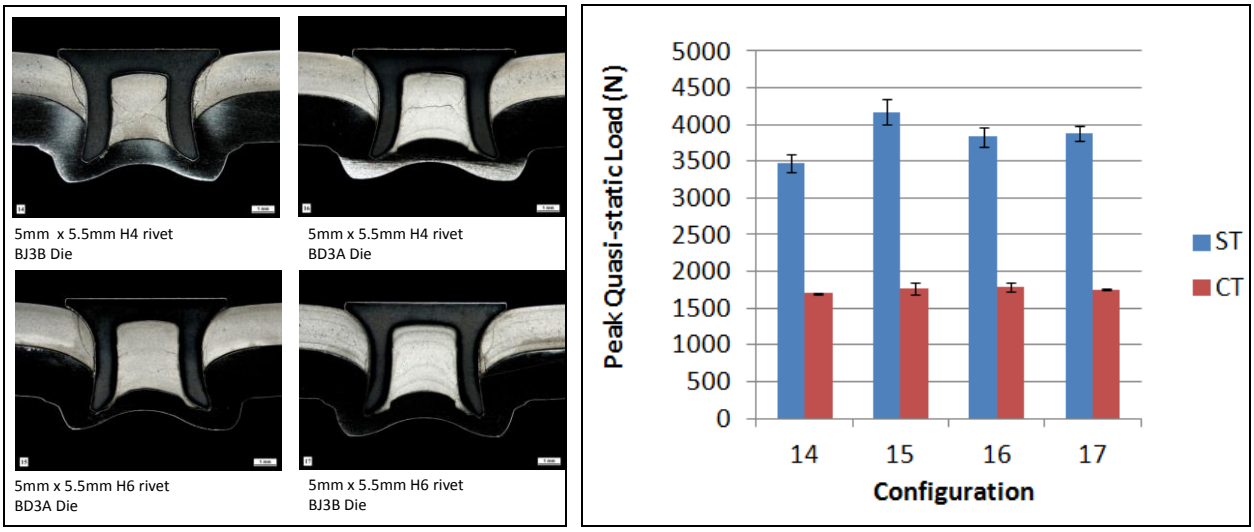

Figure 2: Examples of rivet configurations and joint strengths evaluated for selecting optimum configuration to produce benchmark SPR samples

Once the optimum rivet configuration was identified, SPR joints were produced in the coating configurations shown in Table 4 and subjected to a prescribed matrix of pre-corrosion mechanical/structural testing at AET, and accelerated corrosion testing at FCA US, followed by post-corrosion mechanical/structural testing at AET. In this table, the abbreviation PC indicates powdercoating.

Configuration Number	Upper Sheet			Bottom Sheet			Assembly Coating Configuration
	Material	Thickness (mm)	Coating	Material	Thickness (mm)	Coating	
SPR1	Mg AM60B	2.0	Bare	Al6013-T4	2.2	Bare	Uncoated
SPR2	Mg AM60B	2.0	Pretreated	Al6013-T4	2.2	Pretreated	Powdercoated
SPR3	Mg AM60B	2.0	Pretreated	Al6013-T4	2.2	Pretreated + PC	Uncoated
SPR4	Mg AM60B	2.0	Pretreated	Al6013-T4	2.2	Pretreated + PC	Powdercoated

Table 4: SPR coating configurations

The evaluation plan called for conducting initial (pre-corrosion) benchmark SPR mechanical/structural tests, including microstructure evaluations, joining induced defect characterization, and quasi-static, impact, and fatigue tests of shear and cross tension joint configurations as well as subjecting joined assemblies to 12 weeks of FCA's accelerated corrosion test and evaluating structural/mechanical performance during and after the corrosion test.

Initial (pre-corrosion) Mechanical/Structural Testing and Evaluation

Results of the pre-corrosion mechanical/structural testing are shown in Figures 3 to 6. Quasi-static shear tension and cross tension performance results are shown in Figure 3. Quasi-static vs impact performance results are shown for the SPR2 configuration in Figure 4. Fatigue results are shown for the same configuration in Figure 5. It should be noted, as shown in Figure 6, that all pre-corrosion mechanical/structural joint failures occurred in the Mg parent material.

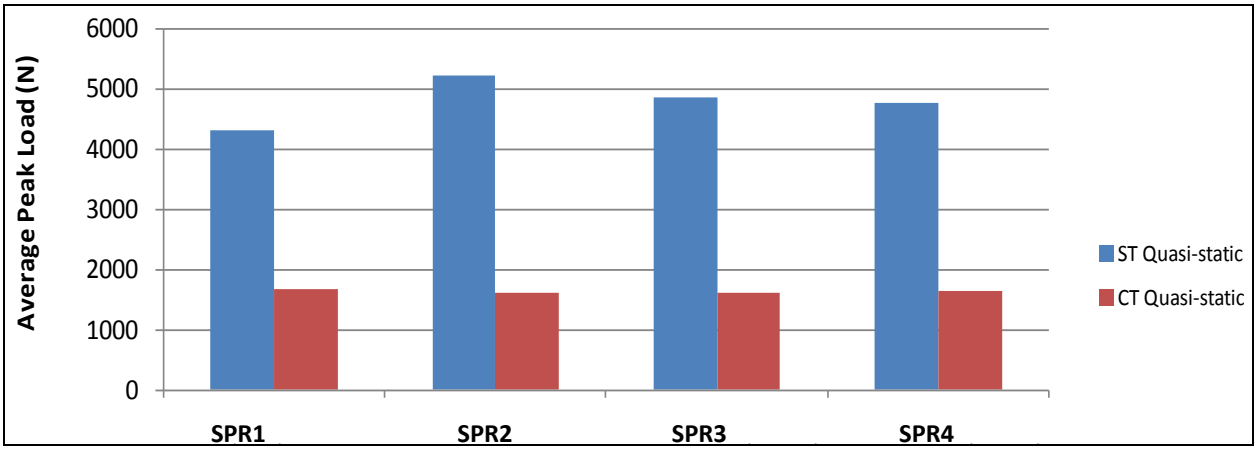

Figure 3: Quasi-static shear tension and cross tension test results for selected coating configurations of Mg AM60B to Al6013 SPR joints

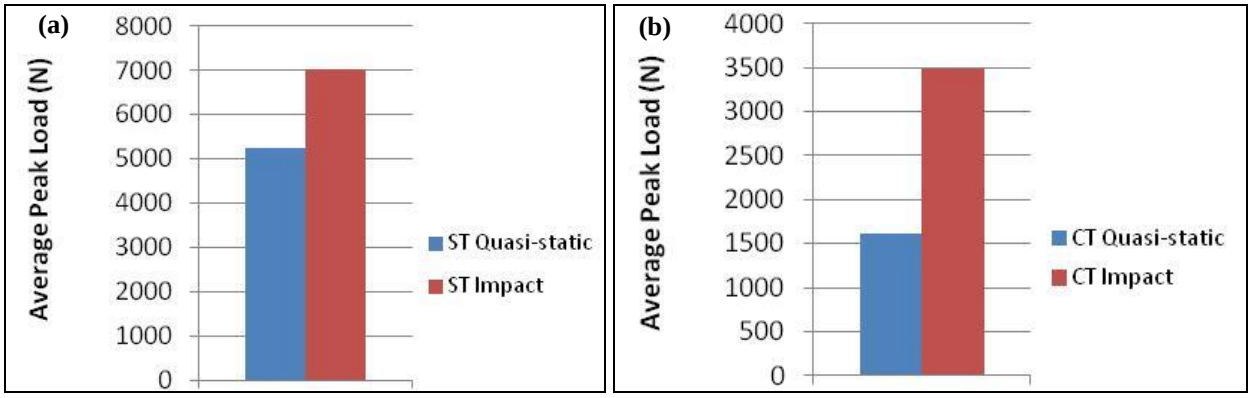

Figure 4: Comparisons of quasi-static vs impact performance for shear tension (a) and cross tension (b) for pretreated Mg AM60B to Al6013 SPR (SPR2) joints

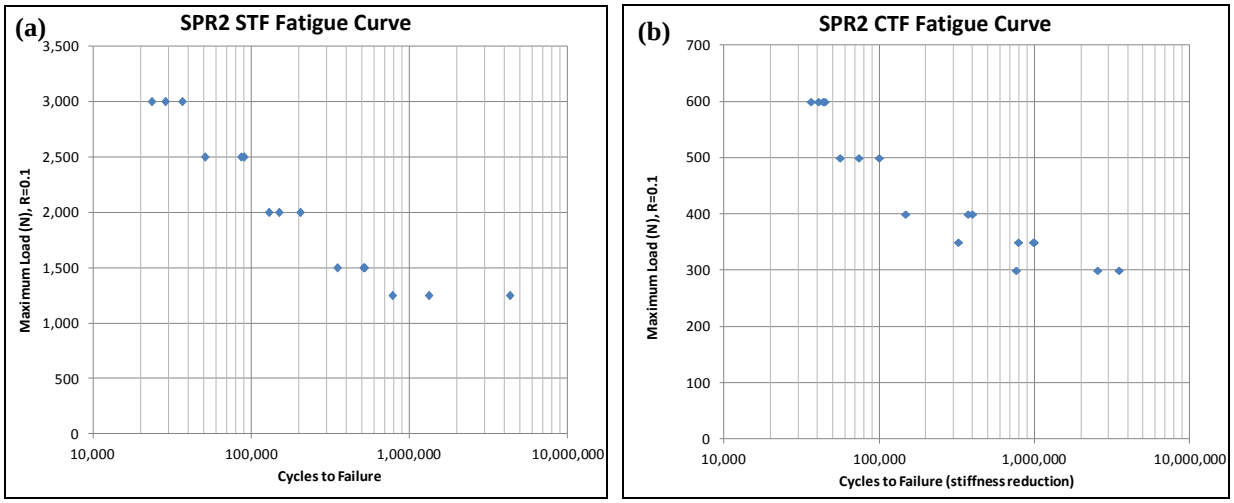

Figure 5: Pre-corrosion fatigue curves for pretreated Mg AM60B to Al6013 SPR2 joints for shear tension joints (a) and cross tension joints (b)

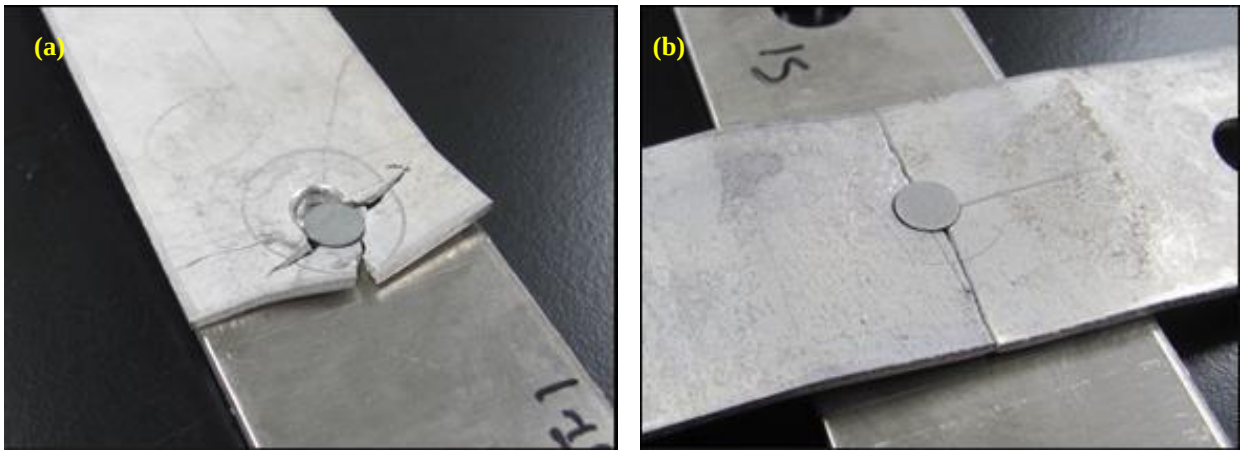

Figure 6: Actual preliminary test samples of SPR1 Mg AM60B to Al6013 joints; shear tension (a) and cross tension (b) showing failure in Mg parent material

Corrosion Testing and Evaluation

Unexpectedly, many of the joined assemblies did not remain intact throughout the prescribed 12-wk accelerated corrosion test, and were removed from the test. Unfortunately, this left an insufficient number of intact samples to conduct all previously defined post-corrosion testing (especially fatigue testing, which typically requires many samples). However, a reduced fatigue test was conducted to allow for later comparison to the UPJ joint performance. Typical joint failure observed during this test after 6-wks of exposure, as shown below in Figures 7 and 8, occurred in the steel SPR rivet itself, not in the Mg or Al material as was expected, although there was clearly extensive corrosion occurring on the Mg and Al coupons as well. Similar failures occurred through 8-wks of exposure as shown in Figure 9, but none of the SPR1 or SPR2 samples remained intact after 8-wks.

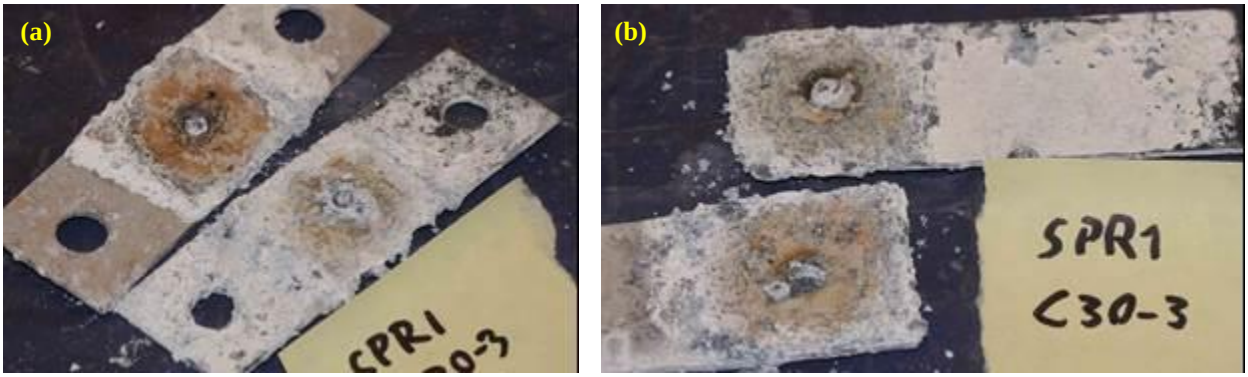

Figure 7: SPR1 cross tension (a) and shear tension (b) joint failure after 6 weeks of accelerated corrosion exposure

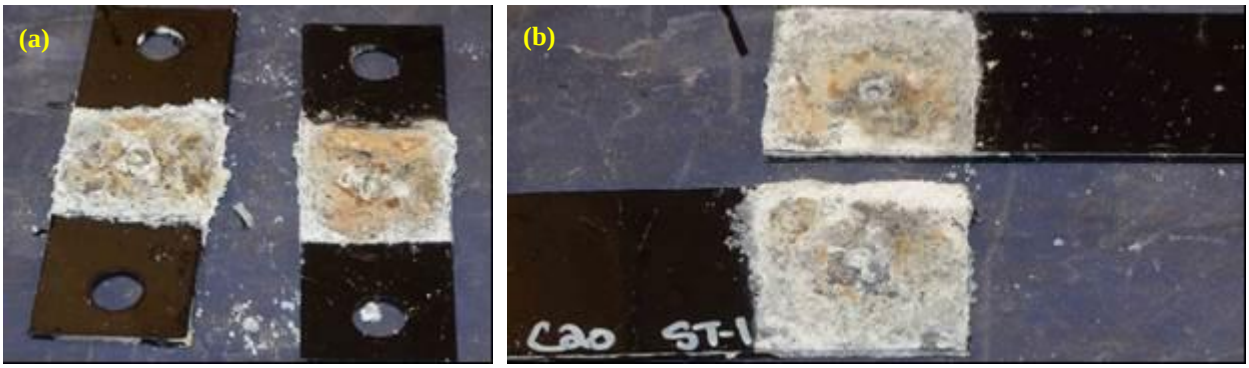

Figure 8: SPR2 cross tension (a) and shear tension (b) joint failure after 6 weeks of accelerated corrosion exposure

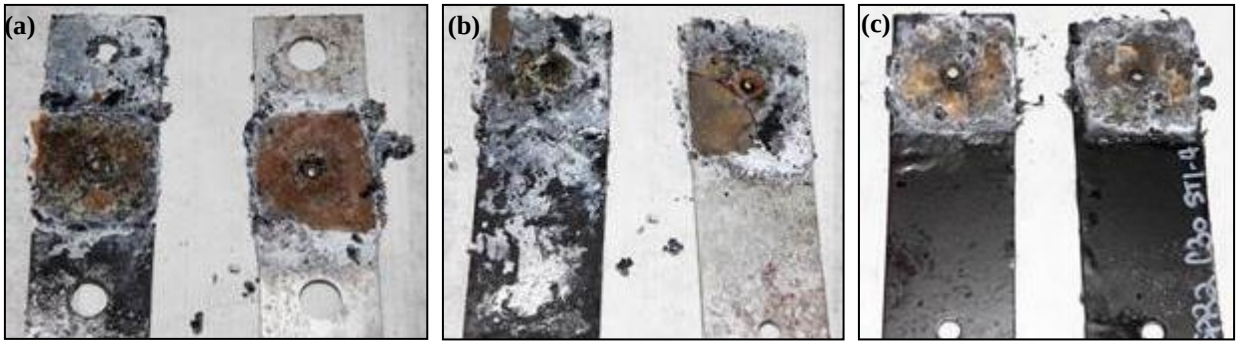

Figure 9: SPR1 cross tension (a) and shear tension (b), and SPR2 shear tension (c) joint failure after 8 weeks of accelerated corrosion exposure

Further SEM evaluation (Figure 10) of one of the SPR1 joints that failed at 6-wks showed the fracture in the steel rivet was a result of hydrogen-induced cracking (hydrogen embrittlement) as a result of high residual stresses on the inner surface of the rivet from the self-pierce riveting process, and a high level of hydrogen generated from the Mg coupon material during the corrosion process and accumulating in the steel rivet (cathode). The rivet was made with high strength steel, which is more susceptible to hydrogen-induced cracking than milder steels.

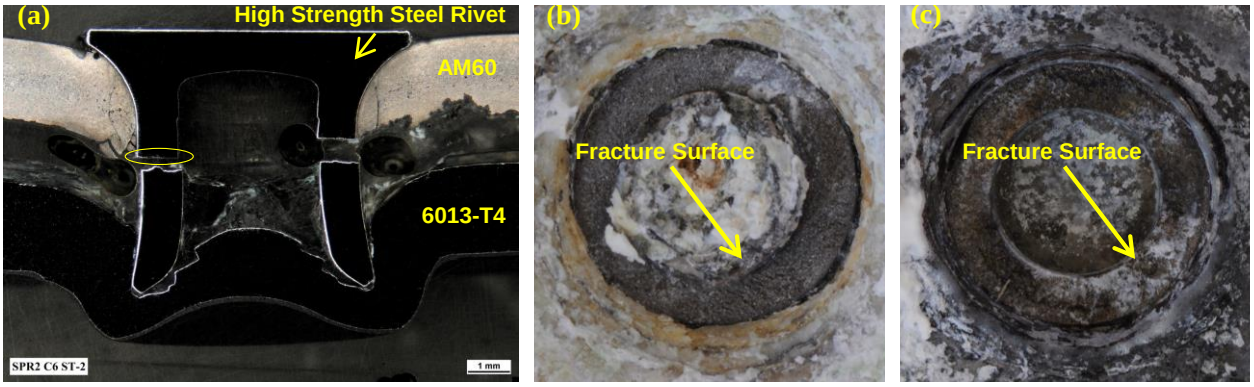

Figure 10: SEM analysis of SPR1 joint failure after 6 weeks of accelerated corrosion exposure

While none of the SPR1 or SPR2 samples remained intact after 8-wks, all the SPR3 and SPR4 samples but one remained intact until the end of the prescribed 12-wk exposure. Photos of SPR3 samples removed at 8-wks can be seen in Figure 11. Note the one SPR3 separation in Figure 11 (c). This sample separated due to the same rivet failure observed in the SPR1 and SPR2 configurations. Photos of SPR4 samples removed at 8-wks are shown in Figure 12. Clearly, coating the Al coupon prior to joining, as in SPR3, resulted in a significant reduction in damage related to galvanic corrosion in the joint and hydrogen embrittlement of the steel rivet. As expected, subsequent coating of the entire assembly, as in SPR4, provided an additional level of protection.

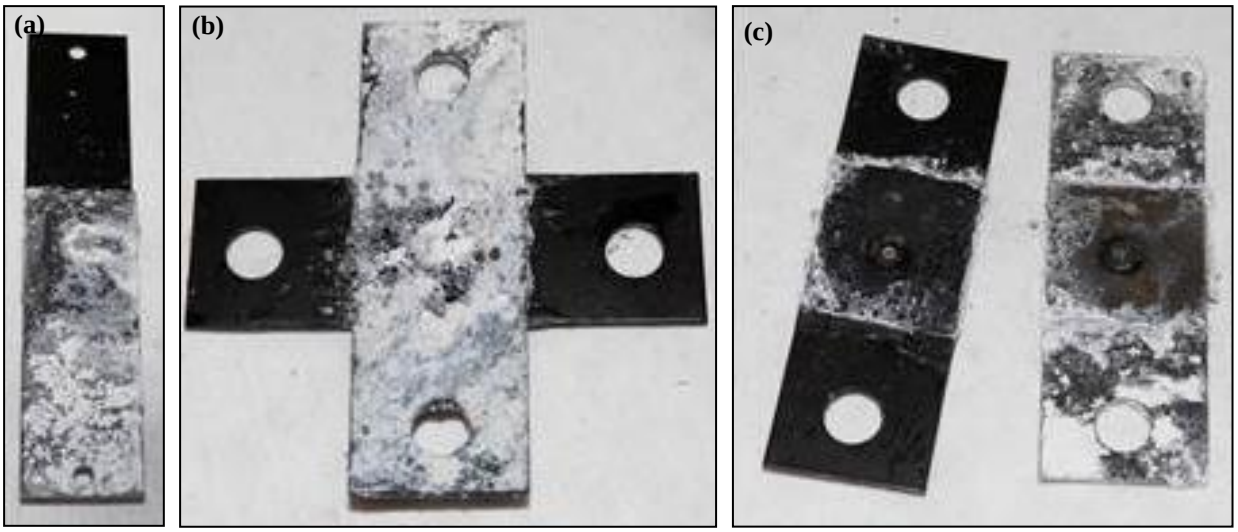

Figure 11: SPR3 joint performance after 8 weeks of accelerated corrosion exposure (a) shear tension specimen, (b) cross tension specimen, and (c) cross tension specimen separated as a result of rivet failure

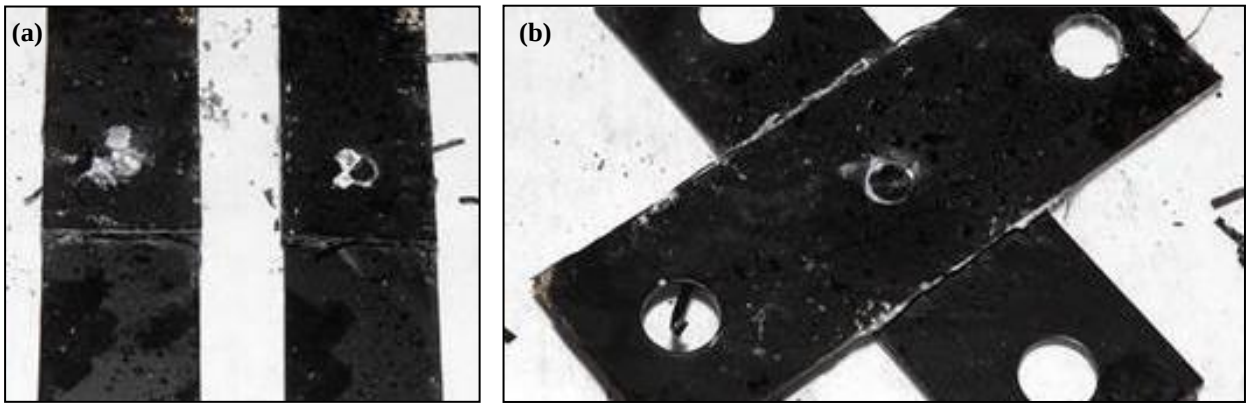

Figure 12: SPR4 shear tension (a) and cross tension (b) joint performance after 8 weeks of accelerated corrosion exposure

Post Corrosion Mechanical/Structural Testing and Evaluation

Post-corrosion mechanical/structural evaluations were conducted on SPR joints in all four coating configurations described in Table 4. Quasi-static lap shear tension test results for SPR coating configurations at various levels of accelerated corrosion testing are shown in Figure 13(a) while impact shear tension test results for the SPR2 coating configuration at pre-corrosion and 8-weeks corrosion exposure are shown in Figure 13(b). Quasi-static cross tension test results for all four SPR coating configurations at various levels of accelerated corrosion testing are shown in Figure 14(a) and impact cross tension test results for the SPR2 coating configuration at pre-corrosion and 8-weeks corrosion exposure are shown in Figure 14(b). Somewhat surprisingly, except for the joints experiencing rivet failures (denoted as RF in the charts), the joint strengths did not drop substantially during accelerated corrosion exposure.

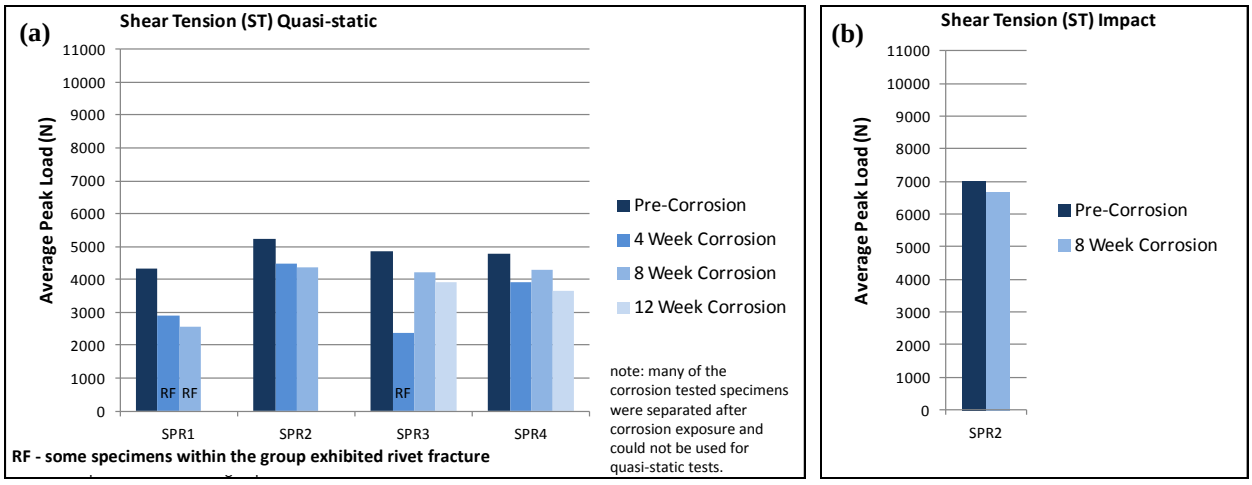

Figure 13: (a) Quasi-static shear tension test results for SPR joints at varying levels of accelerated corrosion exposure and (b) impact shear tension test results for the SPR2 configuration prior to corrosion and after 8-weeks of corrosion exposure

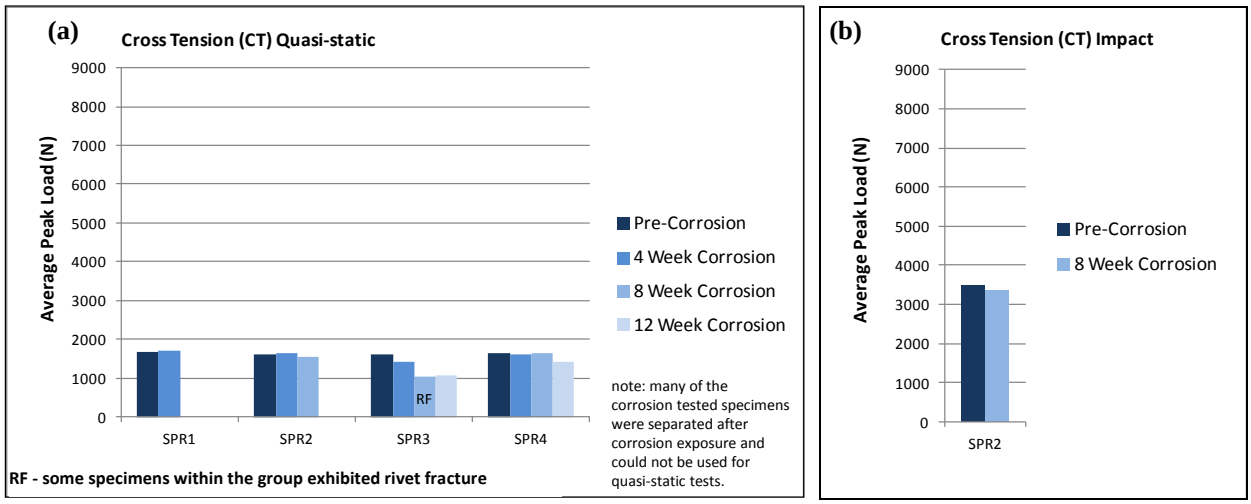

Figure 14: (a) Quasi-static shear tension test results for SPR joints at varying levels of accelerated corrosion exposure and (b) impact shear tension test results for the SPR2 configuration prior to corrosion and after 8-weeks of corrosion exposure

Photos of post-test shear tension and cross tension samples for SPR3 and SPR4 are shown in Figure 15. SPR3 samples are shown in Figure 15(a) while SPR4 samples are shown in Figure 15(b). Note that all failures for these two coating configurations occurred in the Mg parent material. Also note, however, 1) the appearance of the samples, which would not be considered acceptable in exposed applications despite the acceptable joint strength in these configurations, and 2) the substantially increased hole diameter in some of the SPR3 cross tension samples, indicating that the area around the rivet was heavily corroded and likely close to failure prior to removal of the sample from the corrosion chamber.

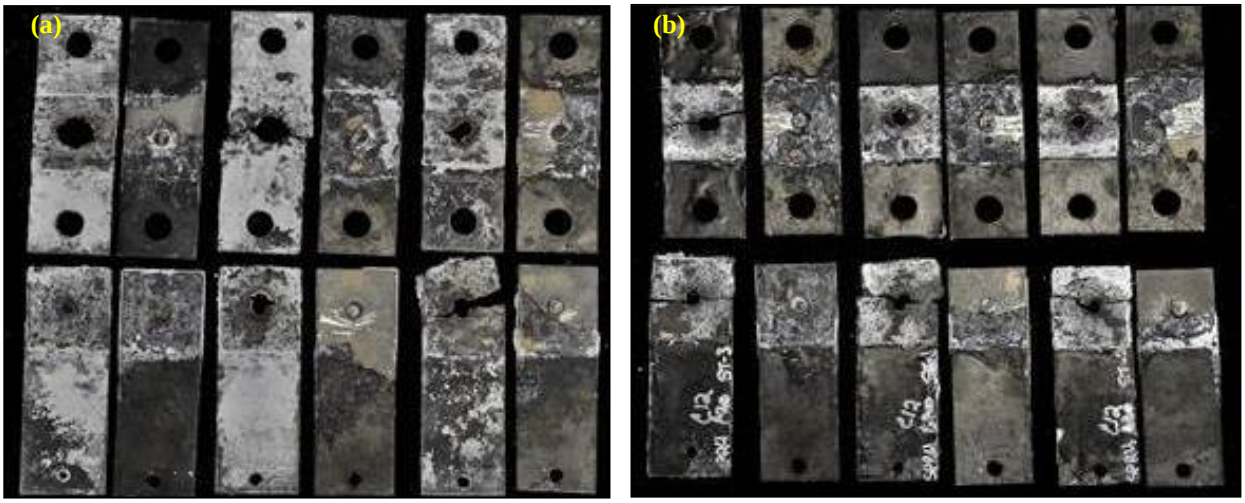

Figure 15: (a) SPR3 post-corrosion samples after quasi-static testing and (b) SPR4 post-corrosion samples after quasi-static testing

Fatigue test results for the SPR2 coating configuration are shown in Figure 16. Shear-tension fatigue results are shown in Figure 16(a) while cross-tension fatigue results are shown in Figure 16(b). The original intent was to conduct a complete fatigue test of the SPR2 samples after 12 weeks of corrosion exposure. However, due to the previously discussed hydrogen embrittlement rivet failures during the accelerated corrosion tests, the exposure was reduced to 8-wks and the number of fatigue tests had to be reduced substantially as well, since more than half of the SPR2 samples separated in the corrosion chamber after

only 8 weeks of exposure. In the charts, the blue points indicate pre-corrosion test results and the red points indicate post-corrosion test results. Again, except for those joints experiencing rivet fractures, the joint fatigue strengths did not drop substantially as a result of accelerated corrosion aging. The low number of post-fatigue data points was a result of the premature separations during the corrosion test.

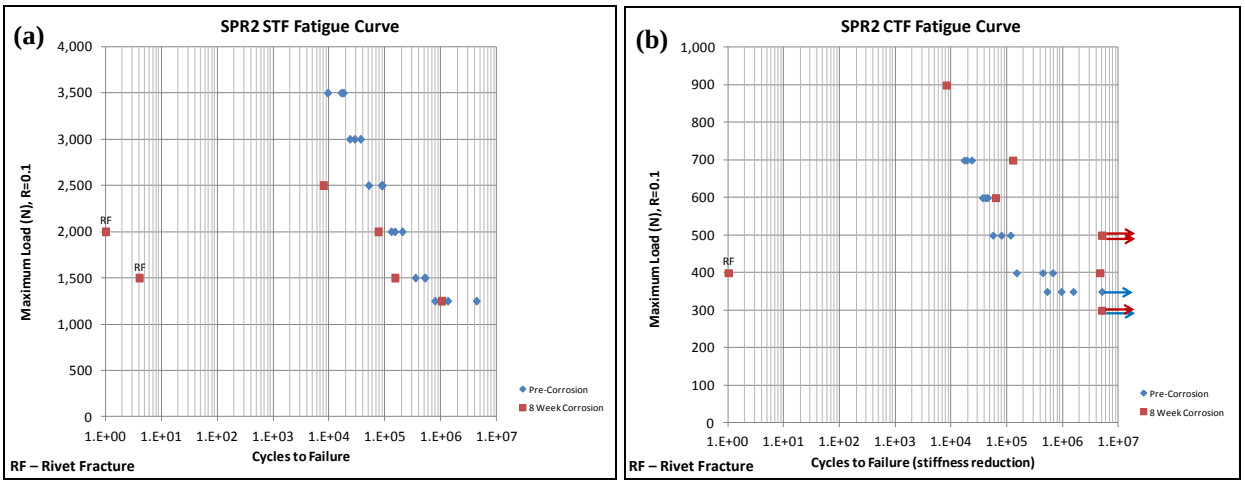

Figure 16: (a) Shear tension fatigue test curves for SPR2 and (b) cross tension fatigue curves for SPR2

MG AM60B THERMO-MECHANICAL MATERIAL CHARACTERIZATION

To better understand the forming behavior of Mg die castings under compression at different temperatures, extensive thermo-mechanical compression behavior characterization for die cast AM60B and AZ91D magnesium alloys was conducted by graduate students from McMaster University at Canmet in Hamilton, Ontario, Canada at eight temperatures and two strain rates using cylindrical shaped compression test specimens cut from die-castings provided by this DoD/DoE funded project. Two additional strain rates were added later to gain a better understanding of the material behavior. It should be noted that the work conducted in Canada was not funded in any way by the U.S. DoD or DoE nor was this work considered as part of the cost share requirements for the DoD/DoE funded project. This information was ultimately used to support computer simulations of UPJ forming behavior to optimize electrode geometries and process parameters. A few early examples of this work are shown in Figures 17 and 18.

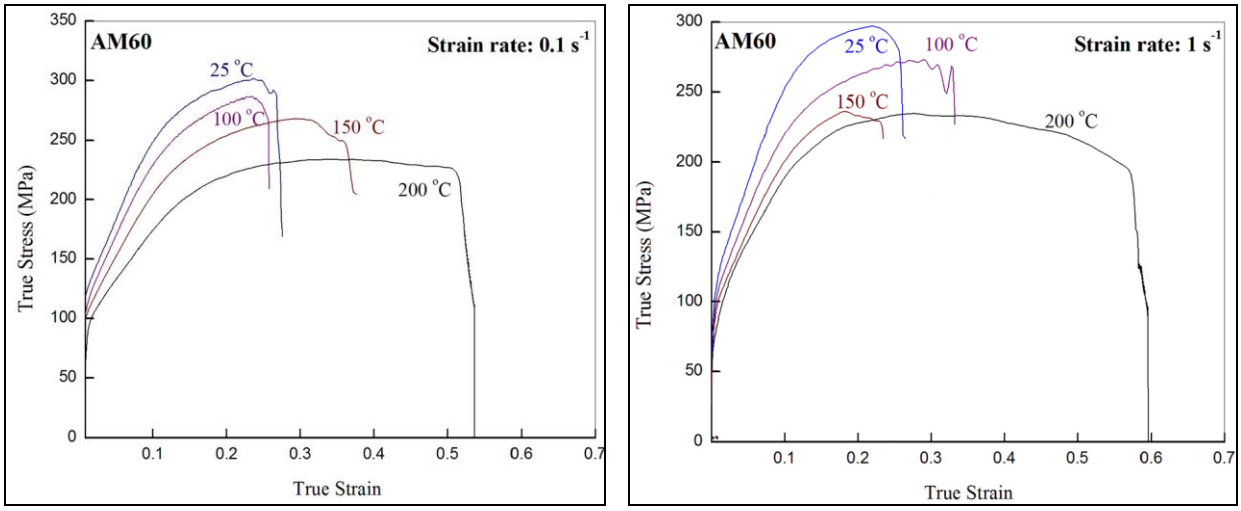

Figure 17: Test results for Mg AM60B alloy at low (<=200ºC) temperatures at 0.1 s^{-1} (left) and 1 s^{-1} (right)

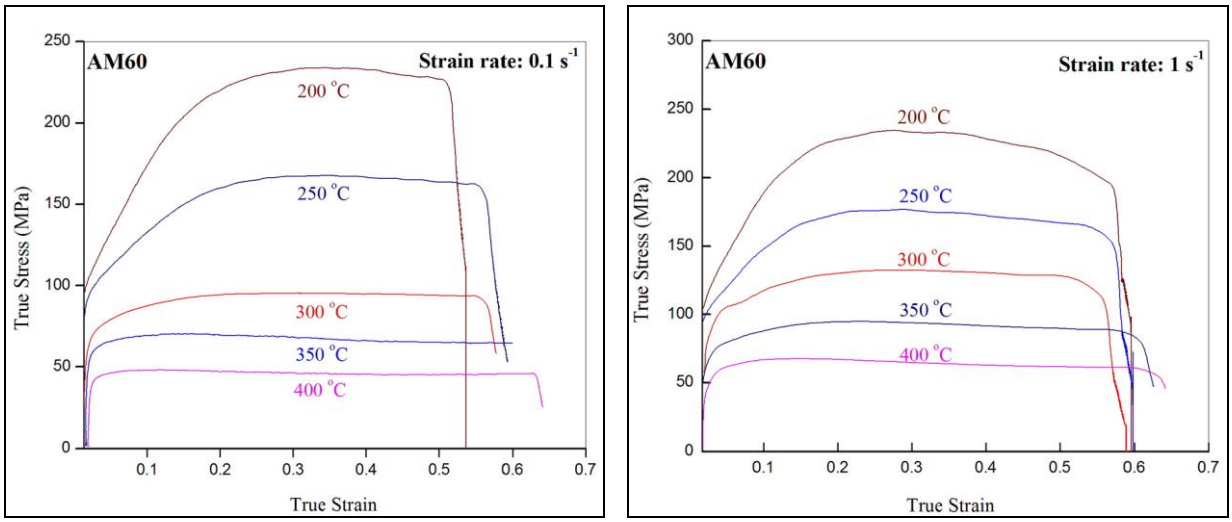

Figure 18: Test results for Mg AM60B alloy at high (>=200ºC) temperatures at 0.1 s^{-1} (left) and 1 s^{-1} (right)

ROUND BOSS UPJ PROCESS DEVELOPMENT AND PERFORMANCE EVALUATION

Generic UPJ Process Development and Optimization

This section provides a ***very*** brief summary of the overall UPJ process development and optimization efforts. Using the thermo-mechanical compression behavior characterization data described briefly in Section C, as well as additional physical experimentation and development on laboratory equipment, the team optimized round boss UPJ joint electrode geometries and process parameters.

Process modeling and simulation development work (examples shown in Figure 19), using the DEFORM-3D software produced by Scientific Forming Technologies Corporation (SFTC), was subcontracted by AET to Upwind Technology, Inc. The simulations (shown on the left) demonstrated good correlation to physical development work (shown on the right) conducted at AET.

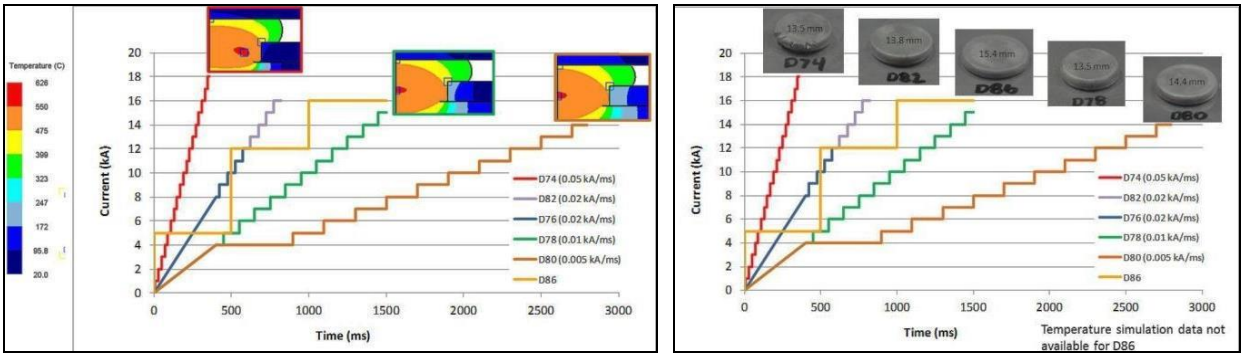

Figure 19: Examples of preliminary process simulation (left) and physical correlation (right) work evaluating effect of current rate on temperature and deformation behavior

Figure 20 shows example process simulation results comparing hoop stress (hoop stress was identified as ***one*** major source of small cracks on the outer perimeter of the formed head) near the end of the formation cycle for two different electrode designs. Figure 21 shows multiple curves characterizing critical parameters during joint development over the entire joining process cycle.

In addition to optimizing the electrode shape, numerous simulations and physical experiments were conducted comparing the joining process performance resulting from increasing current throughout the process at different rates. Several process variations were found to be acceptable. This section shows only a ***very*** small subset of the information that was utilized in the final round boss UPJ process optimization prior to producing joints for testing and evaluation. Extensive additional simulations were conducted for oval boss UPJ and round boss UCR joints as well.

Unfortunately, with the limited time and budget available in this project, it was difficult to accurately and consistently predict cracking during formation of the head shape through simulations, so while the simulations were used to establish a basic starting point, much of the actual process development and optimization was performed with actual machined electrodes and laboratory welding equipment.

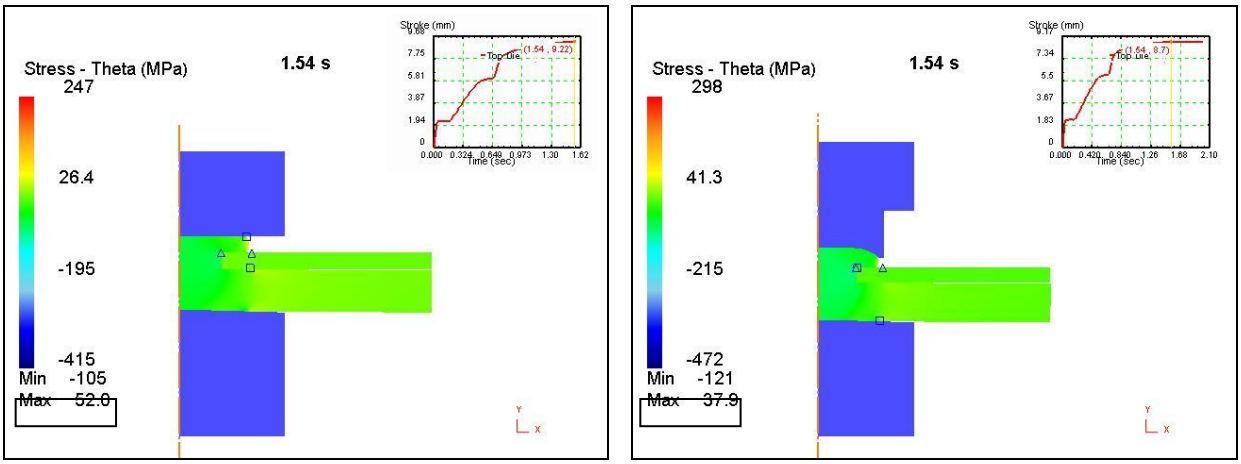

Figure 20: Example simulation comparison of hoop stress created by two different electrode shapes. The one on the left has higher hoop stress and is more likely to crack

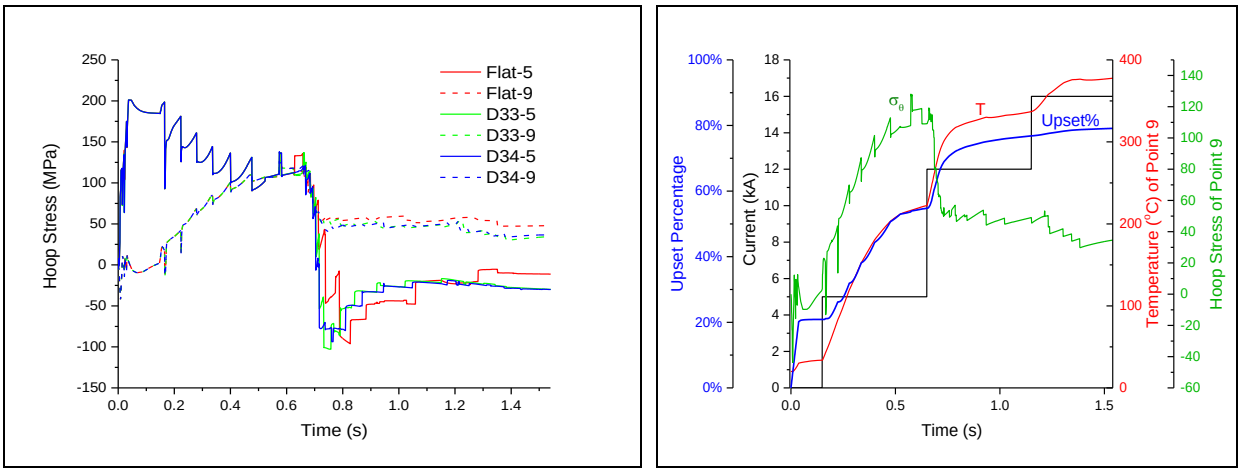

Figure 21: Comparisons of hoop stress at three different points on the UPJ boss outer skin for three different electrode designs (left) and a composite of upset percentage, applied current, temperature, and hoop stress for one electrode design (right)

Round Boss UPJ Development and Performance Evaluation

Beyond the extensive process development and optimization work summarized in the previous section, in order to support the prescribed evaluation of round boss UPJ joints, AET produced several hundred round boss UPJ joints from 11 unique material/coating configurations and two different joint size and material thickness configurations (8-mm diameter bosses were used to join 2.0-mm thick Al 6013 aluminum, 2.0-mm thick AM60B Mg, and 2.2-mm thick DP-590 steel panels to 4-mm thick AM60B Mg plates while 7-mm diameter bosses were used to join 1.0-mm thick Al 6016 panels to 4-mm thick AM60B Mg plates). As with the benchmark SPR evaluations, the prescribed tests included microstructure evaluations, joining induced defect characterization, and quasi-static, impact, and fatigue tests of shear and cross tension joint configurations as well as accelerated corrosion testing and post corrosion structural/mechanical evaluation.

8.0-mm Round Boss UPJ Joint Development and Evaluation

The following section summarizes testing and evaluation of the ***8.0-mm*** diameter round boss joints.

Table 5 shows the material and coating configurations investigated for 8-mm diameter round boss UPJ joints. For these joints, all top sheets were in the 2.0-2.2 mm thickness range, which is close to a practical limitation for this size of boss. The configuration numbers shown in the left column will be used throughout the report to identify specific joint configurations. The two configurations circled in red (UPJ 8-1 and UPJ 8-3) are intended to highlight Mg-steel joints since most performance comparisons of these joints are substantially different than those of the Mg-Al or Mg-Mg joints. Specifically, pre-corrosion mechanical/structural joint strength is typically considerably higher, while corrosion performance results are considerably worse.

Configu-ration Number	Upper Sheet			Bottom Sheet			Assembly Coating Con-figuration
	Material	Thickness (mm)	Coating	Material	Thickness (mm)	Coating	
UPJ8-1	HSS DP-590	2.0	Galvanized	Mg AM60B	4.0	Pretreated	Uncoated
UPJ8-2	Al 6013-T4	2.2	Bare	Mg AM60B	4.0	Bare	Uncoated
UPJ8-3	HSS DP-590	2.0	Galvanized + e-coat	Mg AM60B	4.0	Pretreated	Powdercoated
UPJ8-4	Al 6013-T4	2.2	Pretreated	Mg AM60B	4.0	Pretreated	Powdercoated
UPJ8-5	Al 6013-T4	2.2	Powdercoated	Mg AM60B	4.0	Pretreated	Uncoated
UPJ8-6	Al 6013-T4	2.2	Powdercoated	Mg AM60B	4.0	Pretreated	Powdercoated
UPJ8-7	Mg AM60B	2.0	Bare	Mg AM60B	4.0	Bare	Uncoated

Table 5: 8-mm round boss UPJ material and coating configurations

Figure 22 shows two examples of optimized round boss UPJ joints cross sections. Figure 22(a) shows a section through UPJ8-7 while Figure 22(b) shows a section through UPJ8-2. There is no evidence of cracking or porosity in either of these joints. Furthermore, the head shapes are well formed and provide a substantial overlap to the joined sheet materials to help lock them into place to enable high cross-tension strength. The parameters used to create these joints (with slight modifications for coated samples) were used to create all of the tested 8-mm round boss joints presented throughout the rest of the report.

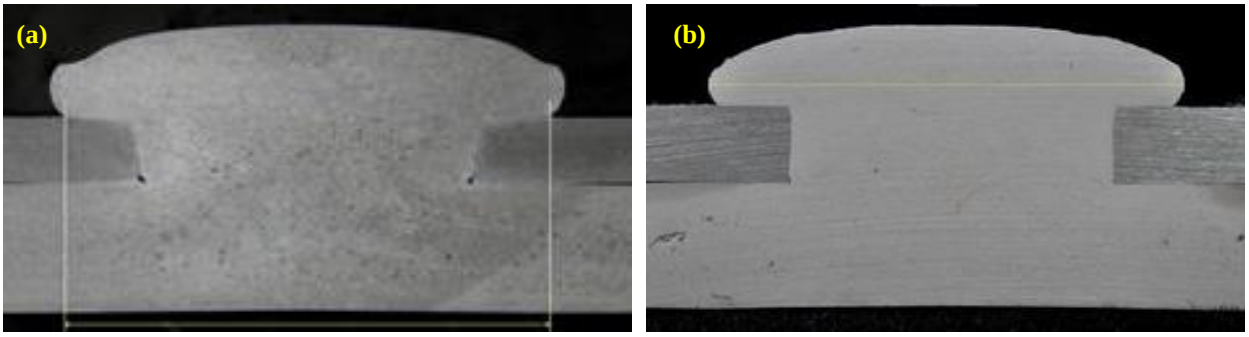

Figure 22: Metallurgical cross-sections of 8-mm round boss UPJ joints UPJ8-7 in (a) and UPJ8-2 in (b)

Figure 23 shows several head formations produced on 8-mm round boss Mg, Al, and steel top sheets in bare, pre-treated, and coated configurations. From these photos, it can be seen that well-formed, crack-free head formations were produced in desired material and coating configurations.

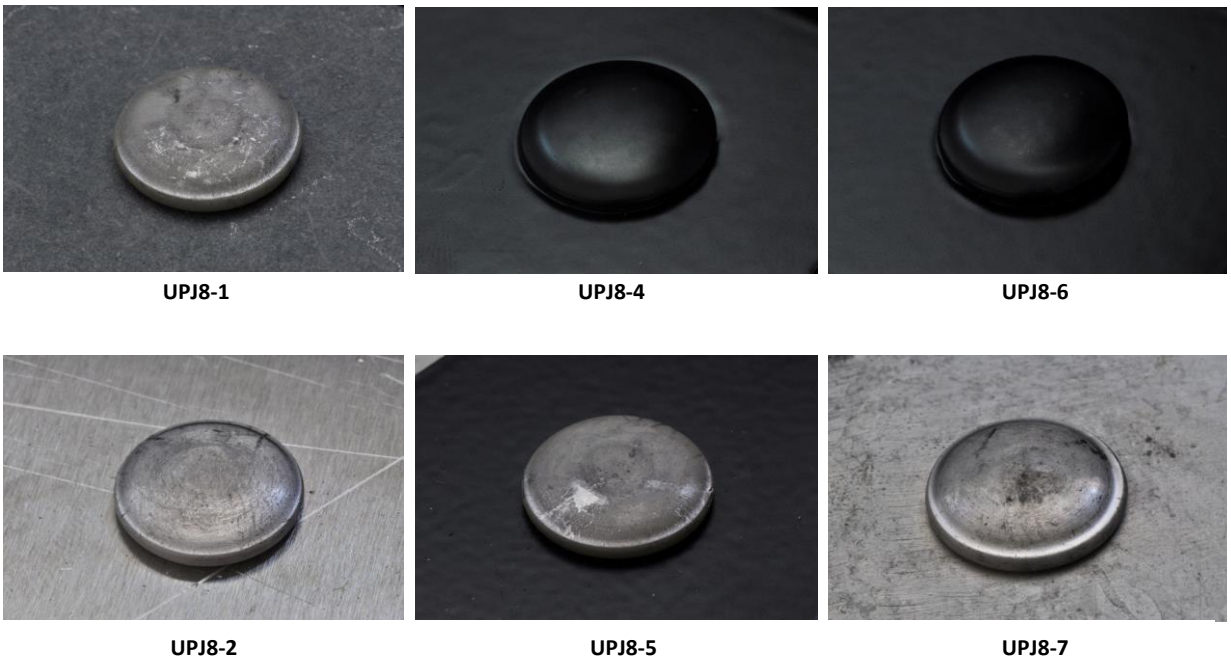

Figure 23: 8-mm round boss UPJ head formations

Figure 24(a) shows a metallurgical cross section for a Mg-steel joint. In this application, the steel top sheet was coated by Agritek Industries with a proprietary cold galvanizing process called Armorgalv. The close-up in 24(b) shows that the steel coating remains intact after the joining process. This was considered to be critical since these parts would be exposed to an accelerated corrosion environment.

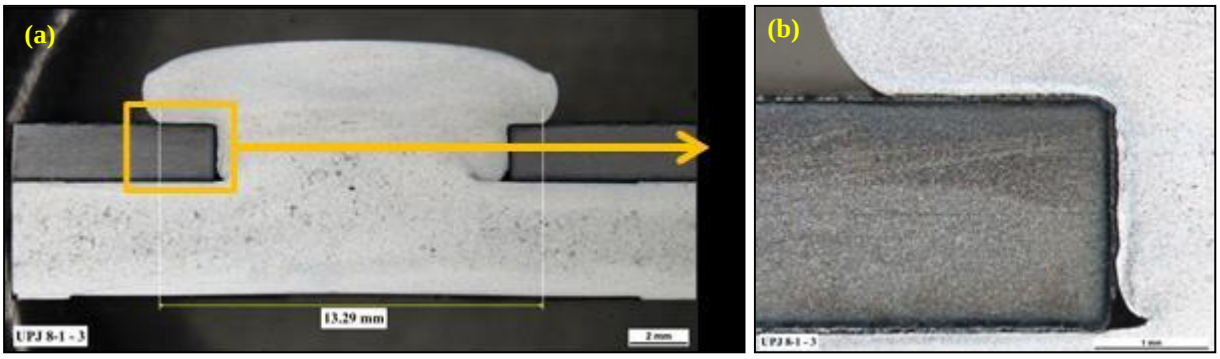

Figure 24: Metallurgical cross-section of 8-mm round boss Mg-Steel UPJ joint

Additionally, due to previous experience at FCA with Mg-steel joints experiencing substantial corrosive attack at the edges of the coupons, which failed well before the actual joint, all the Mg-steel test samples in this study were sealed at the edges as shown in Figure 25. Figures 25(a) and 25(b) show edge sealed shear tension and cross tension assemblies in the UPJ8-1 coating configuration while Figures 25(c) and 25(d) show edge sealed shear tension and cross tension assemblies in the UPJ8-3 coating configuration. The sealer used in both configurations was Henkel's Teroson PV1095 sealer, cured at 177°C.

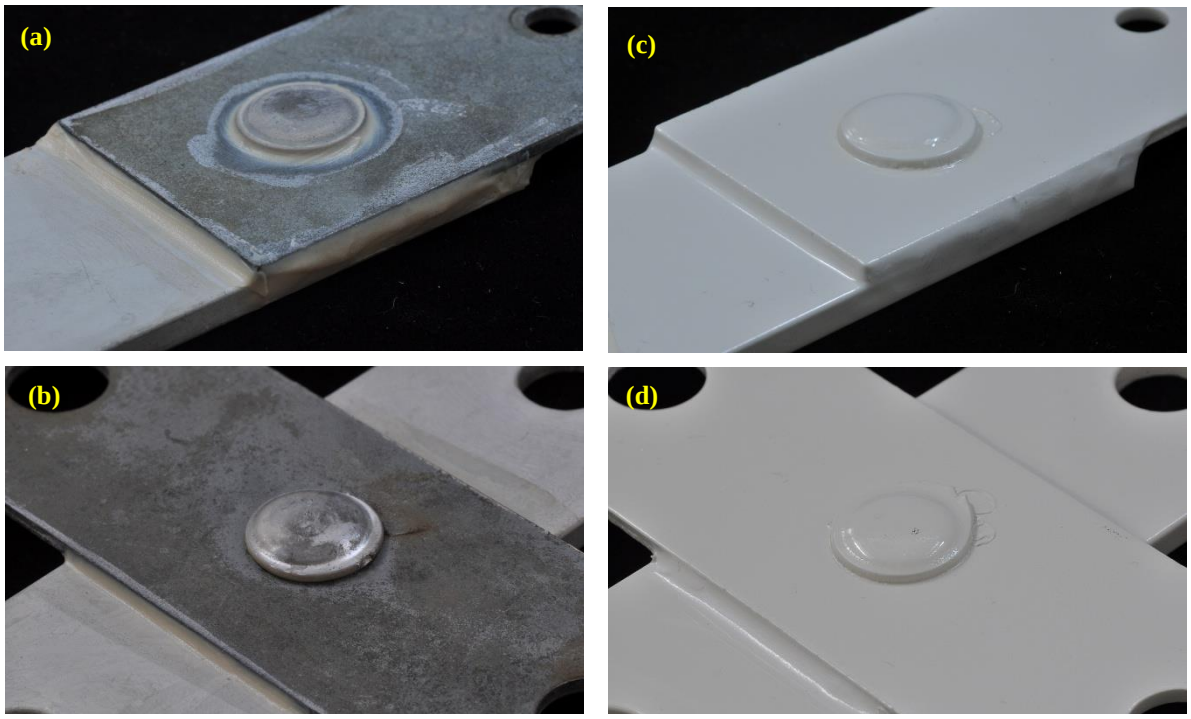

Figure 25: Mg-steel edge sealing

Initial (pre-corrosion) Mechanical/Structural Testing and Evaluation

Quasi-static and impact ***shear*** tension test results are shown in Figure 26 (a) and (b) respectively. While all the configurations exhibit good shear tension strength, it is not clear why, in the quasi-static testing, UPJ8-3 displayed significantly higher shear tension strengths than UPJ8-1. These are both Mg-steel joints with the primary difference being that UPJ8-3 was powder-coated after assembly. While this would be expected to increase the strength of a bake hardenable steel or aluminum alloy, DP590 is ***not*** a bake hardenable alloy. Furthermore, all the Mg-steel and Mg-Al joint failures occurred in the Mg die-casting, which is not known to be affected by paint or powder-coating bake temperatures either.

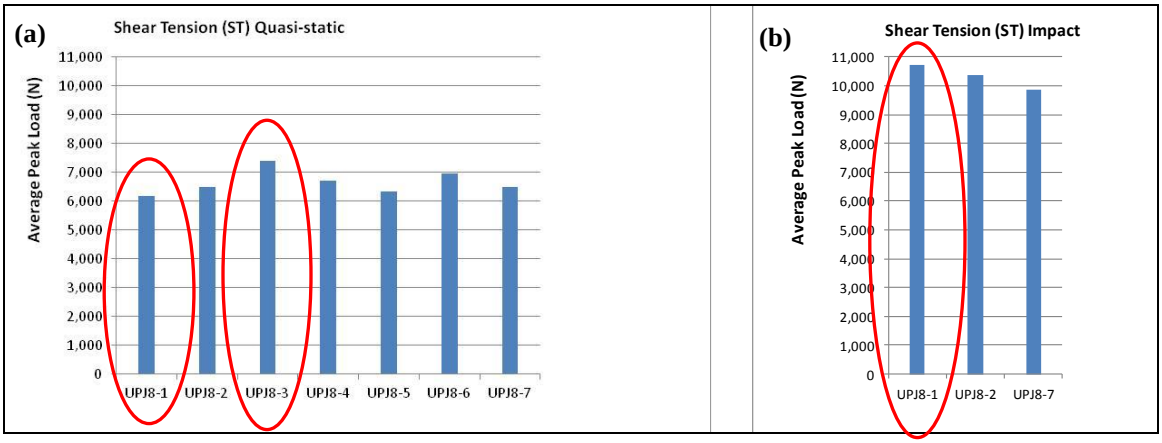

Figure 26: 8-mm round boss UPJ quasi-static (a) and impact (b) shear tension test results

Figure 27 (a) and (b) show quasi-static and impact ***cross*** tension test results for joints produced from an 8-mm diameter boss.

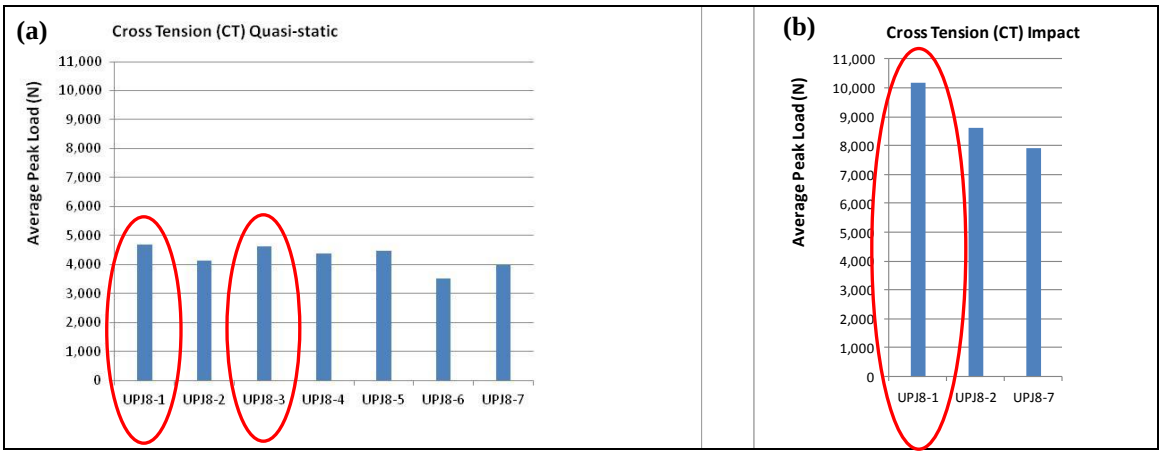

Figure 27: 8-mm round boss UPJ quasi-static (a) and impact (b) cross tension test results

Notably, in both shear tension and cross tension ***impact*** tests, the Mg-Steel joints (UPJ8-1) show significantly higher strength than the Mg-Al joints (UPJ8-2) and Mg-Mg joints (UPJ8-7). This is notable because all these joints failed in the die cast Mg bottom plate. One possible explanation is that the steel top sheet is substantially stiffer than the Al and Mg top sheets. Joint stiffness may have a significant effect on the impact test performance, especially for the cross tension joints.

Shear tension fatigue performance test results for 8-mm diameter round boss UPJ joints are plotted in Figure 28 and cross tension fatigue performance test results are plotted in Figure 29. In both plots, the blue points indicate results for the UPJ8-2 configuration (Al to Mg) while the red points indicate results for the UPJ8-7 (Mg to Mg) configuration. Observation of the failure modes shown in Figures 28(b) and 29(b) indicate that the high cycle fatigue results may be influenced more by the properties of the Mg die castings than by the joining method since the failures always occur in the Mg castings.

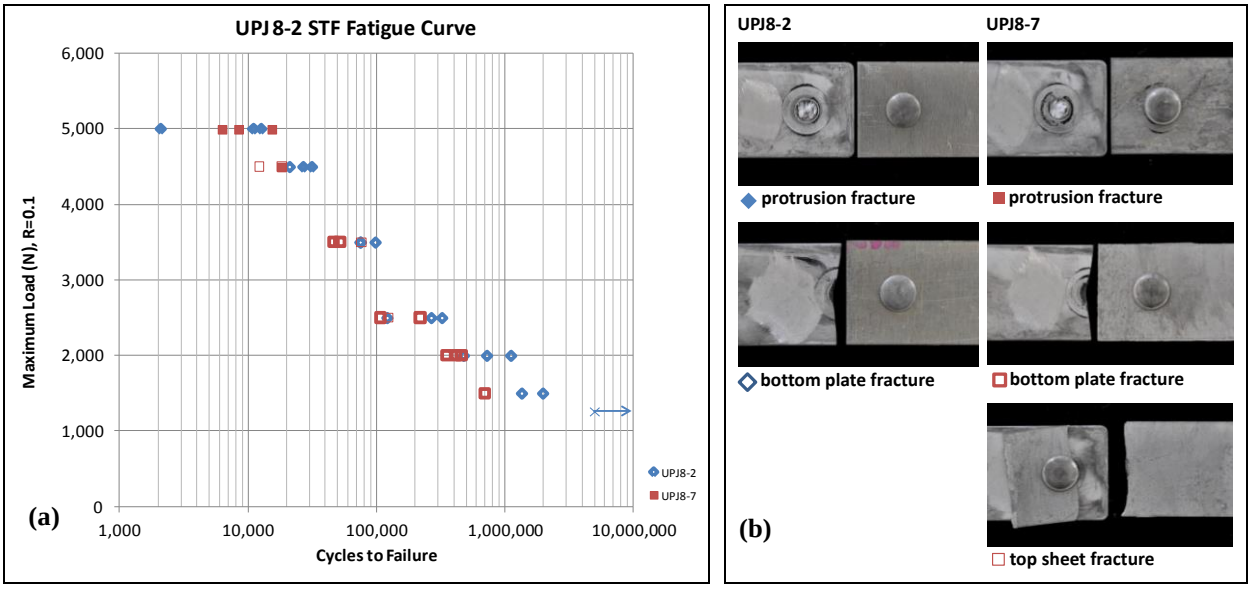

Figure 28: 8-mm round boss UPJ fatigue curves

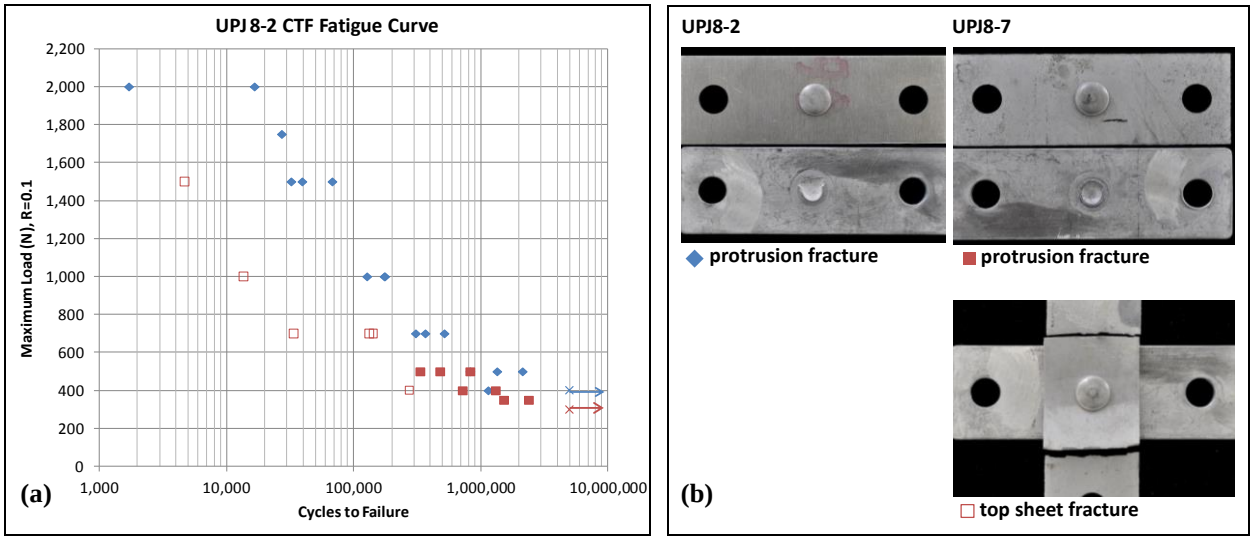

Figure 29: 8-mm round boss UPJ cross tension fatigue curves

Corrosion Testing and Evaluation

Over 250 8-mm diameter round boss UPJ joints were subjected to the FCA accelerated corrosion schedule. As in the case of the benchmark SPR joint evaluations, numerous samples of the bare Mg to bare Al UPJ joints (UPJ8-2) began separating after 6 to 8-wks exposure in the corrosion chamber and could not be evaluated for structural/mechanical performance. However, in the case of UPJ, the effect of galvanic corrosion between the Mg and Al coupons and exfoliation (delamination) corrosion of the Al was more obvious as opposed to fracture of the steel rivet seen in the SPR process. In the case of the Mg to Al6013 joint combination, even with the UPJ process, some level of coatings (e.g., UPJ8-4, UPJ8-5, and UPJ8-6) is required to protect against galvanic corrosion from this high copper containing aluminum alloy. This particular aluminum alloy is a high strength alloy with a higher level of copper than most 6xxx series Al alloys. The combination of high level of copper, acetic acid in the salt spray, and hydrogen given off by the Mg AM60B alloy during corrosion may have exacerbated the exfoliation corrosion of the Al coupons as there were a large number of joints showing this type of corrosion in the bare Mg to bare Al joint combinations.

Examples of separated bare Mg to bare Al (UPJ8-2) joints are shown in Figures 30 and 31. Close up views of the sample showing the extent of corrosion on both the Mg and Al coupons are shown in Figure 31. Note the delamination or “exfoliation” of the Al 6013 coupon in Figure 31(c).

Figure 30: UPJ 8-2 Bare Mg to bare Al joint separation after 6 weeks

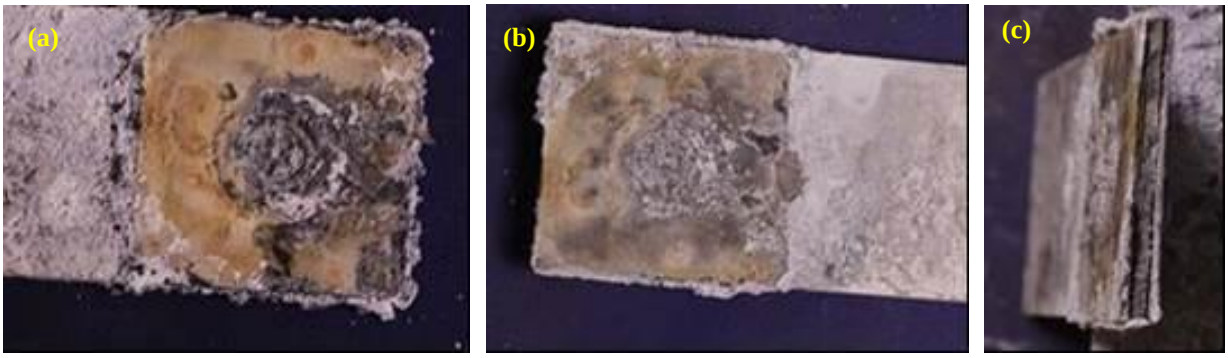

Figure 31: Separated UPJ 8-2 Bare Mg to bare Al joint close-up views (a) Mg plate at joint interface, (b) Al plate at joint interface, (c) edge of Al plate showing delamination or "exfoliation"

The two halves of the assembly were analyzed: Macro-photography was used to document the samples (Figures 32(a) and 33(a)). The samples were then placed in a Scanning Electron Microscope (SEM). Energy Dispersive X-Ray Spectroscopy (EDS) was performed to determine the constituents present at locations A & B on both samples. The EDS spectrum for location A on the magnesium plate contained major peaks for aluminum, oxygen, and sodium (Figure 32(b)). The EDS spectrum for location B on the magnesium plate contained major peaks for magnesium, oxygen, and chlorine (Figure 32(c)).

The EDS spectrum for location A on the aluminum plate contained major peaks for aluminum and oxygen (Figure 33(b)). The EDS spectrum for location B on the aluminum plate contained major peaks for magnesium, oxygen, and chlorine (Figure 33(c)).

The yellow flaky corrosion product observed on both sides of the Mg and Al panels was analyzed by EDS as predominantly aluminum oxide.

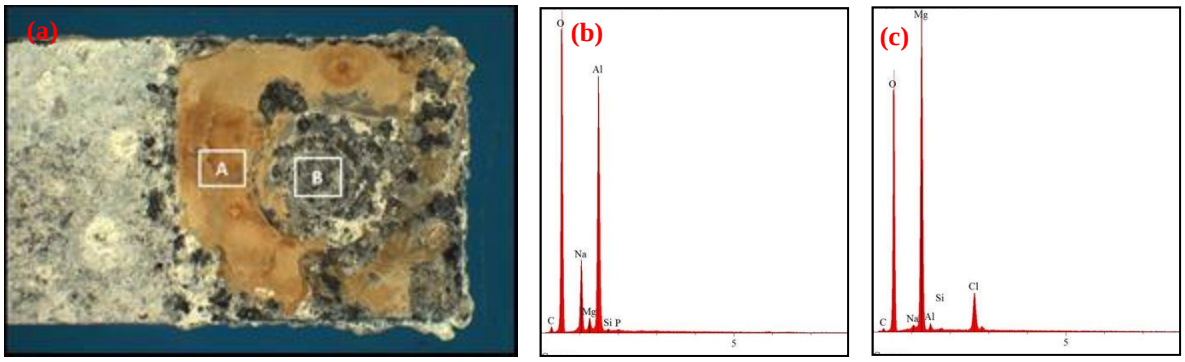

Figure 32: (a) UPJ 8-2 Bare Mg sample macrophotography (b) EDS spectrum analysis showing high level of aluminum and oxygen in location A and (c) EDS spectrum analysis showing high levels of Mg and oxygen in location B

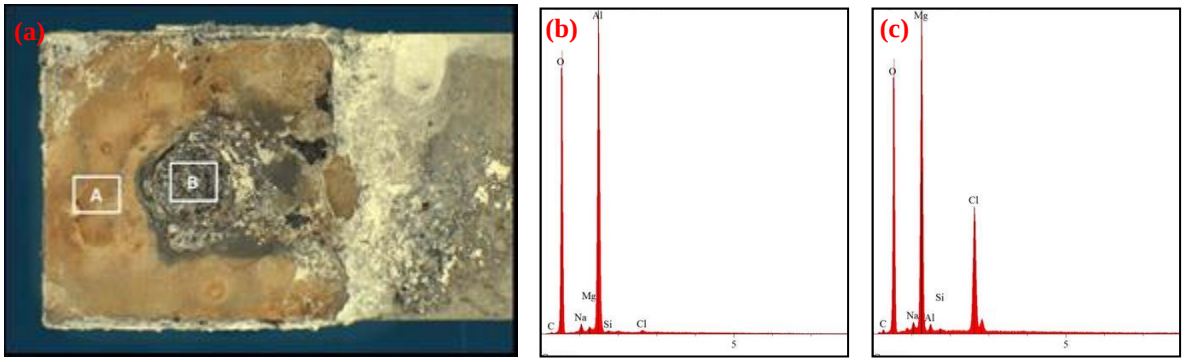

Figure 33: (a) UPJ 8-2 Bare Al sample macrophotography (b) EDS spectrum analysis showing high level of aluminum and oxygen in location A and (c) EDS spectrum analysis showing high levels of Mg and oxygen in location B

Additional bare Mg to bare Al (UPJ8-2) samples separated in a similar manner between 6-wks and 12-wks of exposure. Only one sample of pretreated Mg to pretreated Al (UPJ8-4) separated after 8-wks while none of the samples with coated Al (UPJ8-5 and UPJ8-6) separated even after 12-wks.

Additionally, none of the Mg-steel joint configurations (UPJ 8-1 and UPJ 8-3) were able to withstand the full prescribed 12-wk corrosion exposure testing. These particular configurations include a DP590 steel panel joined to a Mg die-casting. Even the combination of galvanizing, e-coating, sealed edges, etc., was not sufficient isolation to protect the Mg die-casting from the electro-galvanic corrosion activity incited by the coupling to steel in the aggressive accelerated corrosion environment after 6-wks. Examples of separated Mg to steel joints are shown in Figures 34 and 35 where the severe galvanic reaction between the two metals resulted in dissolution of the Mg casting in the areas of contact at the edge of the steel coupon.

Figure 34: UPJ8-1 lap shear tension test coupons separated after 8-wks of accelerated corrosion

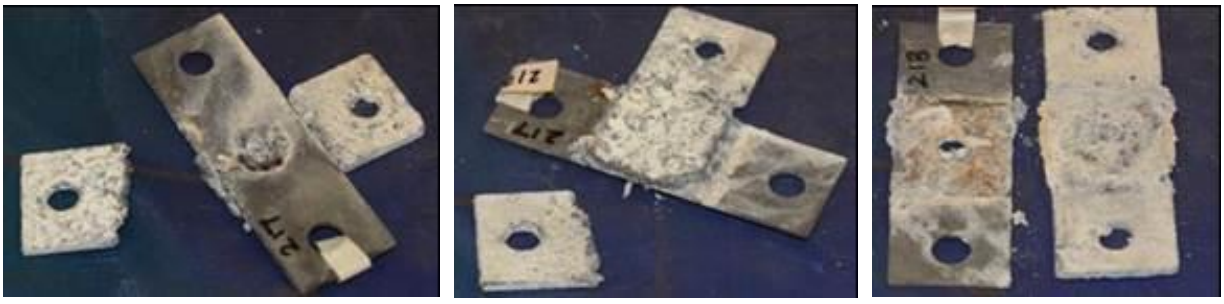

Figure 35: UPJ8-1 cross-tension test coupons separated after 8-wks of accelerated corrosion

Post Corrosion Mechanical/Structural Testing and Evaluation

The quasi-static lap shear and cross tension test results for configurations UPJ8-1 through UPJ8-6 are shown in Figures 36 and 37 prior to corrosion testing and after 4-wks, 8-wks, and 12-wks of accelerated corrosion exposure. Note that there are no results for UPJ8-1 and UPJ8-3 beyond 4-wks of exposure. This is because none of the samples withstood more than 6-wks of corrosion exposure so there were none available for testing at 8-wks. Also, note that all the coated Mg/Al configurations (UPJ8-4, UPJ8-5, and UPJ8-6) maintained good joint strength performance even after 12-wks of exposure. Notably in both lap shear tension and cross tension, of the Mg-Al configurations, only the bare Mg to bare Al (UPJ8-2) configuration displayed any significant reduction in joint strength after 12-wks.

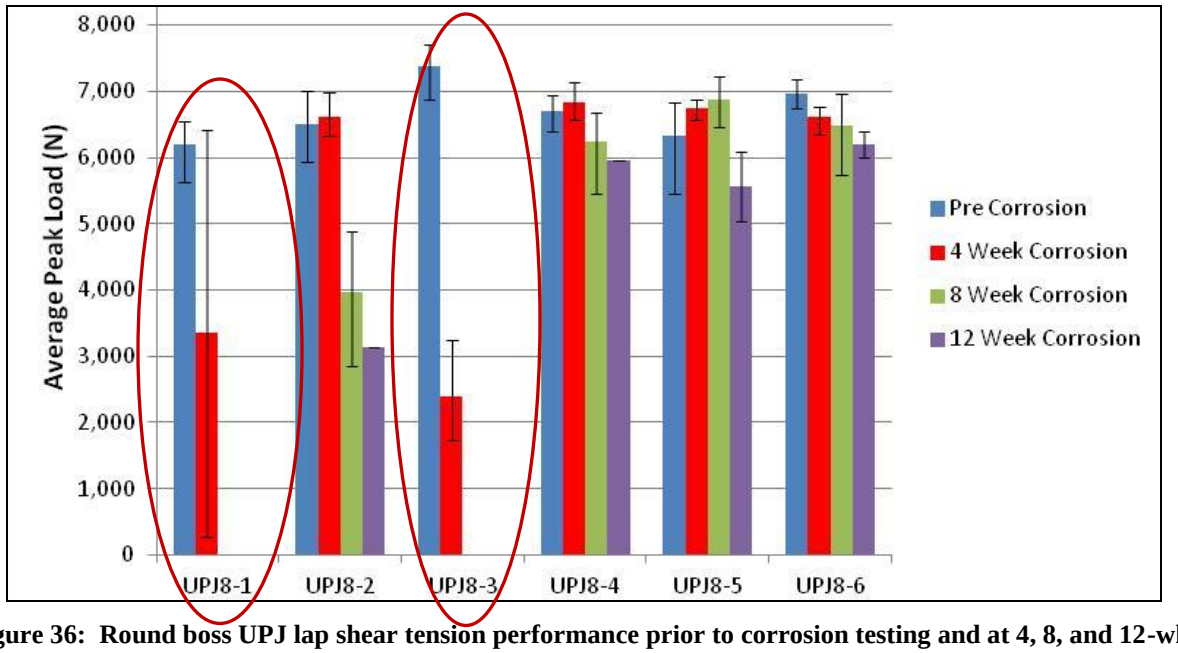

Figure 36: Round boss UPJ lap shear tension performance prior to corrosion testing and at 4, 8, and 12-wks exposure

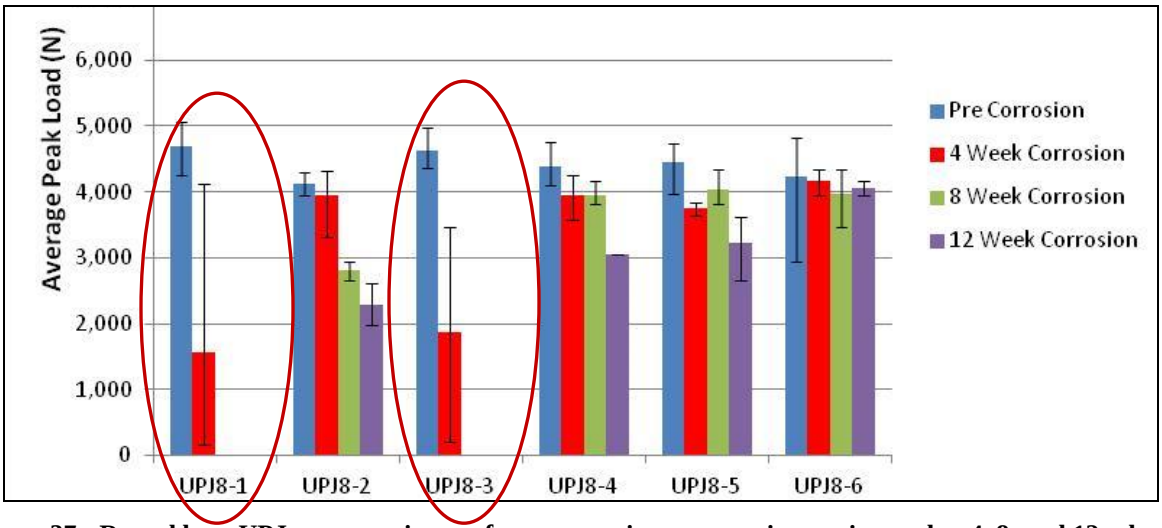

Figure 37: Round boss UPJ cross tension performance prior to corrosion testing and at 4, 8, and 12-wks exposure

Photos of Mg-Al 8-wk lap shear and cross tension samples are shown in Figures 38 and 39 respectively. Note the extensive exfoliation of the Al coupon on the UPJ8-2 joints in Figures 38 and 39. In Figure 38, the Al is shown at the bottom of each photo. In Figure 39, the Al is shown on the left side of each photo.

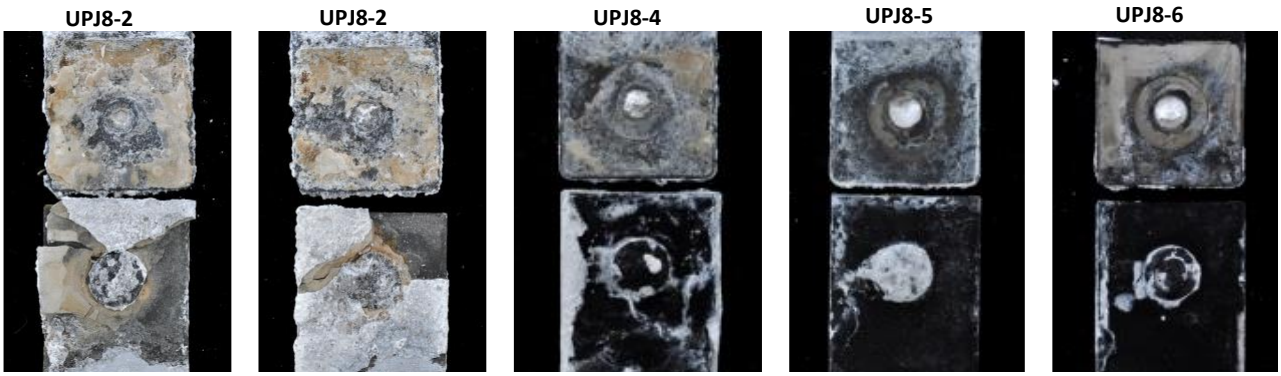

Figure 38: Round boss UPJ samples after 8-wks of accelerated corrosion exposure and lap shear tensile testing

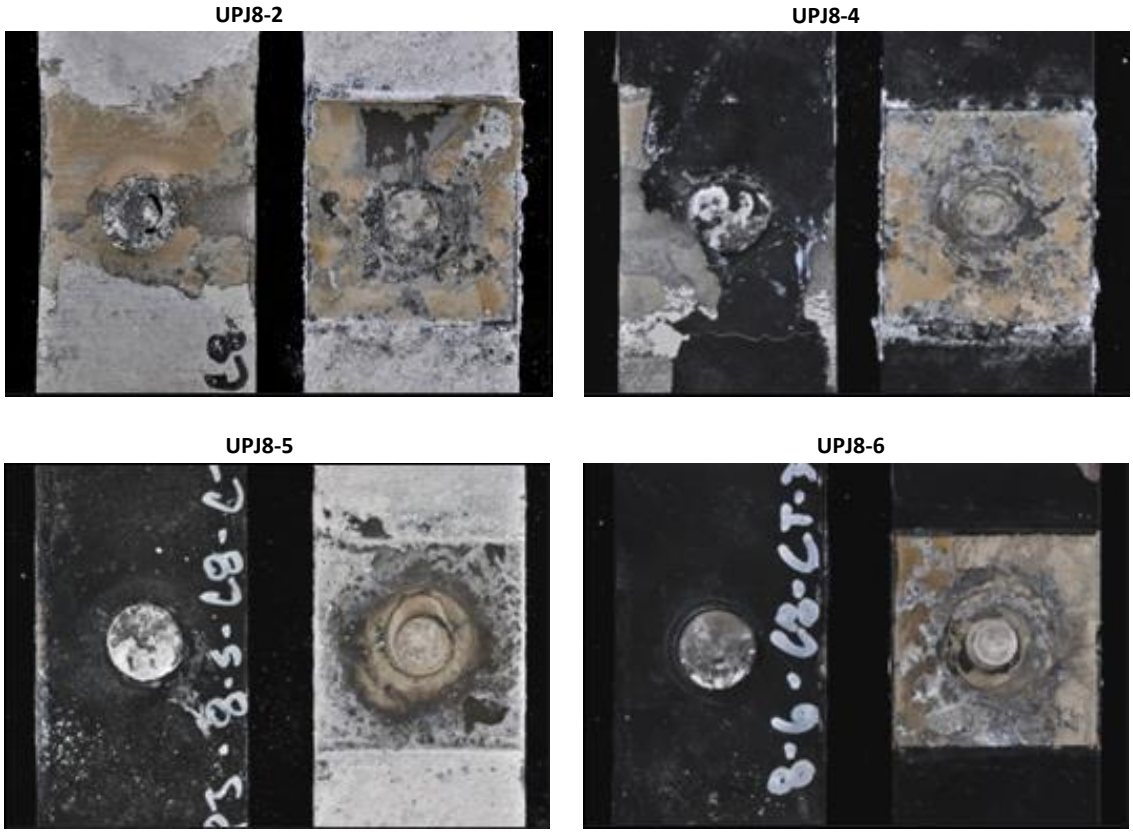

Figure 39: Round boss UPJ samples after 8-wks of accelerated corrosion exposure and cross tension testing

Photos of all 8-mm diameter round boss post-test lap shear and cross tension samples are shown in Figures 40 and 41. There are no photos shown for 8-wks and 12-wks for UPJ8-1 and UPJ8-3 because there were no samples left to evaluate since none of those samples remained intact after corrosion testing beyond 6-wks. In Figure 40, the aluminum sheet (or steel in the case of 8-1 and 8-3) is shown on the bottom of each photo. In Figure 41, the Al sheet is shown on the left side of each photo.

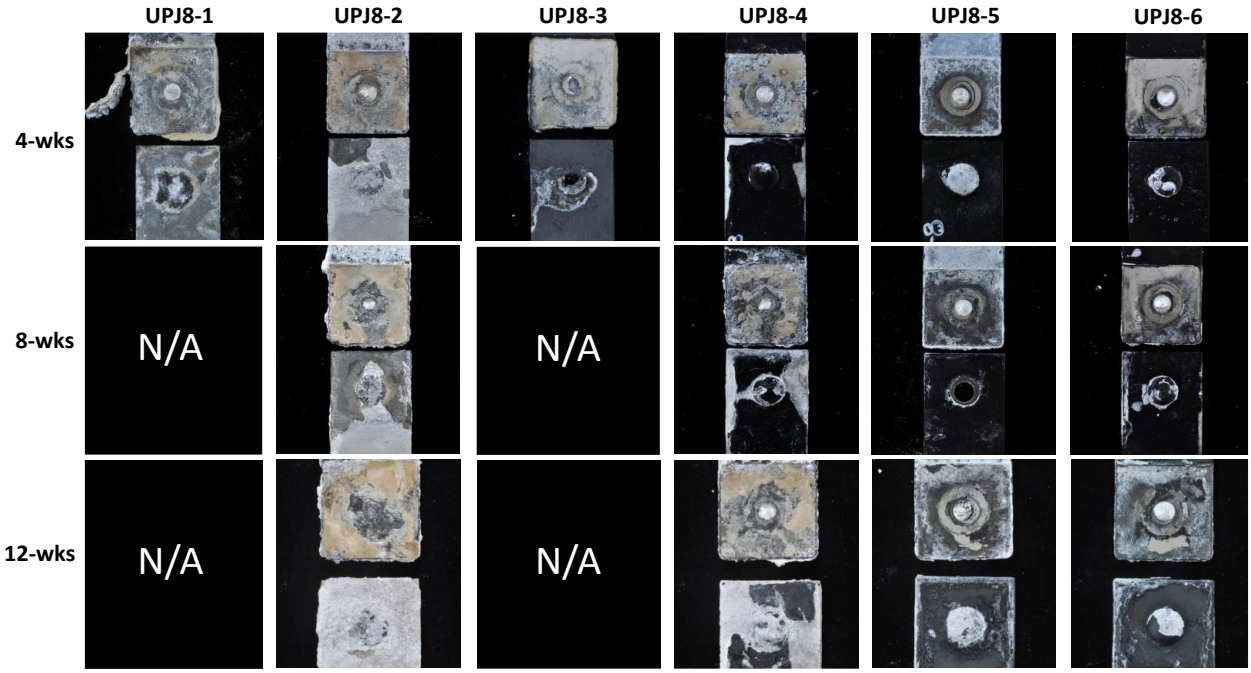

Figure 40: Round boss UPJ samples after 4-wks, 8-wks, and 12-wks of accelerated corrosion exposure and lap shear tension testing

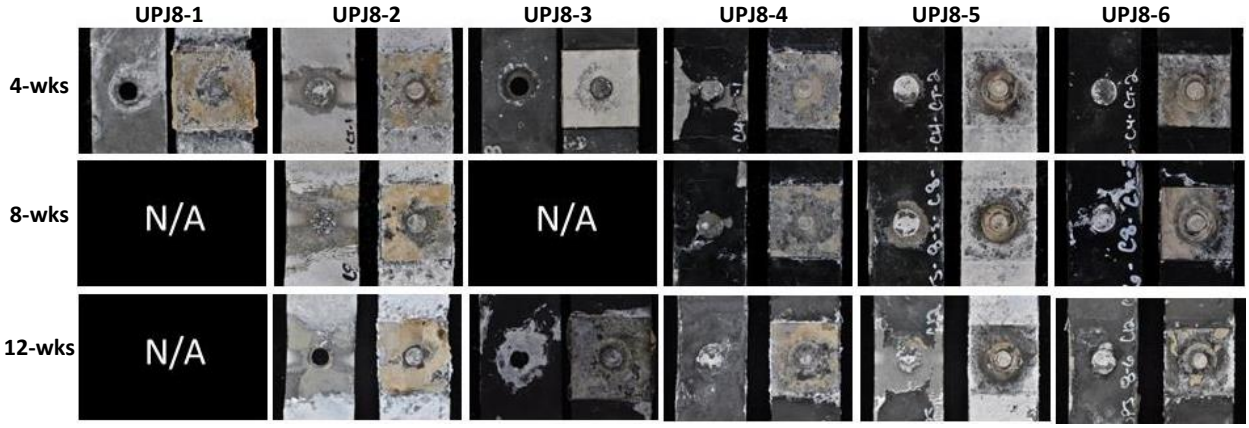

Figure 41: Round boss UPJ samples after 4-wks, 8-wks, and 12-wks of accelerated corrosion exposure and cross tension testing

The ***impact lap shear tension*** test results for configurations UPJ8-2 and UPJ8-4 are shown in Figure 42 prior to corrosion testing and after 12-wks of accelerated corrosion exposure (left) and the failure mode for UPJ8-4 after corrosion is shown in Figure 42 (right). This sample failed through shearing of the protrusion. It should be noted that, although there is not a substantial drop in impact performance after corrosion exposure, the data ***range*** for the results has increased substantially.

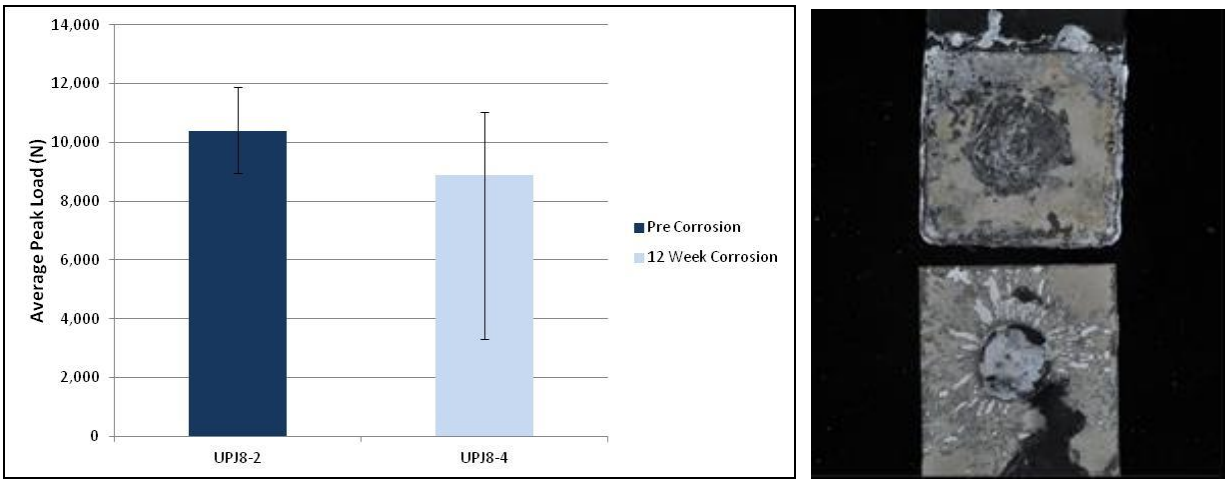

Figure 42: 8-mm round boss UPJ lap shear tension impact performance prior to corrosion testing and at 12-wks exposure (left) and failure mode after corrosion testing (right)

The ***impact cross tension*** test results for configurations UPJ8-1, UPJ8-2, UPJ8-3, and UPJ8-5 are shown in Figure 43 prior to corrosion testing and after 12-wks of accelerated corrosion exposure. The failure modes for UPJ8-3 and UPJ8-5 after corrosion are shown in Figure 44. These samples failed through partial thickness protrusion pull-out, head of protrusion fracturing, and base of protrusion fracturing.

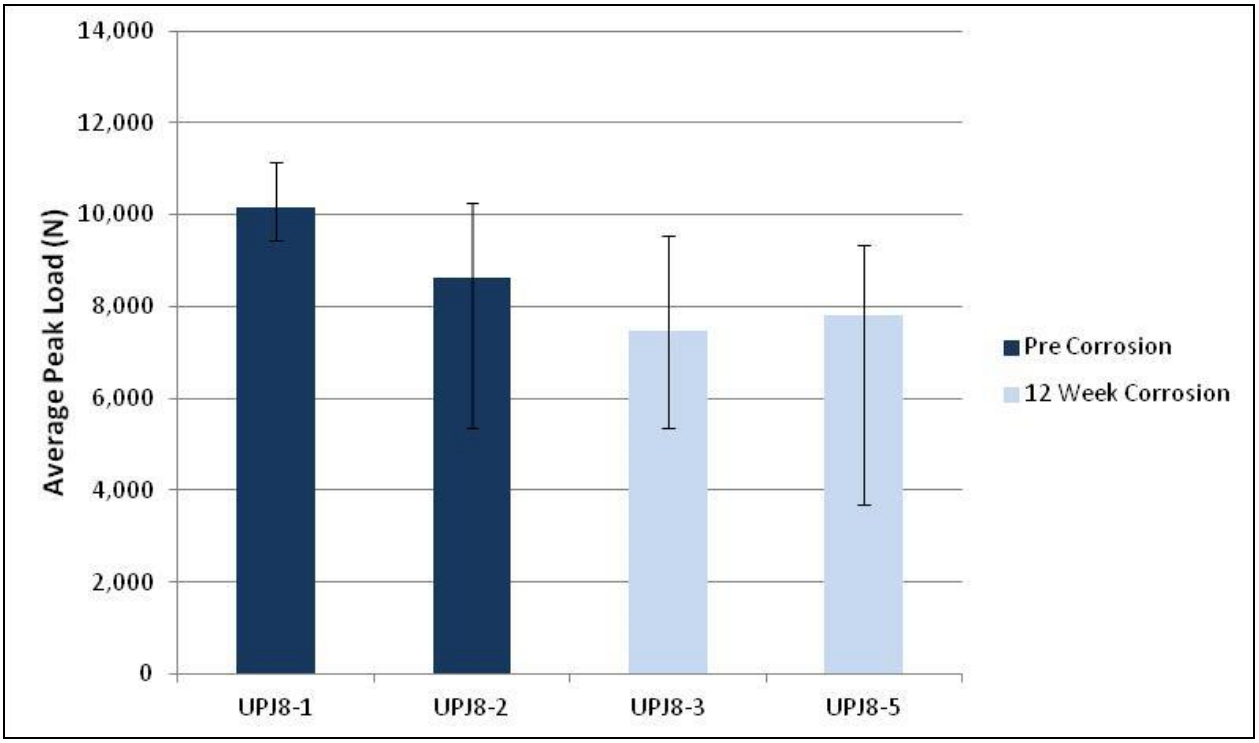

Figure 43: 8-mm round boss UPJ cross tension impact performance prior to corrosion testing and at 12-wks exposure

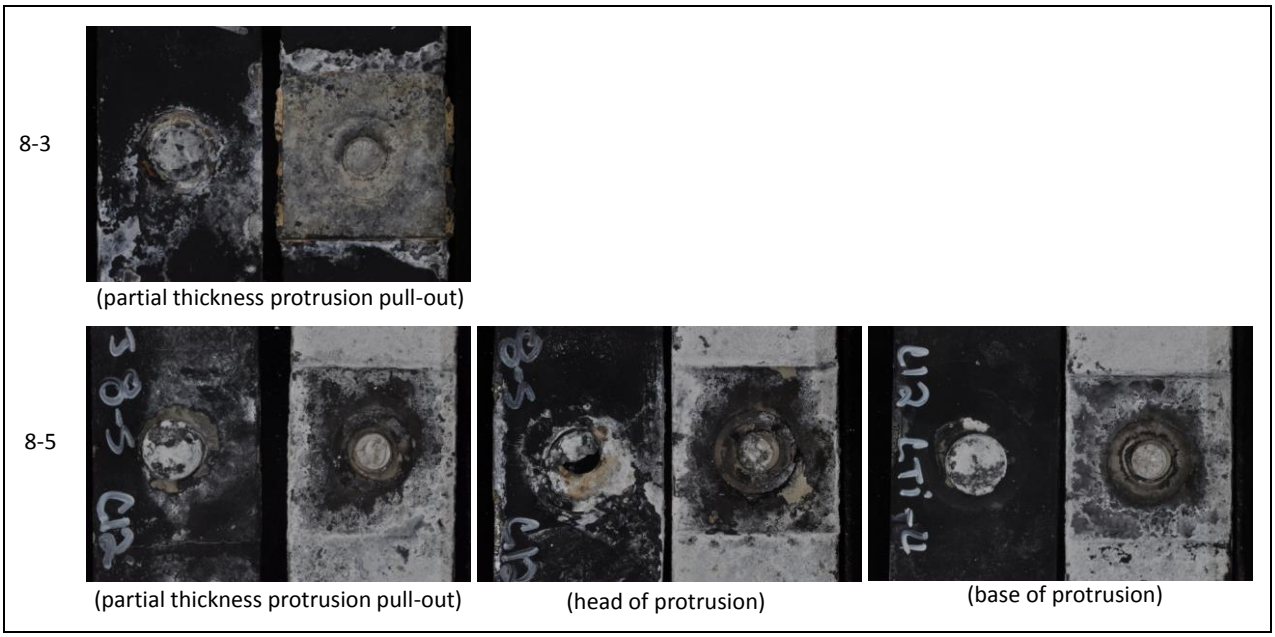

Figure 44: 8-mm round boss UPJ impact cross tension samples at 12-wks exposure

Lap-shear tension fatigue results prior to corrosion and after 12-wks corrosion exposure are shown in Figure 45. It is interesting to note that, for lap shear tension fatigue, the post corrosion samples (shown in purple) failed at lower levels than the pre-corrosion samples in low cycle fatigue, but not at high cycle fatigue.

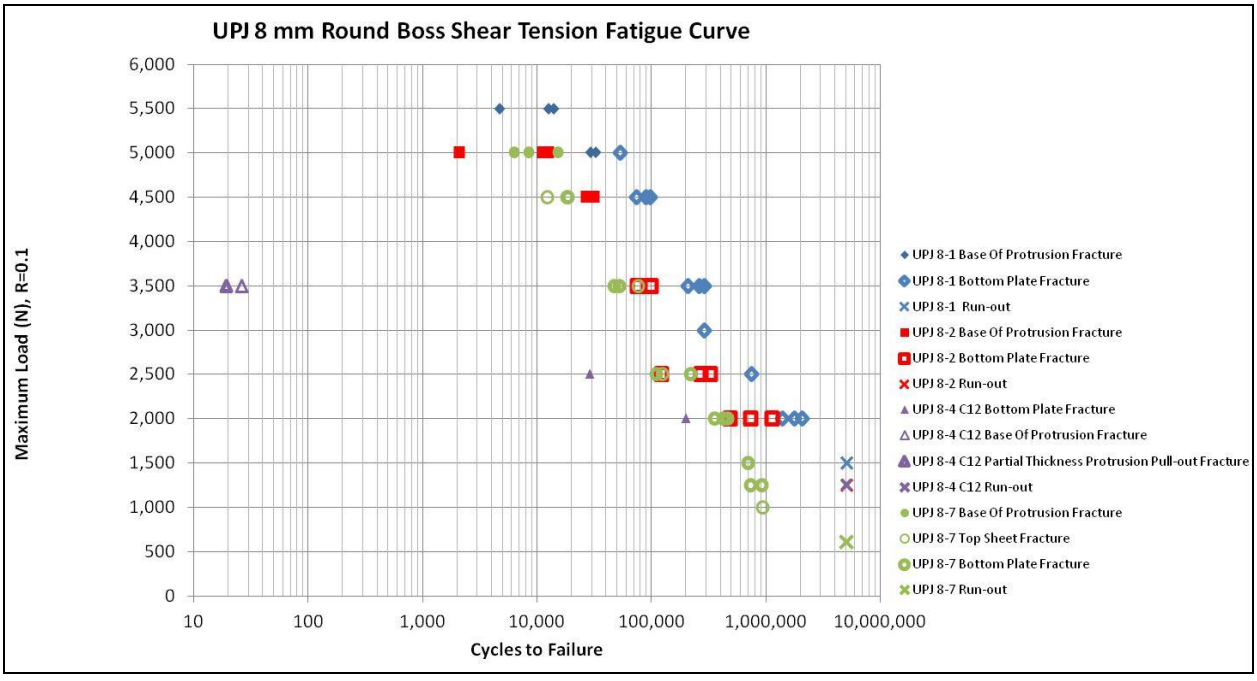

Figure 45: Comparison of round boss UPJ lap-shear tension fatigue performance prior to corrosion testing and at 12-wks exposure

Cross tension fatigue results are shown in Figure 46. For cross tension fatigue, the post corrosion samples (again shown in purple) failed at dramatically higher levels (2-3 times higher) than the pre-corrosion samples in high cycle fatigue. This was completely unexpected, and the reason for this increase remains unclear, especially since the observed failure mode (shown in Figure 47) matched that of the pre-corrosion samples.

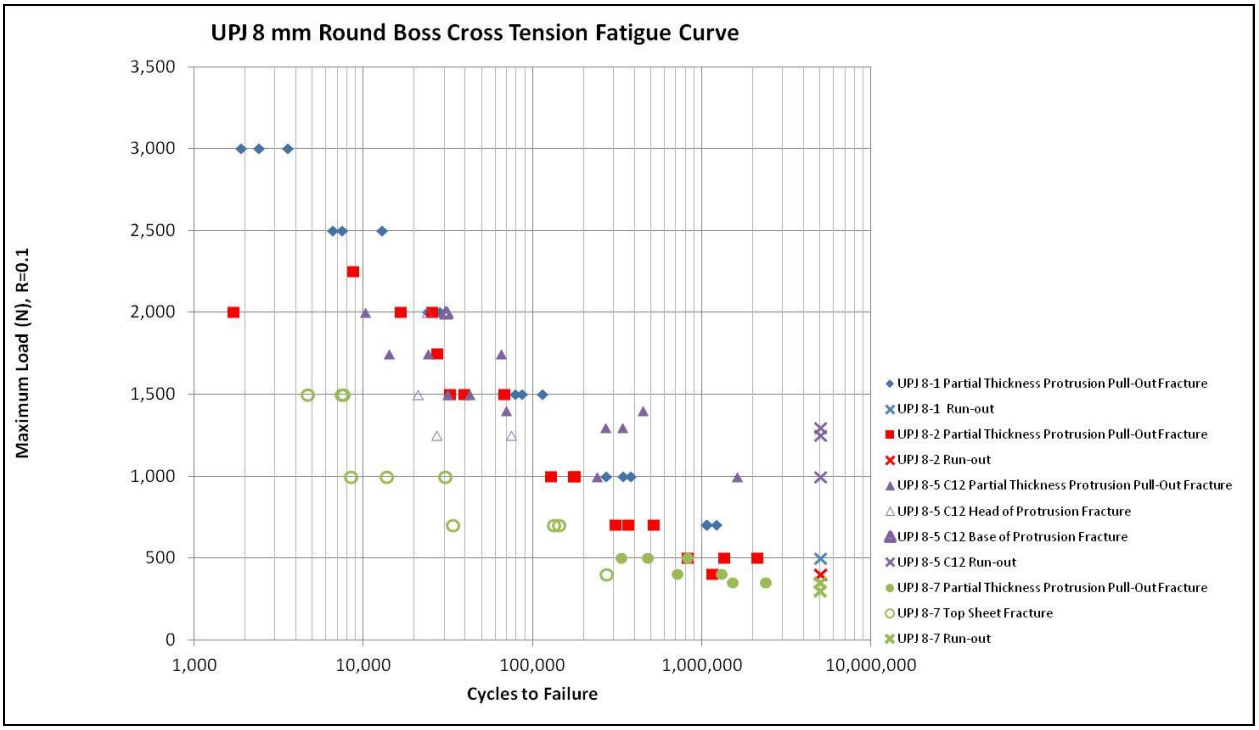

Figure 46: Comparison of round boss UPJ cross tension performance prior to corrosion testing and at 12-wks exposure

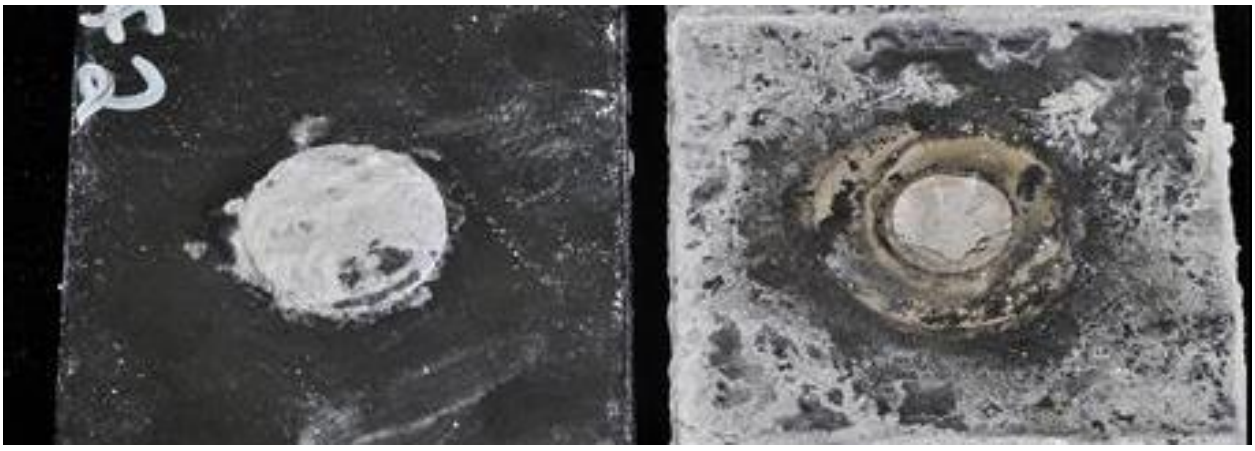

Figure 47: Failure mode for UPJ8-5 post corrosion high cycle fatigue sample

One possible explanation considered for the performance discrepancy is the fact that the post corrosion samples (UPJ8-5, pretreated Mg to coated Al) were from a different coating configuration than the pre-corrosion samples (UPJ8-2, bare Mg to bare Al. In the original test matrix, the UPJ8-2 configuration was intended to be evaluated both before and after corrosion exposure. This would have allowed for comparing the effect of corrosion exposure on fatigue performance of the UPJ8-2 configuration, and additional

post-corrosion testing of the UPJ8-5 configuration would have identified if there was any impact as a result of the coatings. However, since none of the UPJ8-2 samples remained intact at the end of the 12-wk corrosion exposure, a direct comparison was not possible.

Since the post corrosion samples were coated, they were exposed to a different set of processing parameters (force, time, heat) than the pre-corrosion samples. Because of the higher contact resistance of the coated samples, the actual forming process has to be conducted at a slower rate. This slower heating rate could have had an advantageous effect on the microstructure of the boss. To evaluate this theory, microstructures and micro-hardness of both configurations were evaluated prior to corrosion exposure.

Figure 48 shows the microstructure (left) and micro-hardness (right) of UPJ8-2 while Figure 49 shows the microstructure (left) and micro-hardness (right) of UPJ8-5. While there is clearly a difference in the micro-hardness maps of these two configurations, the actual numerical difference in micro-hardness is not large, so it is still not completely clear if this is the source of the unexpectedly high fatigue corrosion performance for the UPJ8-5 configuration.

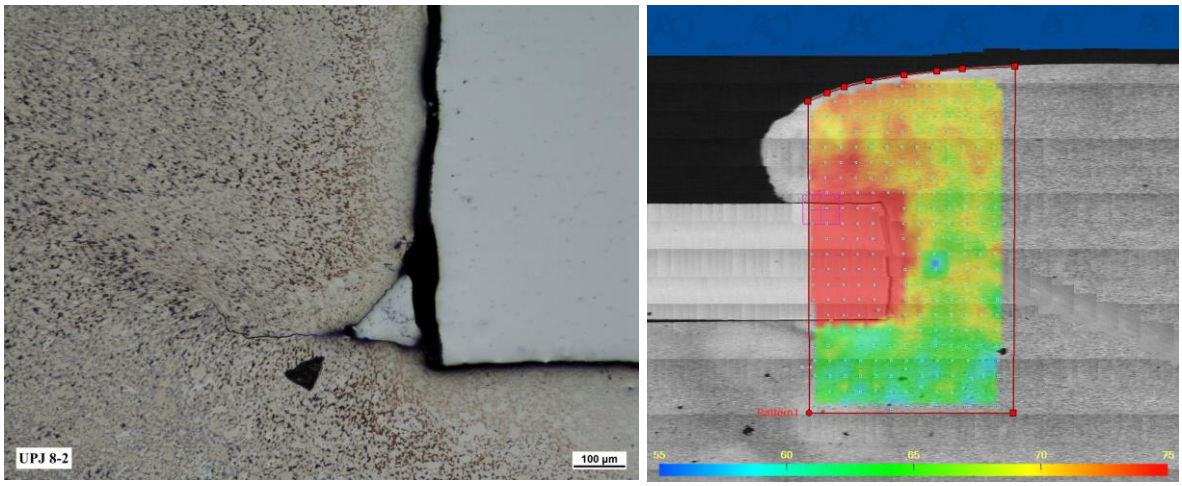

Figure 48: UPJ8-2 pre-corrosion microstructures (left) and micro-hardness maps (right)

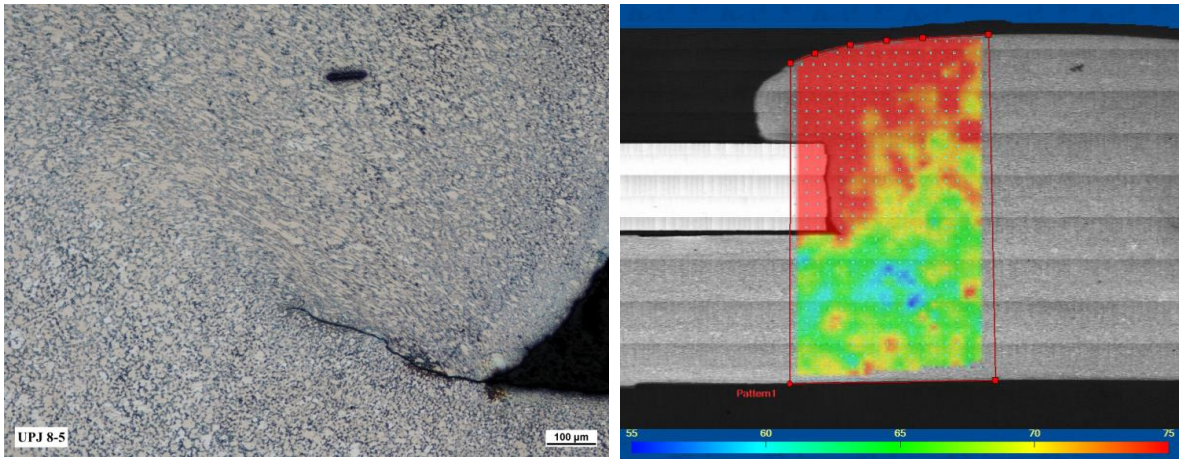

Figure 49: UPJ8-5 post-corrosion microstructures (left) and micro-hardness maps (right)

Since the microstructure and micro-hardness evaluations were inconclusive, and the UPJ8-2 configuration would not survive the 12-wk corrosion exposure, then additional UPJ8-5 samples were prepared and sub-

jected to fatigue testing without being subjected to a corrosion test. This would at least provide a direct comparison of pre- and post-corrosion fatigue performance of the same coating configuration and clarify if there was any difference in fatigue performance as a result of the coatings or process parameters. As can be seen in Figure 50, there does not appear to be any significant difference in the pre-corrosion fatigue performance of the coated UPJ8-5 (denoted by the dark blue triangles and x's) and uncoated UPJ8-2 (denoted by the light blue diamonds, squares, and x's) configurations. This would appear to indicate that the substantial increase in post-corrosion fatigue performance of the UPJ8-5 configuration compared to the pre-corrosion performance is indeed a result of the corrosion exposure, although the reason for this is still unclear.

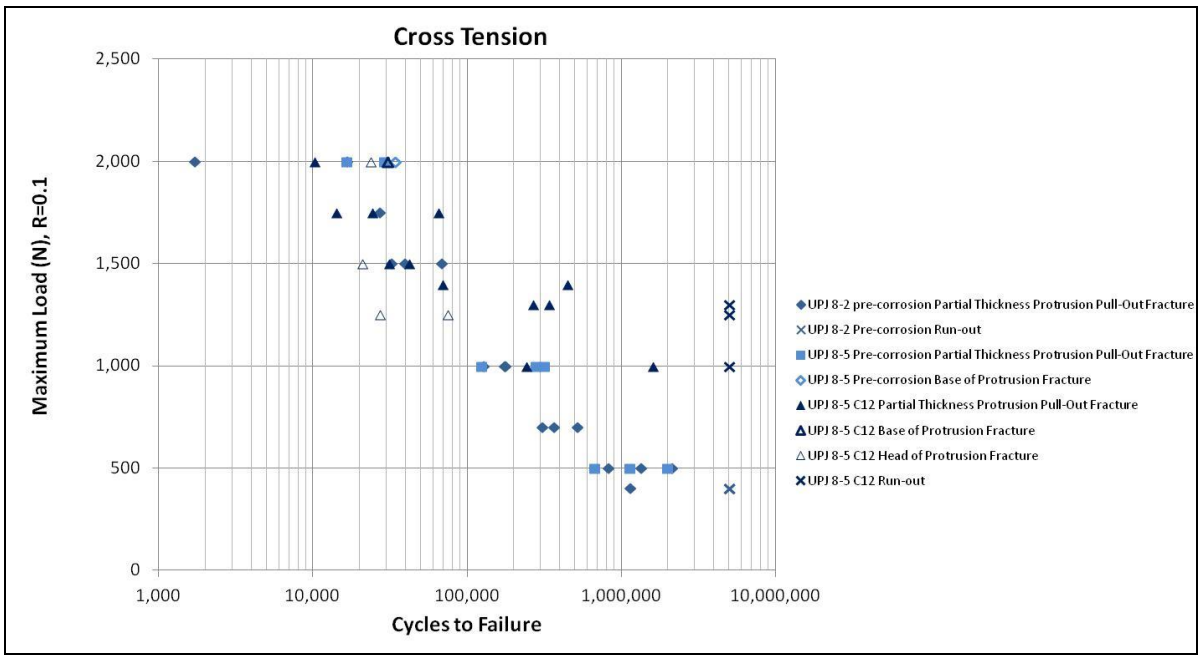

Figure 50: 8-mm round boss UPJ cross tension fatigue test results prior to corrosion testing and after 12-wks exposure

8.0-mm Round boss UPJ vs SPR Performance Comparisons

In order to accommodate direct comparison of initial mechanical/structural performance of UPJ joints to the baseline SPR tests, all of the test results for the round boss UPJ examples presented in this section of the report are shown immediately to the right of the comparable SPR test results.

Comparisons of quasi-static lap shear tensile test and cross-tension test results for round boss UPJ joints and benchmark SPR joints are shown in Figures 51 and 52 prior to corrosion, and after 4-wks, 8-wks, and 12-wks of accelerated corrosion exposure. The benchmark SPR data was presented earlier in the report but is repeated here to facilitate a direct comparison of the round boss UPJ joints. When viewing these figures, note that UPJ8-2 and SPR1 are both bare Mg to bare Al joints; UPJ8-4 and SPR2 are pretreated Mg to pretreated Al with the whole assembly being powder-coated; UPJ8-5 and SPR3 are pretreated Mg to powder-coated Al; and finally UPJ8-6 and SPR4 are pretreated Mg to powder-coated Al with the whole assembly being powder-coated after assembly.

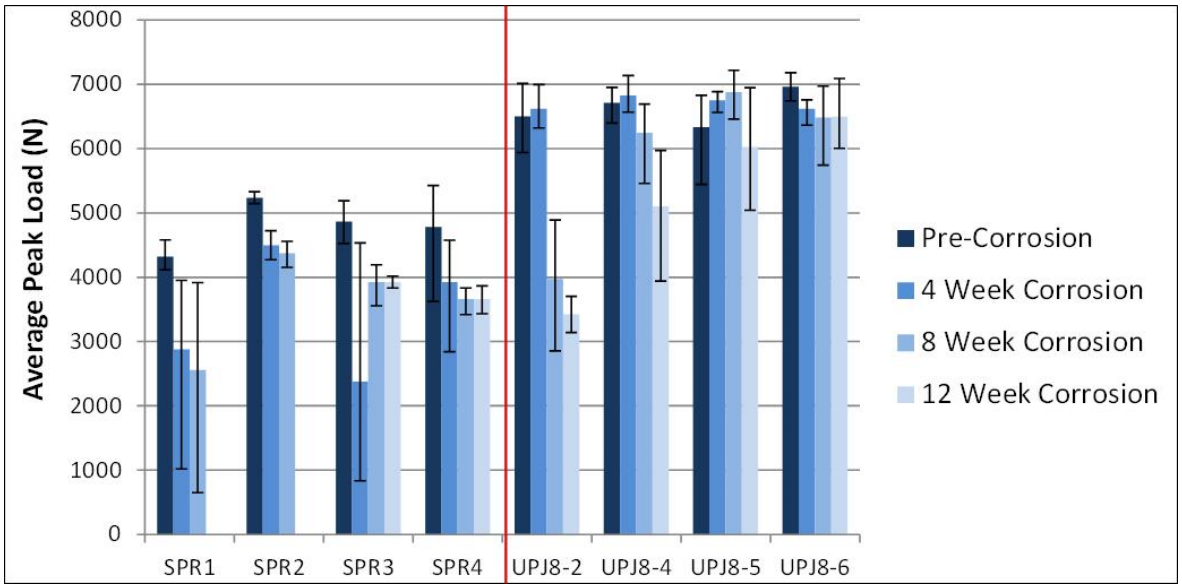

Figure 51: Comparison of round boss UPJ lap shear tension performance prior to corrosion testing and at 4, 8, and 12-wks exposure to performance of benchmark SPR joints

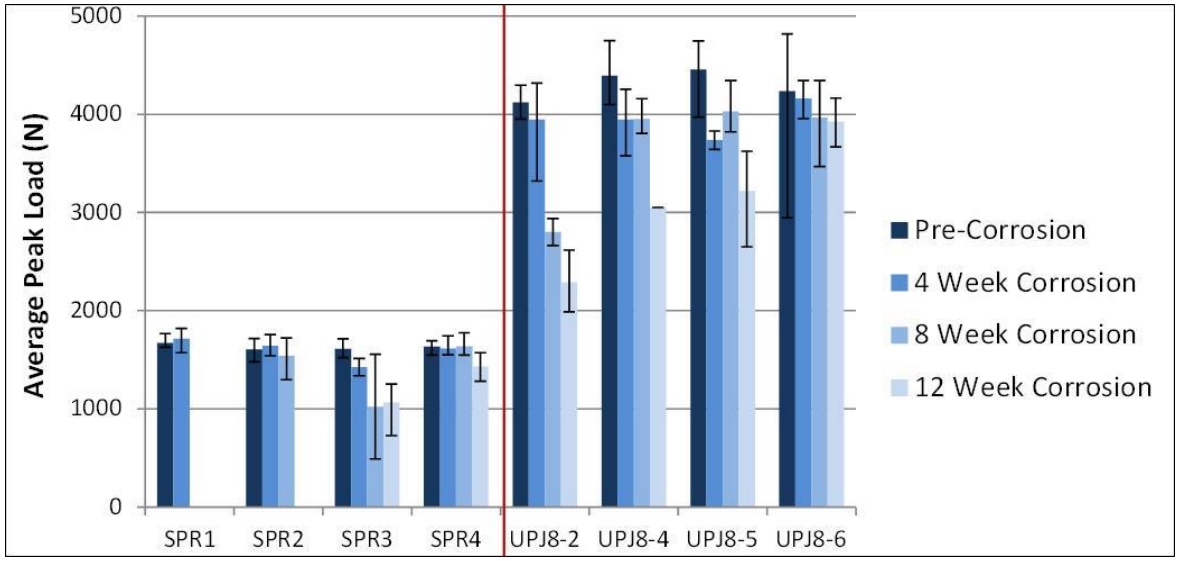

Figure 52: Comparison of round boss UPJ cross tension performance prior to corrosion testing and at 4, 8, and 12-wks exposure to performance of benchmark SPR joints

Although the UPJ joints exhibit substantially higher levels of strength across the board (~35-40% for lap shear tension and ~160-170% for cross-tension), primarily due to geometry where the UPJ bosses are larger diameter than the SPR rivets (increasing the lap shear strength) and have considerably larger heads (increasing the cross-tension strength), the real purpose of this comparison is to evaluate the effect of corrosion exposure on performance. It can be seen that both SPR and UPJ joints perform well when the Mg is pretreated and the Al is powder-coated (SPR3, SPR4, UPJ-5, and UPJ-6), although there were a couple of rivet fractures in the SPR3 configuration; the UPJ joints perform somewhat better than SPR when both Mg and Al are bare (SPR1 and UPJ8-2), although this can be misleading since there were multiple early separations in both SPR and UPJ for this configuration but there were more UPJ joints available; however, the configuration with the greatest improvement for UPJ over SPR is SPR2 and UPJ8-4, where both

the Mg and Al samples are pretreated and the assembly is powder-coated. In this configuration, there were multiple rivet fractures in the SPR joints resulting in no SPR samples surviving to 12-wks of exposure whereas only two UPJ joints separated before 12-wks of exposure.

Impact test results for round boss UPJ configurations UPJ8-2 (Mg to Al) and UPJ8-7 (Mg to Mg) are shown in Figure 53(b) and (d) while the comparable SPR joints for configuration SPR2 are shown to the left of these in Figure 53(a) and (c). Again, the pre-corrosion results for the UPJ joints are dramatically higher than those of the comparable SPR joints. The results here are similar to the quasi-static test results with the UPJ joints showing substantial improvements (~45%) over SPR for the shear tension tests and dramatic improvements (~150%) for the cross tension tests. The post corrosion results are not directly comparable since the SPR samples were tested after 8-wks while the UPJ samples were tested after 12-wks.

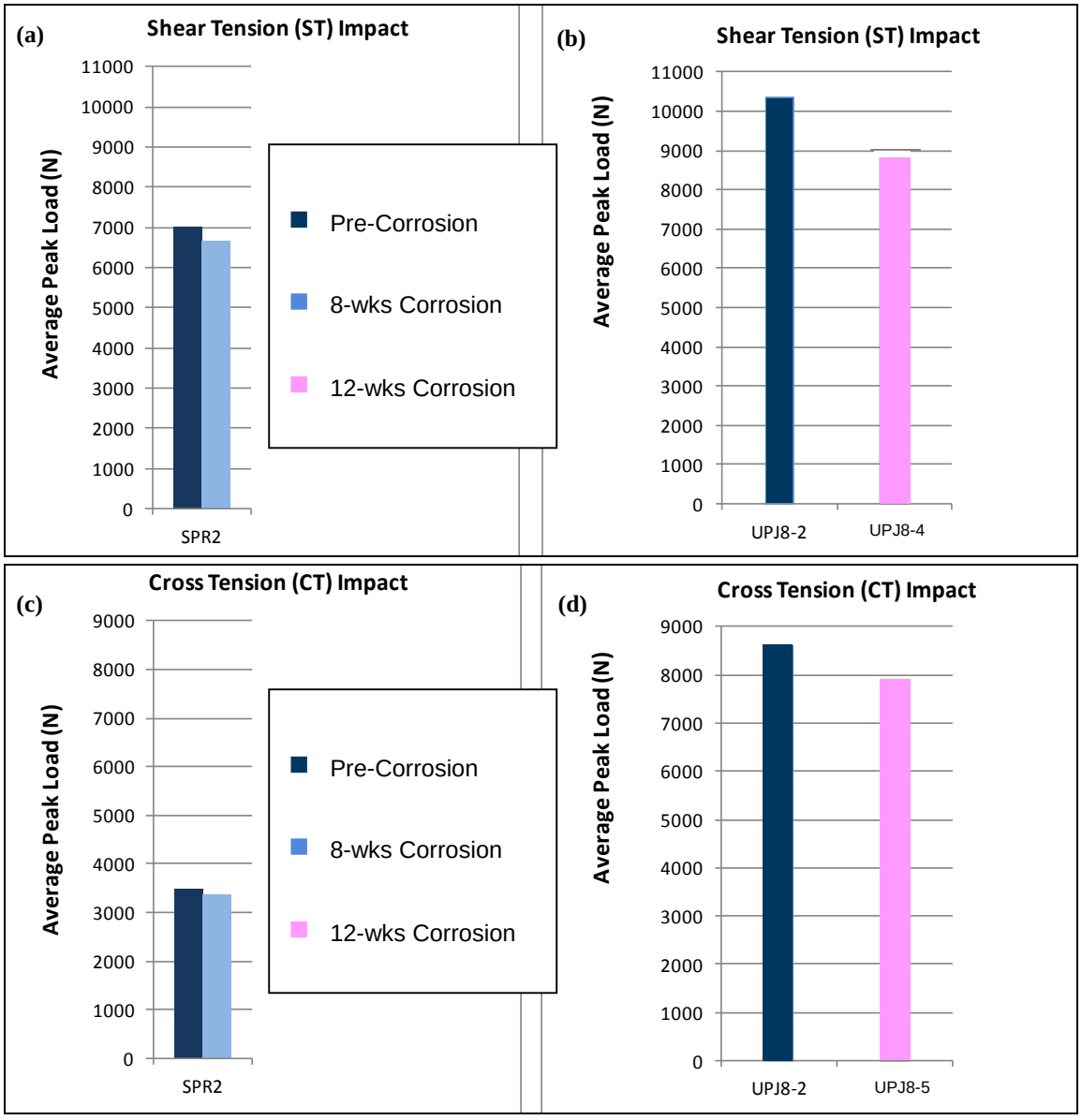

Figure 53: (a) Impact shear tension test results for SPR2; (b) impact shear tension test results for UPJ round boss joints; (c) impact cross-tension test results for SPR2; and (d) impact cross-tension for UPJ round boss joints

Shear tension fatigue performance test results comparing 8-mm diameter round boss UPJ joints to SPR joints are plotted in Figure 54 and cross tension fatigue performance test results are plotted in Figure 55. For the round boss UPJ joints shown in Figures 54(b) and 55(b), the blue points indicate results for the UPJ8-2 configuration (Al to Mg) while the red points indicate results for the UPJ8-7 (Mg to Mg) configuration. It is noteworthy that even though the low cycle fatigue results for the UPJ joints are substantially higher than for the SPR joints shown in Figures 54(a) and 55(a), there is very little difference in the high cycle fatigue results. As noted earlier in the report, observation of the failure modes shown in Figures 28(b) and 29(b) indicate that the high cycle fatigue results for the UPJ process may be influenced more by the properties of the Mg die castings than by the actual UPJ joint strength since the failures always occur in the Mg castings.

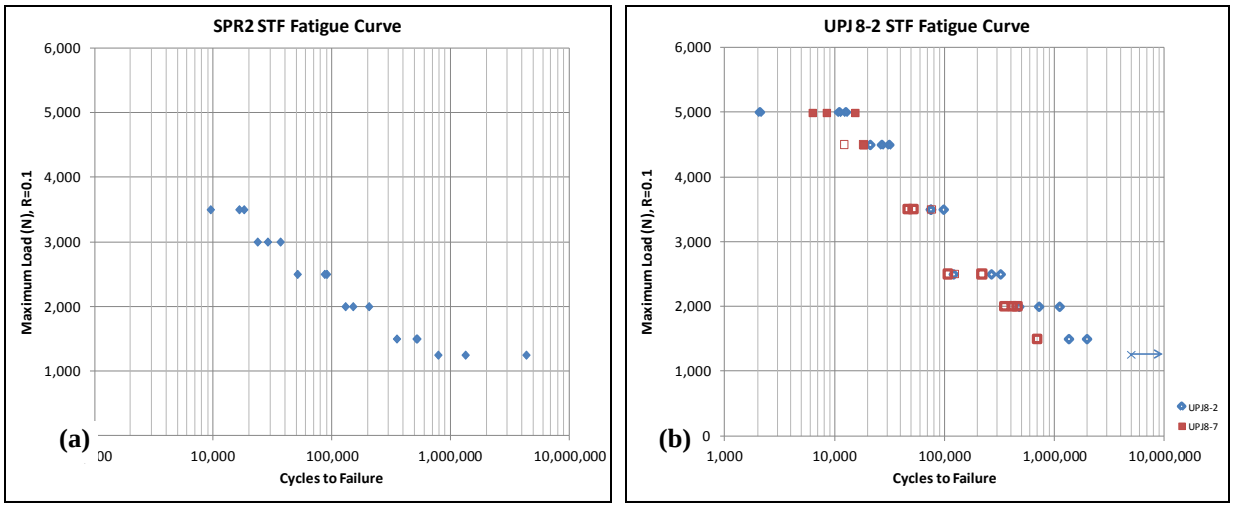

Figure 54: (a) Pre-corrosion shear tension fatigue test curves for SPR2 and (b) 8-mm diameter round boss UPJ joints of Mg to Al (blue points) and Mg to Mg (red points)

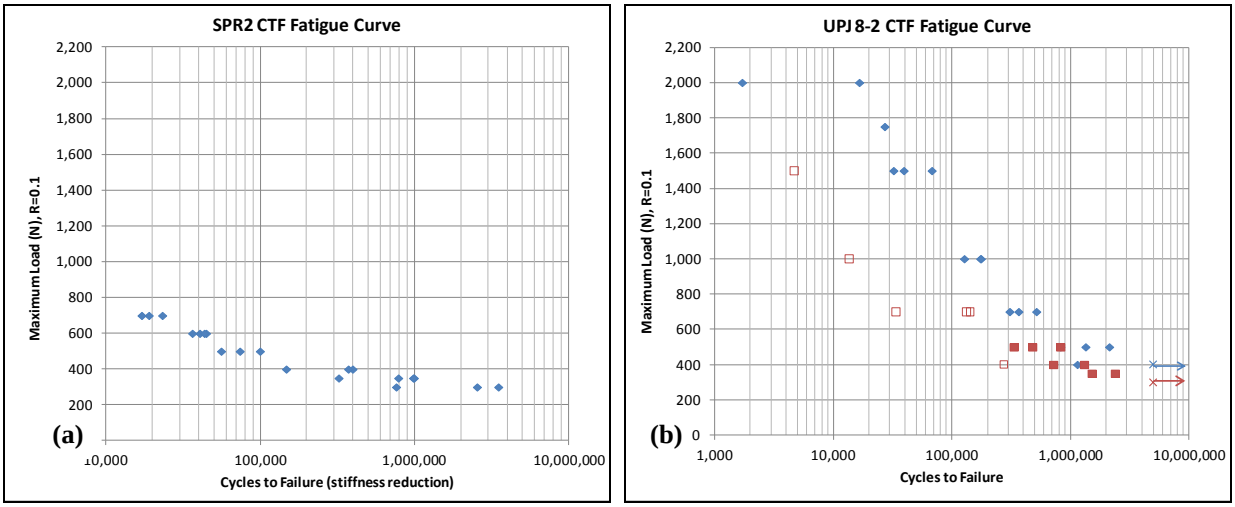

Figure 55: (a) Pre-corrosion cross tension fatigue test curves for SPR2 and (b) 8 mm diameter round boss UPJ joints of Mg to Al (blue points) and Mg to Mg (red points)

7.0-mm Round Boss UPJ Joint Development and Evaluation

The following section summarizes testing and evaluation of the ***7.0-mm*** diameter round boss joints. Note that for all 7-mm diameter round boss UPJ joints discussed in this section, the top sheet investigated is a 1.1 mm thick bake-hardenable Al6016-T43 alloy sheet.

Table 6 shows material and coating configurations investigated for 7-mm round boss UPJ joints. The configuration numbers shown in the left column will be used throughout the report to identify specific joint configurations.

Configuration Number	Upper Sheet			Bottom Sheet			Assembly Coating Configuration
	Material	Thickness (mm)	Coating	Material	Thickness (mm)	Coating	
UPJ7-1	Al6016-T43	1.1	Bare	Mg AM60B	4.0	Bare	Uncoated
UPJ7-2	Al6016-T43	1.1	Pretreated	Mg AM60B	4.0	Pretreated	Powdercoated
UPJ7-3	Al6016-T43	1.1	Powdercoated	Mg AM60B	4.0	Pretreated	Uncoated
UPJ7-4	Al6016-T43	1.1	Powdercoated	Mg AM60B	4.0	Pretreated	Powdercoated

Table 6: Round boss UPJ material and coating configurations

Figure 56 shows three examples of optimized round boss UPJ joints cross sections. Figure 56(a) shows a section through a bare Mg to bare Al joint (UPJ7-1) while Figure 56(b) shows a section through a pre-treated Mg to pretreated Al joint (UPJ7-2) and Figure 56(c) shows a section through a pretreated Mg to pretreated and coated Al joint (UPJ7-3 and UPJ7-4). There is no evidence of cracking or porosity in any of these joints. Furthermore, the head shapes are well formed with substantial overlap to the joined sheet material to help lock it into place and enable high cross-tension strength.

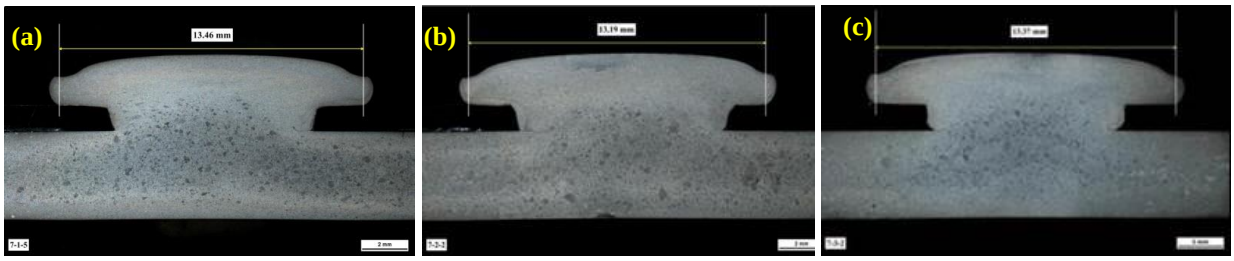

Figure 56: Metallurgical cross-sections of 7-mm round boss UPJ Mg-Al joints (a) UPJ7-1, (b) UPJ7-2, and (c) UPJ7-3, 4

Figure 57 shows head formations produced on 7-mm round boss Mg to Al joints in bare, pre-treated, and coated configurations. From these photos, it can be seen that fully-formed, crack-free head formations were produced in all desired coating configurations.

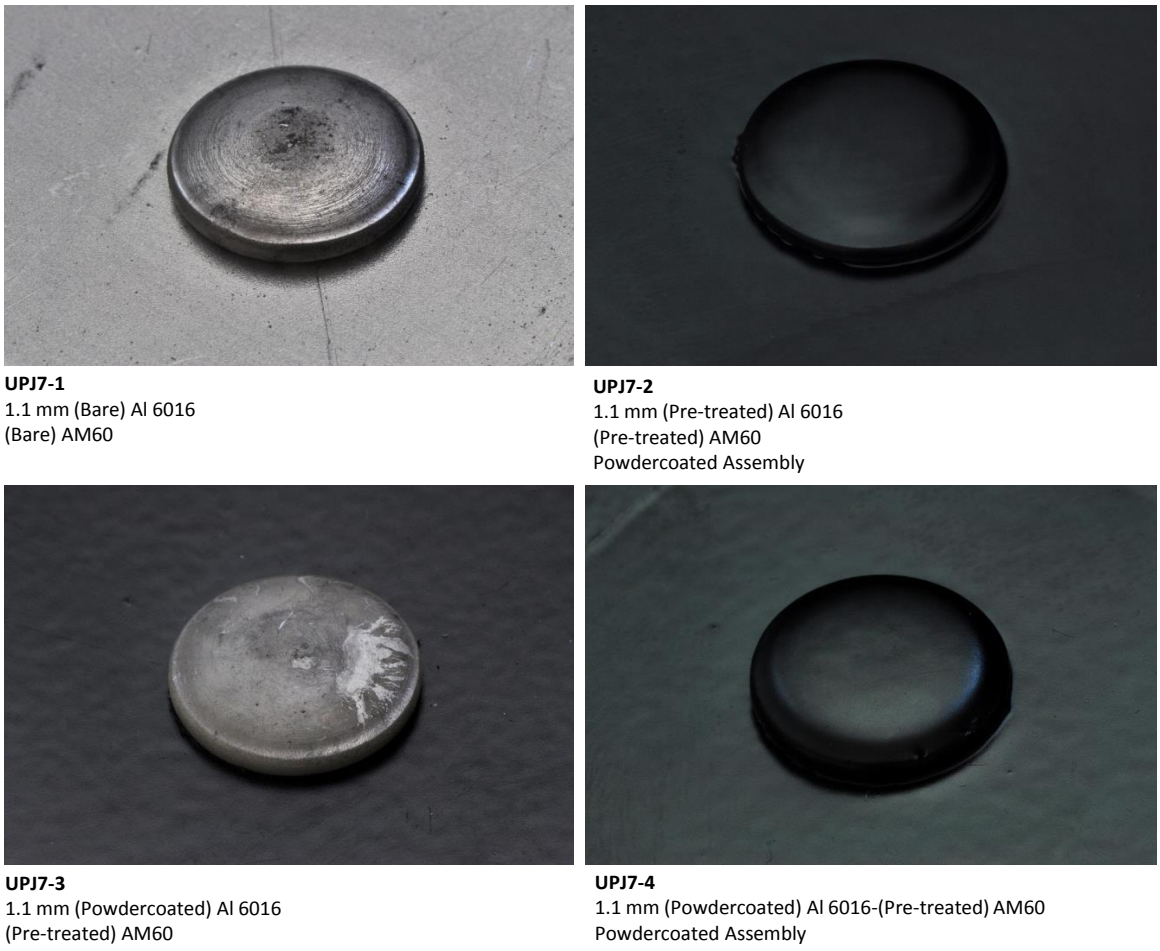

UPJ7-1
1.1 mm (Bare) Al 6016
(Bare) AM60

UPJ7-2
1.1 mm (Pre-treated) Al 6016
(Pre-treated) AM60
Powdercoated Assembly

UPJ7-3
1.1 mm (Powdercoated) Al 6016
(Pre-treated) AM60

UPJ7-4
1.1 mm (Powdercoated) Al 6016-(Pre-treated) AM60
Powdercoated Assembly

Figure 57: 7-mm round boss UPJ head formations

Initial (pre-corrosion) Mechanical/Structural Testing and Evaluation

Figure 58 shows quasi-static and impact ***shear*** tension test results for 7-mm diameter round boss UPJ joints. The substantial difference in joint strength between UPJ7-1 and the other configurations is that in all of the other configurations, the bake hardenable Al-6016 top sheet was powdercoated and baked afterwards, resulting in a substantial increase in the strength of this thin Al top sheet. In the case of these joints, since the Al-6016 top sheet is only 1.1 mm thick, then the primary failure mode for these joints is in the top sheet. Therefore, the bake hardening of this top sheet produces a substantial improvement in the joint strength.

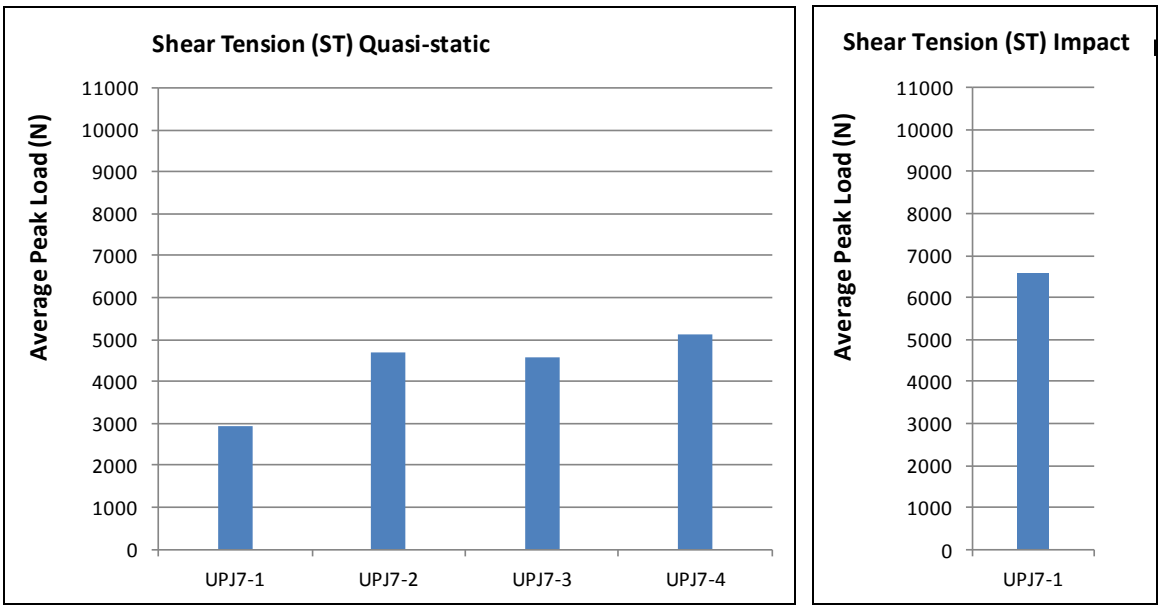

Figure 58: 7-mm round boss UPJ Quasi-static (left) and Impact (right) Shear Tension (ST) joint strength performance

Figure 59 shows ***cross*** tension test results for 7-mm diameter round boss UPJ joints. These joints included 1.1 mm Al-6016 top sheets and 7-mm diameter round bosses. Unlike the shear tension tests, in the case of the cross tension tests, the joint strength of UPJ7-1 was essentially equivalent to that of the other joints. The failure of the cross tension joints for these thin Al-6016 top sheets is a result of the top sheet bending around the head of the protrusion and then ultimately tearing around the head of the protrusion. It is likely that the joint strength in this mode is as much related to the stiffness of the top sheet as to the yield strength. Since the bake hardening only affects the strength of the material and not the modulus, then the top sheet stiffness is not affected and therefore the joint strength is not affected.

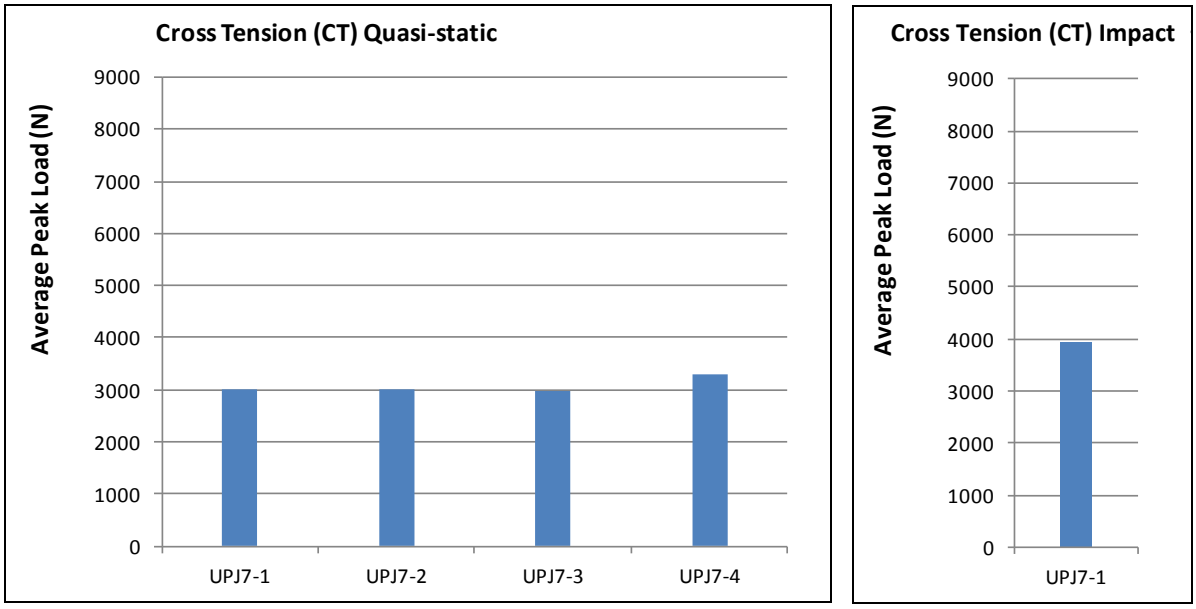

Figure 59: 7-mm round boss UPJ Quasi-static (left) and Impact (right) Cross Tension (CT) joint strength performance

Corrosion Testing and Evaluation

All 7-mm diameter round boss UPJ joint samples successfully completed the prescribed 12-wk FCA accelerated corrosion evaluation with no joint separations observed during the test. Figure 60 shows the results accelerated corrosion testing for Bare Mg AM60B to Bare Al 6016 lap shear tension test samples (UPJ7-1). Figure 61 shows similar results for pretreated Mg to pretreated Al joints with the powder-coating applied after assembly (UPJ7-2). Figure 62 shows results for pretreated Mg to powder-coated Al without any coating being applied after assembly (UPJ7-3). Figure 63 shows results for pretreated Mg to powder-coated Al with additional powder coating being applied after assembly (UPJ7-4).

The significantly improved results for these samples compared to the 8-mm round boss samples discussed in the previous section is primarily due to the lower copper content in the Al6016 alloy compared to the high copper content found in the higher strength Al6013 alloy. Copper is well known to be aggressive to Mg when exposed to an acidic environment and, as can be seen from the previous samples, also has a very detrimental effect on the inter-granular exfoliation corrosion of the aluminum sheet material as well.

Even though these configurations maintained good joint integrity throughout the testing, the substantial cosmetic corrosion and coating delamination (for a good example, note the blistering and peeling on UPJ7-4 shown in Figure 63) would likely preclude the use of any of these configurations in applications where appearance is critical. While the coating delamination is significantly worse on the Mg coupons, it is certainly obvious on the Al coupons as well.

Figure 60: UPJ7-1 bare Mg to bare Al lap shear tension test coupons before corrosion exposure (left) and after 12-wks of exposure (right)

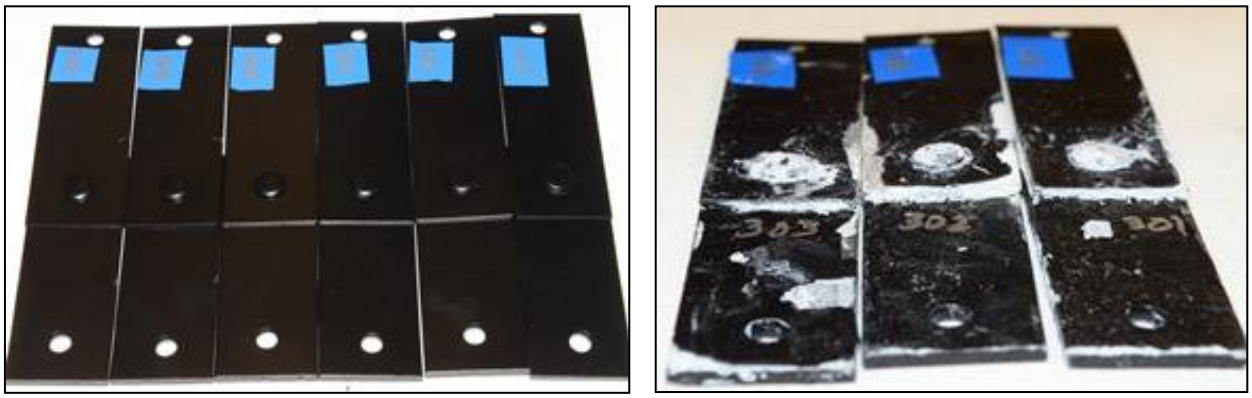

Figure 61: UPJ7-2 pretreated Mg to pretreated Al lap shear tension test coupons with powder coating applied after assembly, before corrosion exposure (left) and after 12-wks of exposure (right)

Figure 62: UPJ7-3 pretreated Mg to powder-coated Al lap shear tension test coupons, before corrosion exposure (left) and after 12-wks of exposure (right)

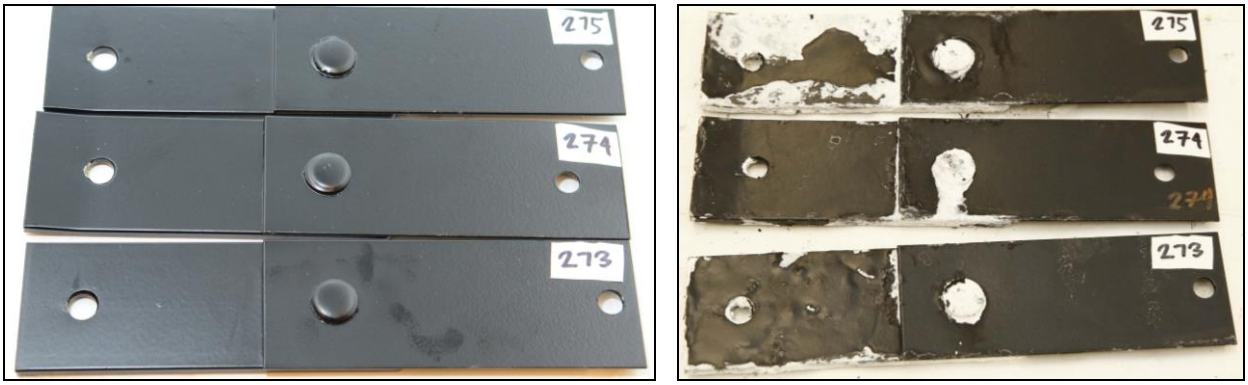

Figure 63: UPJ7-4 pretreated Mg to powder-coated Al lap shear tension test coupons with additional powder coating applied after assembly, before corrosion exposure (left) and after 12-wks of exposure (right)

Interestingly, while none of the cross tension samples separated during the 12-wk corrosion exposure, one sample from each coating configuration did experience substantial corrosion of the Mg coupons well away from the joint. Figure 64 shows some of the cross tension samples with damage to the Mg coupons. The reason for this is not immediately clear since: (a) none of the lap shear samples experienced the same type of damage, and (b) this particular type of damage was not observed in the previous corrosion testing with the Mg to Al 6013 or Mg to steel joints. The most likely culprit for this damage is that electrolyte was allowed to pool in the holding trays during the test, thereby creating excessive corrosion on the ends of the samples that were resting in the pooled electrolyte. In any case, it does not appear to be related to the joining process.

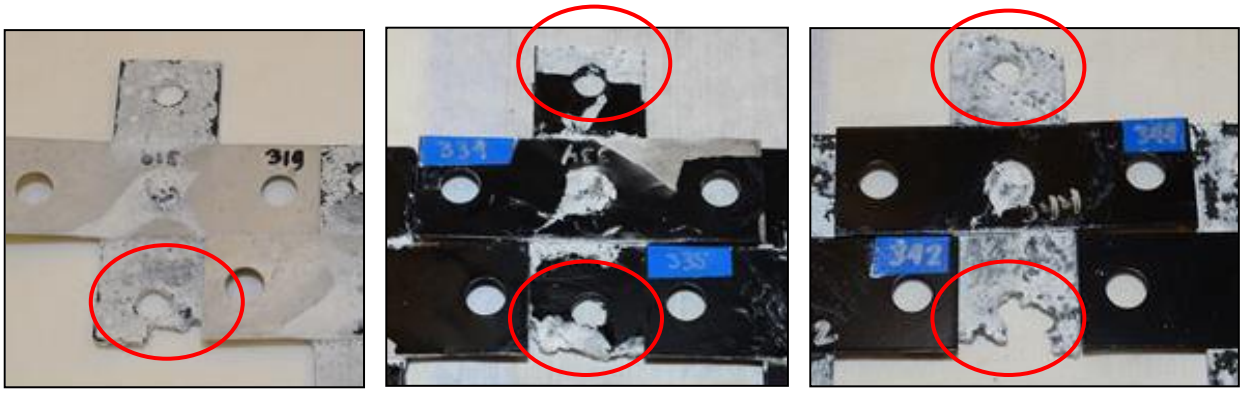

Figure 64: From left, UPJ7-1, 7-2, and 7-3 Mg to Al cross tension test coupons after 12-wks of exposure

Post Corrosion Mechanical/Structural Testing and Evaluation

The ***quasi-static lap shear tension*** results for all 7-mm round boss UPJ joints are shown in Figure 65 prior to corrosion testing and after 4-wks, 8-wks, and 12-wks of accelerated corrosion exposure. As discussed earlier, all of these configurations incorporate a 6016 alloy which has a lower level of copper than the 6013 alloy used in the 8-mm round boss UPJ Mg to Al configurations, so the general level of performance degradation (especially related to exfoliation corrosion) after corrosion exposure is expected to be less. It should also be noted that the aluminum panel in this configuration is only 1.1 mm thick so the overall strength levels in both lap shear tension testing and cross tension testing are lower than the 8-mm round boss UPJ configurations.

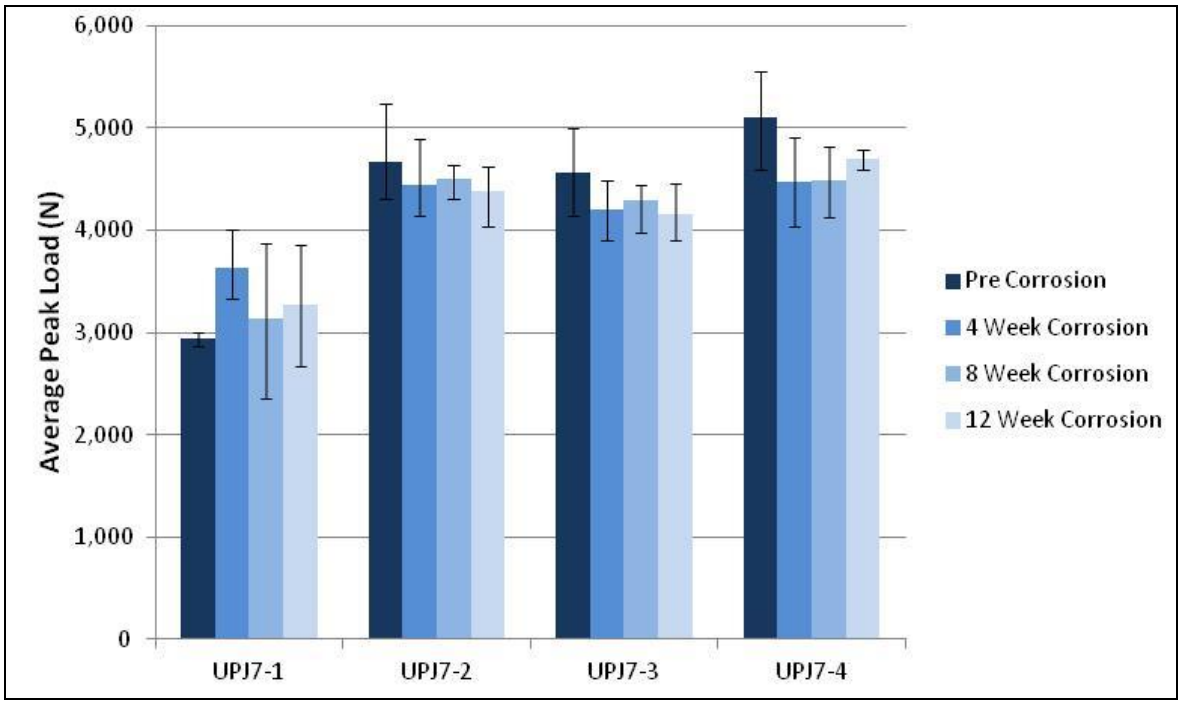

Figure 65: 7-mm round boss UPJ quasi-static lap shear tension performance prior to corrosion testing, at 4-wks, 8-wks, and 12-wks accelerated corrosion exposure

The failure modes for all four configurations through 12-wks of exposure are shown in Figure 66. The failures occur consistently by deformation and tearing in the thin 1.1 mm aluminum top sheet. In this figure, for each photograph, the aluminum sheet is shown on the bottom.

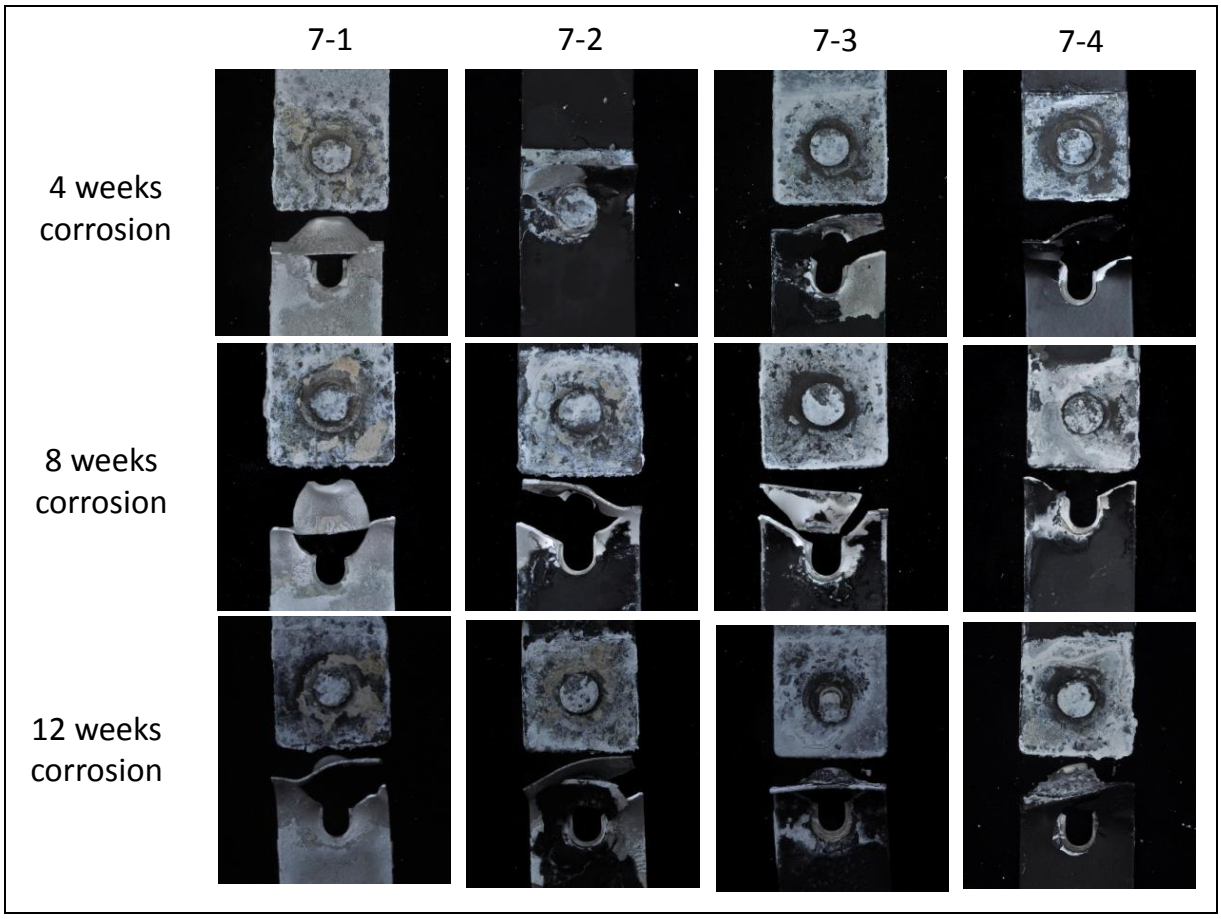

Figure 66: 7-mm round boss UPJ quasi-static lap shear tension performance failure modes after accelerated corrosion exposure

The ***quasi-static cross tension*** results for 7-mm round boss UPJ joints are shown in Figure 67 prior to corrosion testing and after 4-wks, 8-wks, and 12-wks of accelerated corrosion exposure.
Again, as in the case of the lap-shear tension testing, due to the lower level of copper in the Al-6016 coupons vs. the Al-6013 alloys evaluated with the 8-mm round boss UPJ joints, none of the joints separated during the accelerated corrosion testing, even the UPJ 7-1 configuration, which consists of bare Al joined to bare Mg with no pretreatments or coatings on either material.

Note, that unlike the lap-shear tension testing, in cross-tension testing, the UPJ7-1 configuration did not exhibit significantly lower joint strength than the other configurations. This is because in cross-tension, the joint strength is more dependent on the material stiffness than in lap-shear, so the additional strength gained through paint baking has less effect on the overall joint strength.

A more interesting observation is that the UPJ7-3 configuration displayed significantly better joint strength retention and consistency than the other configurations throughout the post-corrosion testing.

The failure modes for all four configurations through 8-wks of exposure are shown in Figure 68. The failure modes are primarily related to deformation in the thin 1.1 mm upper aluminum sheet, although UPJ7-3 failed by partial protrusion pull-out. While it can be seen that this was the only configuration that did not fail primarily through deformation in the clearance hole in the thin 1.1 mm upper aluminum sheet,

and this may explain the higher level of strength retention, it is not clear as to why this was the only configuration that failed in this manner. It may be that three samples of each configuration is not sufficient to compare some of the configurations. In this figure, for each photograph, the aluminum sheet is shown on the left.

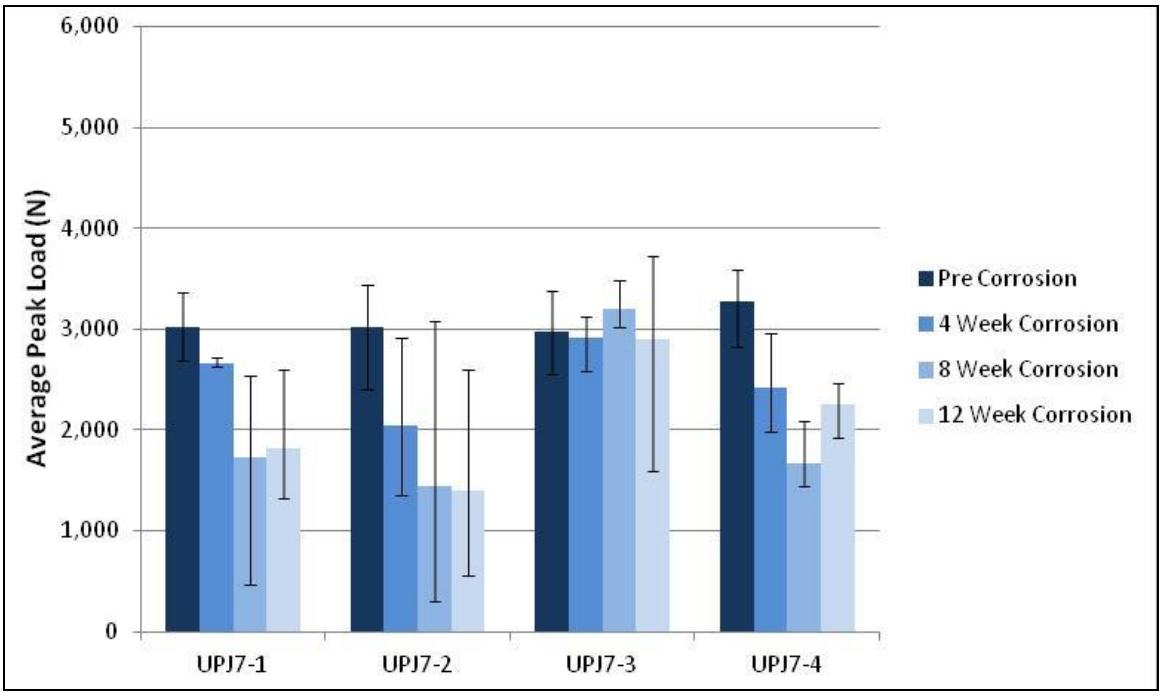

Figure 67: 7-mm round boss UPJ quasi-static cross tension performance prior to corrosion testing and at 4-wks, 8-wks, and 12-wks accelerated corrosion exposure

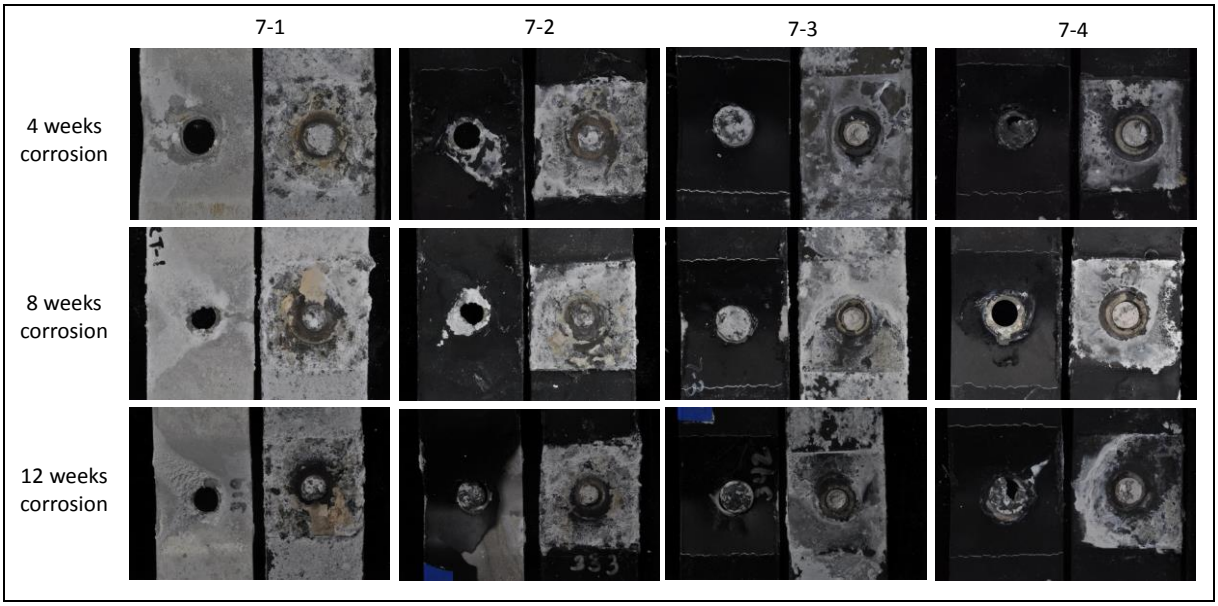

Figure 68: 7-mm round boss UPJ quasi-static cross tension performance failure modes after accelerated corrosion exposure. The aluminum sheet is shown on the left

The ***impact lap shear tension*** results for UPJ7-1 and UPJ7-4 are shown in Figure 69 prior to corrosion testing and after 12-wks of accelerated corrosion exposure. The failure modes are shown in Figure 70. Similar to the quasi-static testing, the failures occur consistently by deformation and tearing in the thin 1.1 mm aluminum top sheet. In this figure, for each photograph, the aluminum sheet is shown on the bottom.

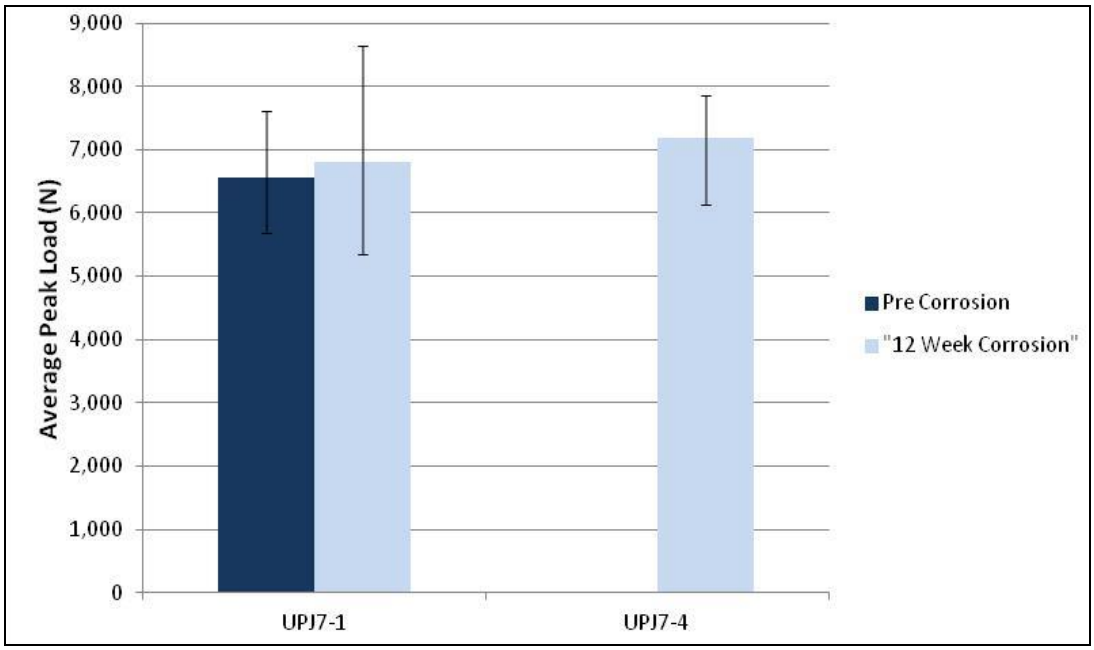

Figure 69: 7-mm round boss UPJ impact lap-shear tension samples prior to corrosion and after 12-wks

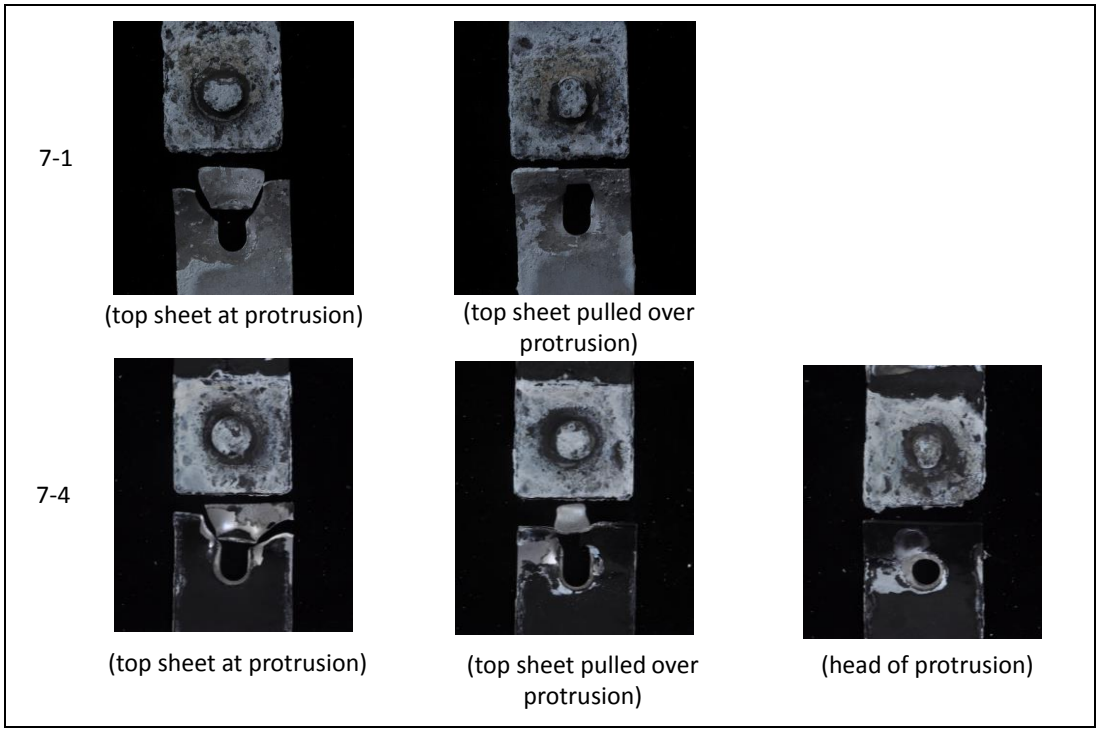

Figure 70: 7-mm round boss UPJ impact lap-shear tension performance failure modes after accelerated corrosion exposure. The aluminum sheet is shown on the bottom

The ***impact cross tension*** results for UPJ7-1 and UPJ7-4 are shown in Figure 71 prior to corrosion testing and after 12-wks of accelerated corrosion exposure. The failure modes are shown in Figure 72. Failures occurred by deformation in the thin 1.1 mm aluminum top sheet and by partial protrusion pull-out. In this figure, for each photograph, the aluminum sheet is shown on the left.

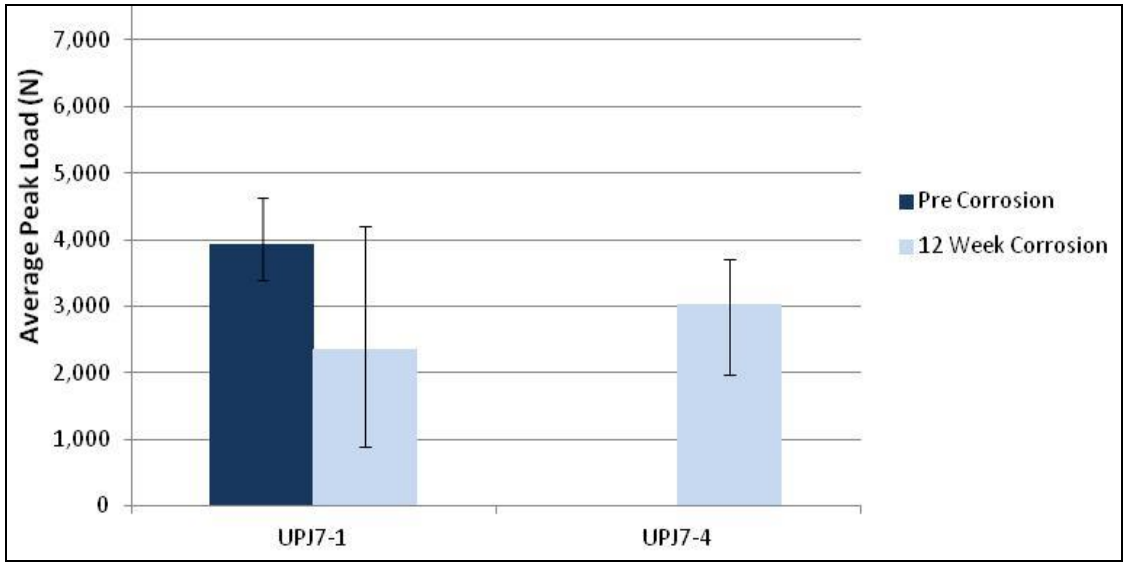

Figure 71: Comparison of round boss UPJ cross tension impact performance prior to corrosion testing and at 12-wks exposure

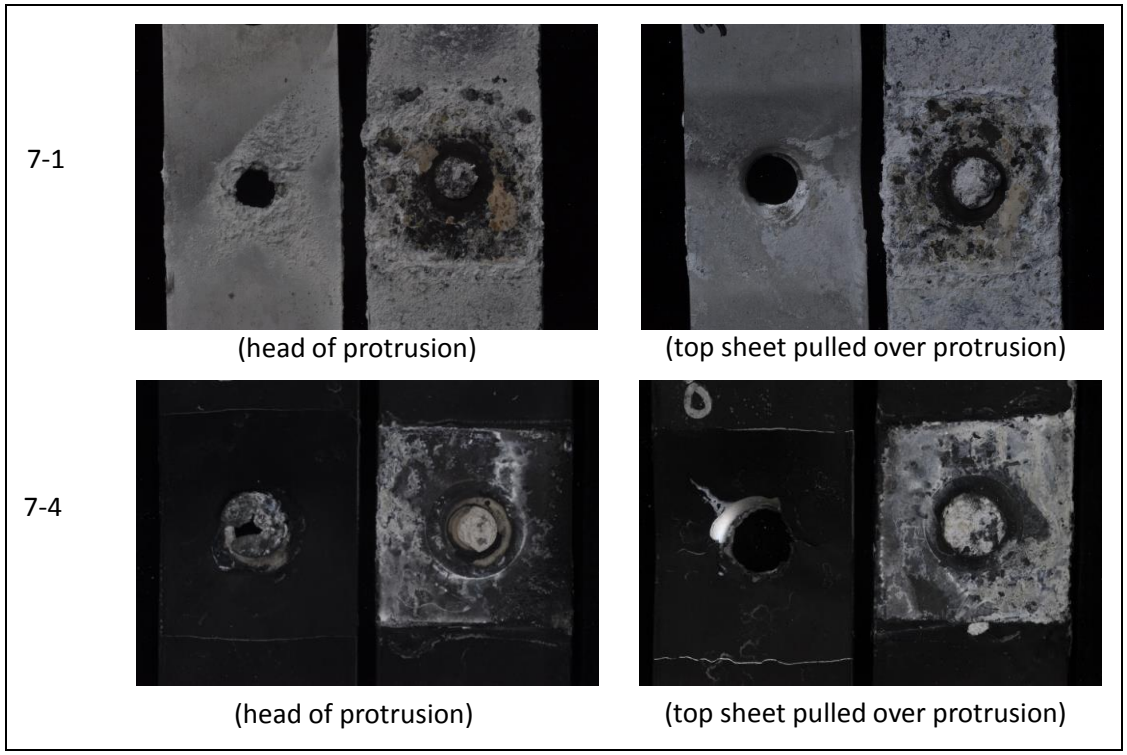

Figure 72: 7-mm round boss UPJ impact cross tension performance failure modes after 12-wks of accelerated corrosion exposure

Alternative Coating Process Evaluation

Because the most common commercially available coatings did not provide sufficient protection to prevent significant galvanic corrosion in many of the joint configurations, the team decided to take a cursory look at a few alternative (less widely used in the automobile industry) coatings.

The United States Army Tank Automotive Research, Development and Engineering Center (TARDEC) provided 75 steel test coupons with the military spec Chemical Agent Resistant Coating (CARC) coating process to see if this coating could provide improved galvanic isolation between the steel and Mg samples compared to the previously evaluated conventional automotive coating processes. However, as can be seen in Figure 73, this coating was unable to withstand the UPJ process temperatures and forces. Due to the obvious extensive coating damage in the area of the UPJ joint, no corrosion testing was conducted.

Figure 73: Photo of two joined lap-shear tension assemblies utilizing the CARC coating on the steel coupons

Henkel provided 40 Mg AM60B test coupons with an experimental pretreatment to see if this pretreatment could provide improved corrosion performance of the Mg samples compared to the previously evaluated, more commonly used Alodine 5200 pretreatments. This treatment converts the outer layer of the Mg material to a semi-conductive ceramic. However, this treatment was unable to withstand the UPJ process forces, as can be seen in Figure 74 where most of the black coating flaked away from the boss in the form of a very fine powder when the UPJ force was applied prior to application of any electrical current. This did not prevent the formation of a good mechanical joint as can be seen in Figure 74(c). Parts were returned to Henkel for evaluation where it was determined that even though most of the black color was gone from the boss, approximately 50-75% of the actual surface treatment thickness still remained.

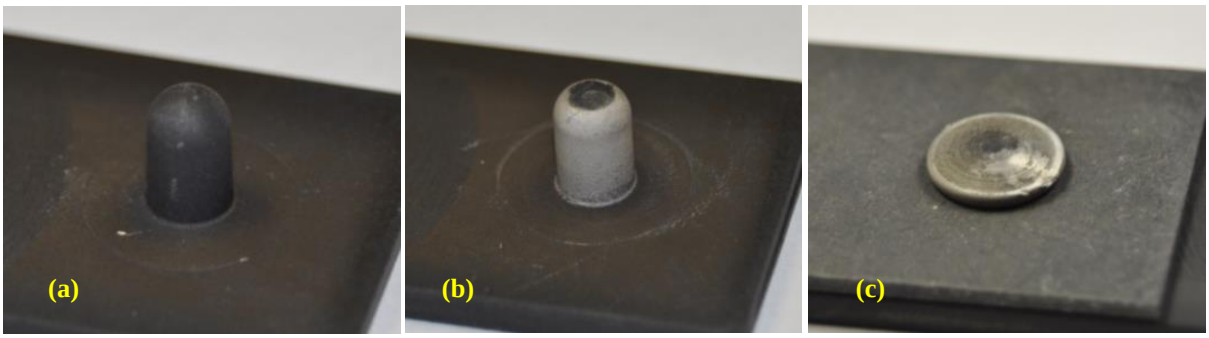

Figure 74: Photos of experimental pretreated Mg lap-shear tension coupons (a) prior to contact by the electrode, (b) after application of initial contact force by the electrode but prior to application of electrical current, and (c) after full forming operation with force and current

Nevertheless, subsequent corrosion testing showed no noticeable improvement over the previous results using Alodine 5200. However, there was no powder-coat or paint applied, and it may be that the experimental treatment is more dependent than Alodine 5200 on the application of powdercoat and paint. The two photos shown in Figure 75 show the UPJ head after only one week of corrosion exposure for Mg to Steel joints with the experimental pretreatment on the Mg and the Armorgalv treatment on the steel.

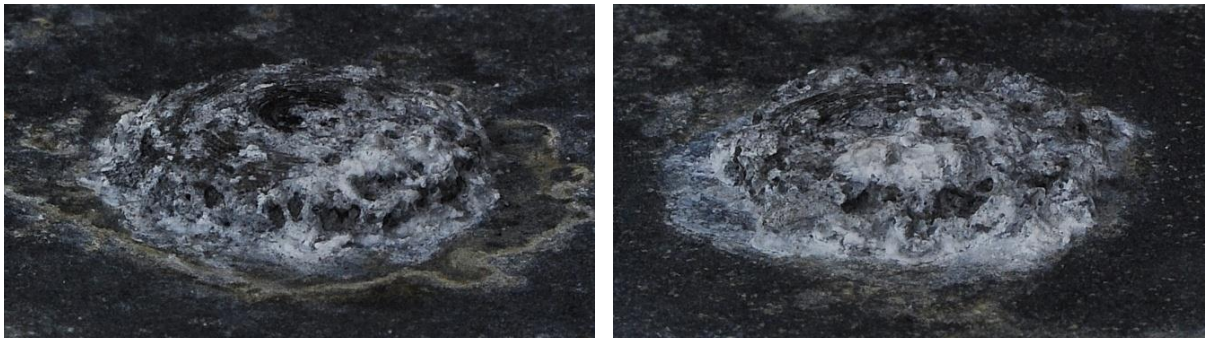

Figure 75: Photos of experimentally pretreated Mg UPJ joints to Armorgalv treated steel test coupons after 1-wk of ASTM G85-A2 accelerated corrosion exposure. Photos are of different specimens of the same joint and coating configuration

AET also conducted preliminary evaluations of Mg to steel joints with alternative Zn-Mg-Al treatments on the steel coupons and subjected assemblies to up to 12-wks exposure of the ASTM G85-A2 schedule per the matrix shown in Table 7. The steel material was provided in 120 and 250 g/m^2 density by Arcelor Mittal (Zagnelis) and Tata (MagiZinc). For these joints, the corrosion performance evaluations are primarily visual with mechanical testing conducted only prior to corrosion and post corrosion.

For UPJ 7-9, the specified adhesive was Henkel's Teroson EP 5089 adhesive. The sealer specified was Henkel's 1097 sealer. All coated assemblies were coated to the FCA specifications for Powder primer (PCV70500) and base coat (HWB90394P bright white). The corrosion performance evaluations are primarily visual with mechanical testing conducted only prior to corrosion and post corrosion.

Configuration Number	Upper Sheet			Bottom Sheet			Assembly Coating Configuration
	Material	Thickness (mm)	Coating	Material	Thickness (mm)	Coating	
UPJ 7-5	A 120	0.8	Bare	Mg AM60B	4.0	Bare	Uncoated
UPJ 7-6	A 120	0.8	E-coat	Mg AM60B	4.0	Pretreated	Coated
UPJ 7-7	B 120	0.8	Bare	Mg AM60B	4.0	Bare	Uncoated
UPJ 7-8	B 120	0.8	E-coat	Mg AM60B	4.0	Pretreated	Coated
UPJ 7-9	B 120	0.8	E-coat	Mg AM60B	4.0	Pretreated	Adhesive, coated, sealed edges
UPJ 7-10	B 250	0.8	Bare	Mg AM60B	4.0	Bare	Uncoated
UPJ 7-11	B 250	0.8	E-coat	Mg AM60B	4.0	Pretreated	Coated

Table 7: Round boss UPJ material and coating configurations

As can be seen in Table 8, only one coating configuration (UPJ 7-9) completed the entire 12-wks of exposure while other configurations were removed at 4-wks and 8-wks because the corrosion damage was so extensive that extending the test any longer would not have left any samples available for mechanical testing.

Configuration Number	Test Type Configuration	Number of wks exposure	Number of specimens corrosion tested	Number of specimens mechanically tested
UPJ 7-5	Lap-shear	4	3	0
	Cross-tension	4	3	2
UPJ 7-6	Lap-shear	8	3	3
	Cross-tension	8	3	3
UPJ 7-7	Lap-shear	4	3	3
	Cross-tension	4	3	2
UPJ 7-8	Lap-shear	8	3	3
	Cross-tension	8	3	3
UPJ 7-9	Lap-shear	12	3	3
	Cross-tension	12	3	3
UPJ 7-10	Lap-shear	4	3	3
	Cross-tension	4	3	2
UPJ 7-11	Lap-shear	8	3	3
	Cross-tension	8	3	3

Table 8: Round boss UPJ alternative corrosion treatment test matrix

Figure 76 shows three examples of round boss UPJ joints cross sections with the new steel coatings. Although we did not expect the new coatings to adversely affect the process, it was important to verify this. Figure 76(a) shows a section through UPJ 7-5, while Figure 76(b) shows a section through UPJ 7-6, and Figure 76(c)shows a section through UPJ 7-9. In all cases (including the ones not shown here), the head shape is well formed and provides a substantial overlap to the joined sheet material to help lock it into place to enable high cross-tension strength. The same process parameters used previously in this project to create Mg-steel joints were used to create the tested joints presented throughout the rest of the report.

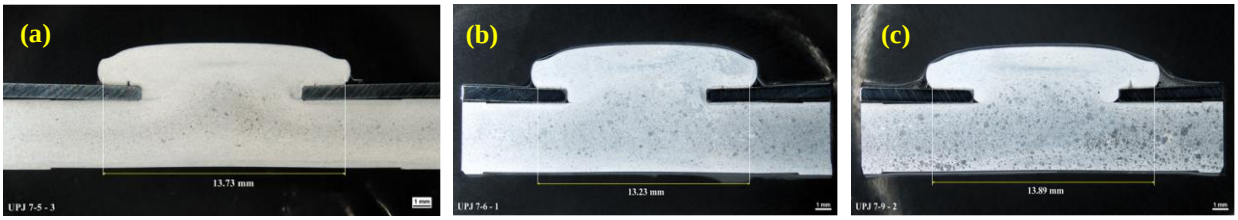

Figure 76: Typical joint metallographic cross sections

Quasi-static lap-shear tension results for all UPJ joints are shown in Figure 77 both prior to and after accelerated corrosion exposure. Except for UPJ7-9 (which has adhesive in addition to the UPJ joint and therefore substantially higher lap-shear tension strength), results are consistent among the different configurations. Note: UPJ 7-5 samples separated during corrosion testing at 3-weeks

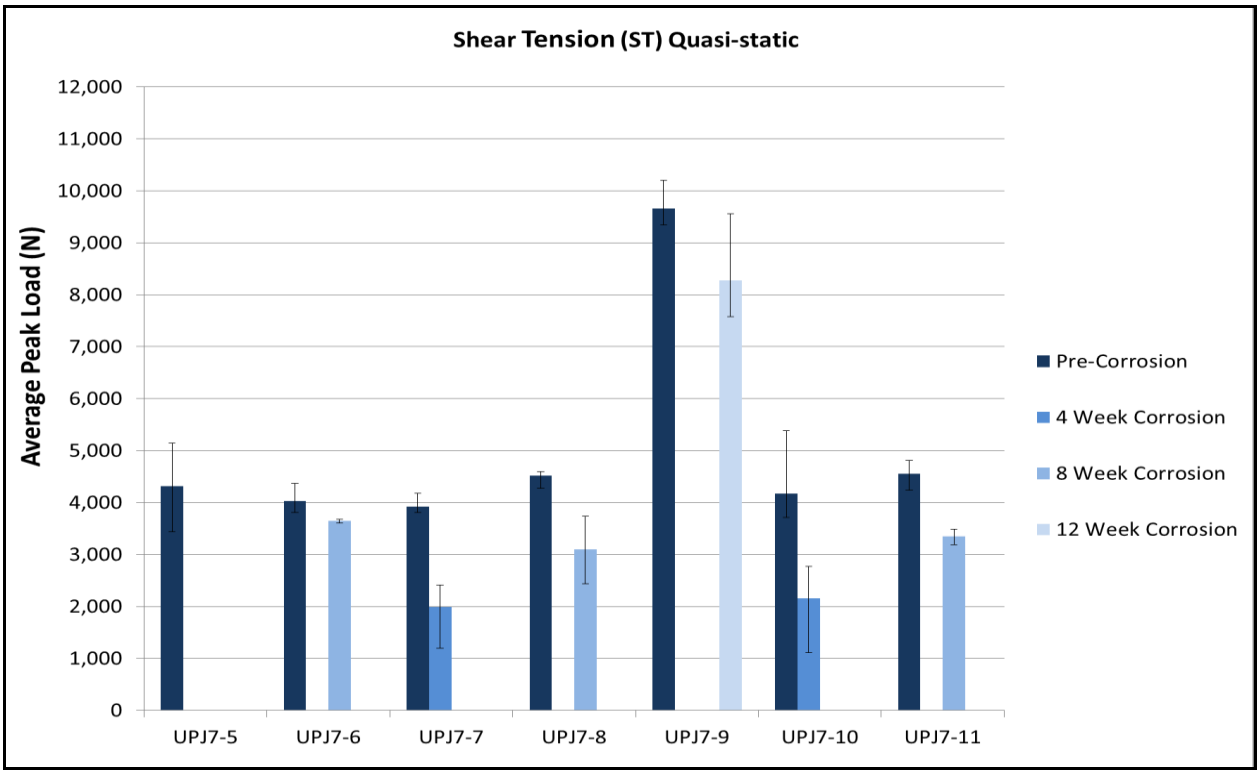

Figure 77: Quasi-static lap-shear tension results prior to corrosion and at selected corrosion intervals

As can be seen in Figure 78, pre-corrosion joint failures are consistently a result of deformation and tearing in the 0.8 mm thick upper steel sheet whereas post-corrosion joint failures often result from the head pulling off the die-cast Mg protrusion or by the protrusion breaking at the base plate as shown in Figure 79.

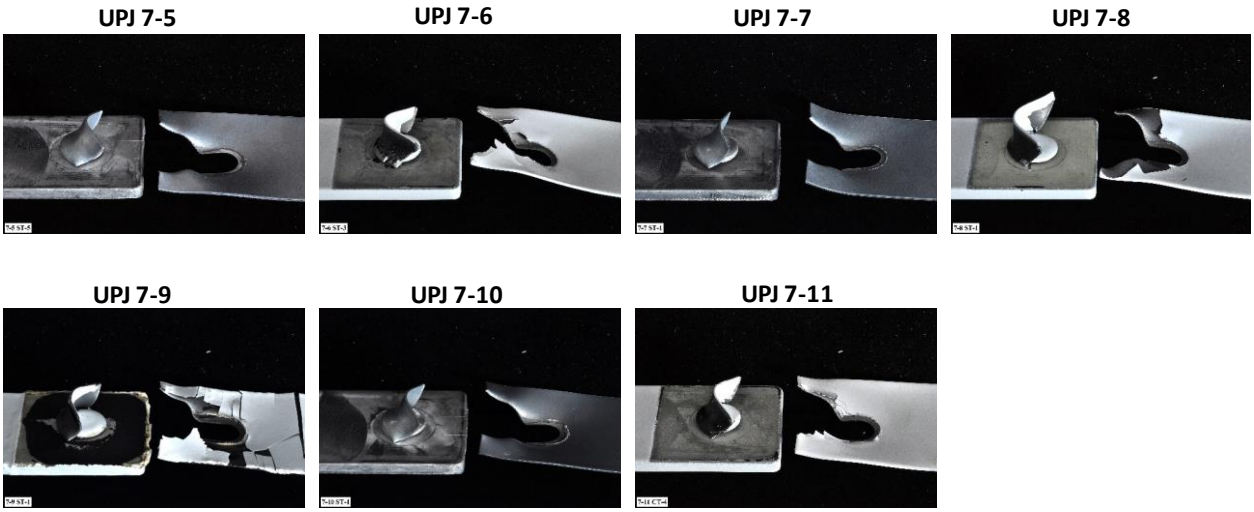

Figure 78: Pre-corrosion quasi-static lap-shear tension failure modes

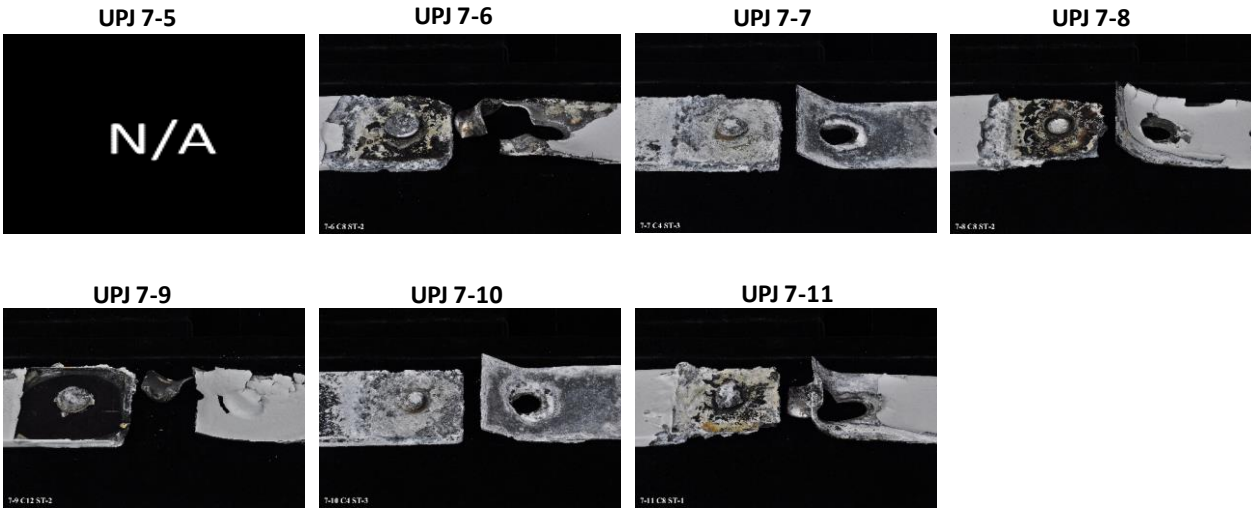

Figure 79: Post-corrosion quasi-static lap-shear tension failure modes

Quasi-static cross tension results for all UPJ joints are shown in Figure 80 both prior to and after accelerated corrosion exposure. Unlike the lap-shear tension configurations, adhesive does not play a significant role in cross-tension joint strength performance. Pre-corrosion failure modes are shown in Figure 81 while post-corrosion failure modes are shown in Figure 82. In both cases, joint failure resulted from primarily from deformation in the upper sheet, while a few others failed because of the head pulling off the die-cast Mg protrusion or by the protrusion breaking at the base plate.

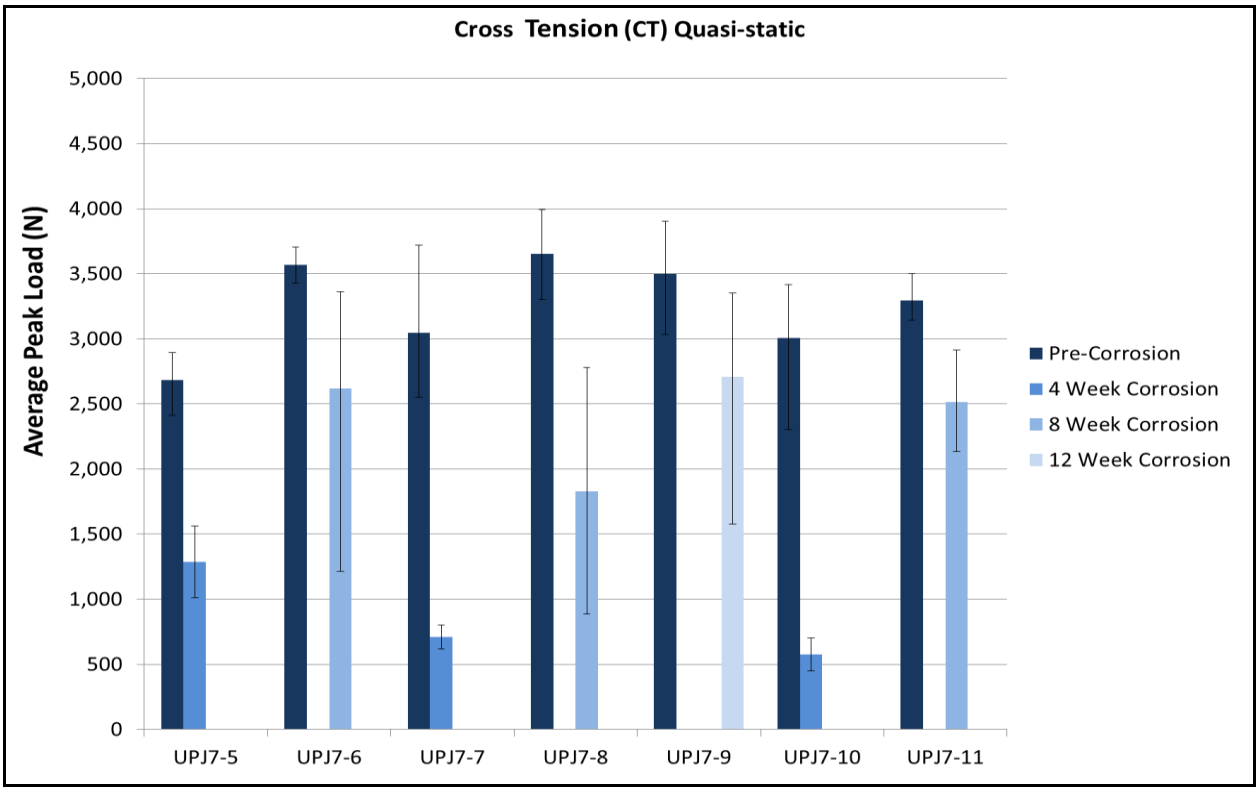

Figure 80: Quasi-static cross tension results prior to corrosion and at selected corrosion intervals

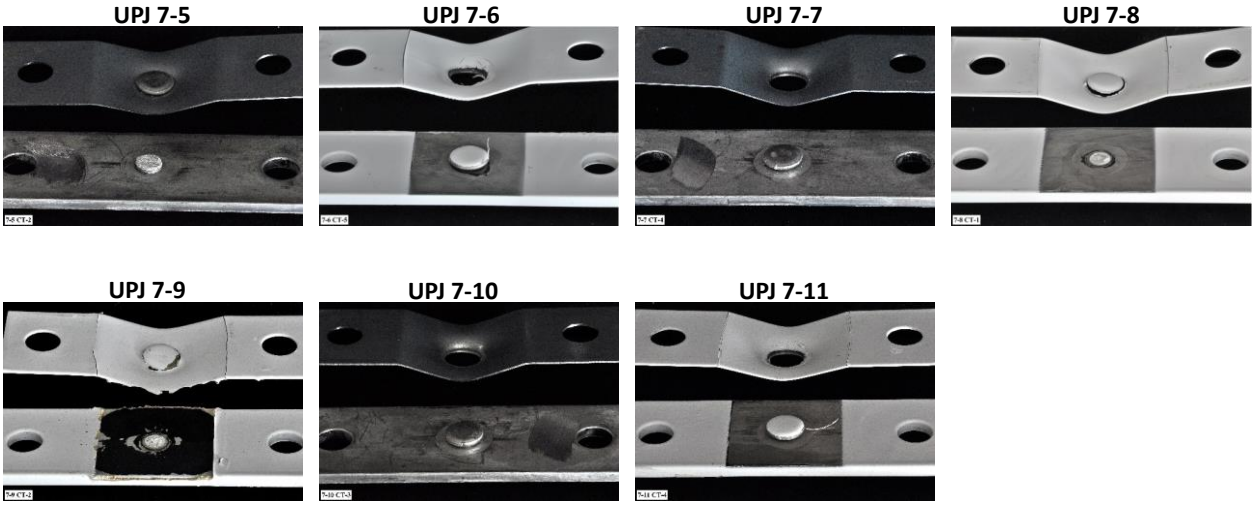

Figure 81: Pre-corrosion quasi-static cross tension failure modes

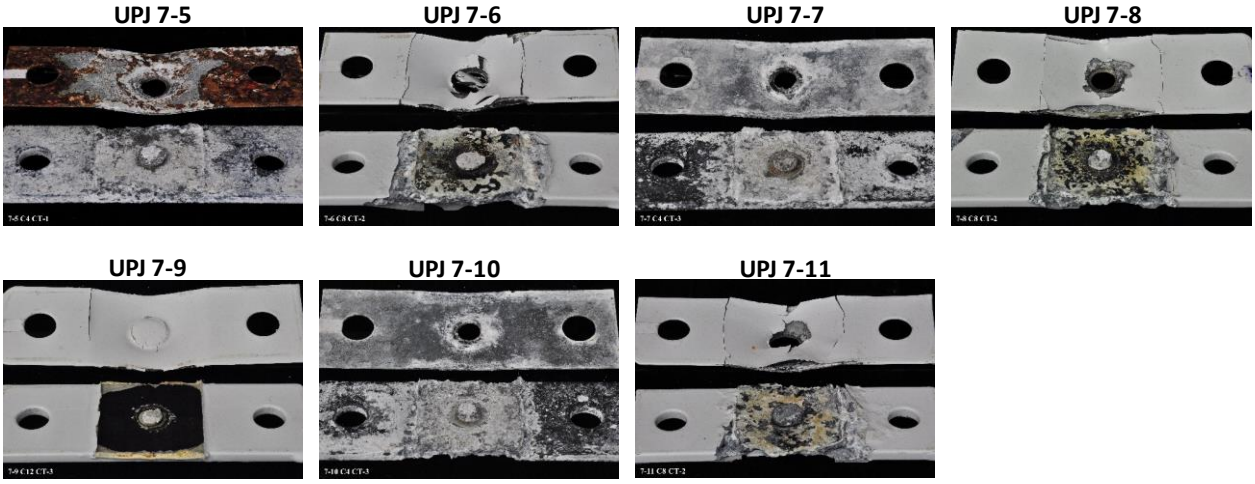

Figure 82: Post-corrosion quasi-static cross tension failure modes

Figure 83 shows typical corrosion progression through 2-wks of salt fog exposure for lap-shear tension samples while Figure 84 shows progression through wks 4-12. There was no notable difference in performance of the uncoated Mg/steel configurations (UPJ 7-5, 7-7, and 7-10). All of these samples were removed from corrosion exposure after 4-wks in order to have samples that could be tested for mechanical performance. For the painted samples, however, there was some observable difference. UPJ 7-9 showed a substantial improvement over the others. This configuration included adhesive and edge sealing, which obviously makes a dramatic difference. Additionally, UPJ 7-6 showed improvement over UPJ 7-8 even though both configurations have the same 120 g/m^2 surface density, and appeared to be equivalent to UPJ 7-11 (which has a 250 g/m^2 surface density) despite that configuration having twice the coating density. All of the coated configurations, except for UPJ 7-9, were removed from corrosion exposure after 8-wks to ensure a sufficient quantity of samples for post-corrosion testing. Because UPJ 7-9 was showing very little effect from the corrosion exposure, the samples from this configuration were returned to the corrosion chamber for another 4-wks. The performance of this configuration clearly validates the benefit of adding adhesive between the coupons and sealer to the edges.

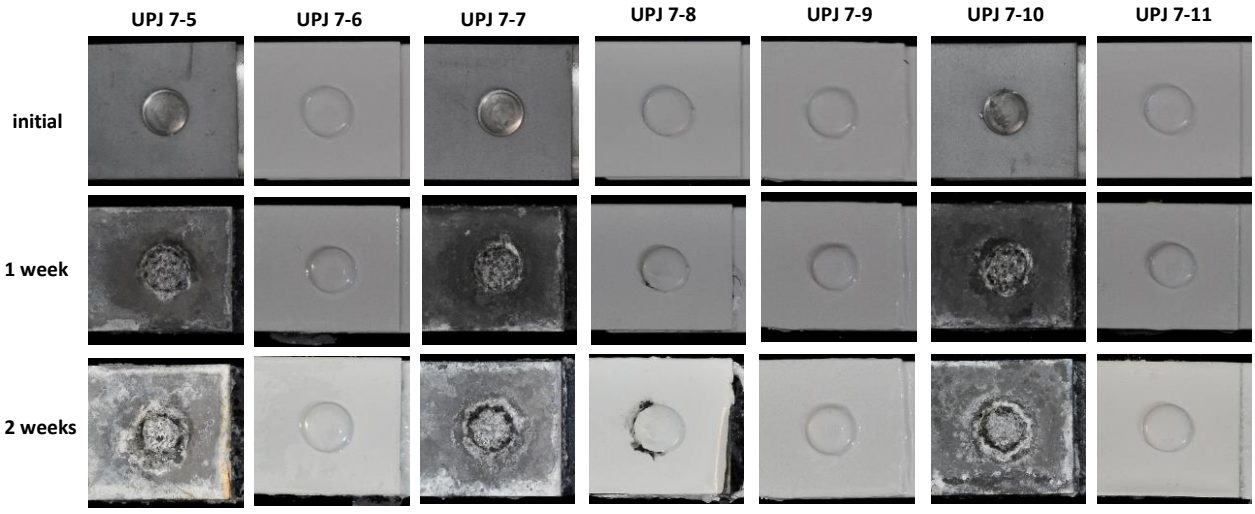

Figure 83: Typical corrosion progression – lap shear tension samples through 2 weeks

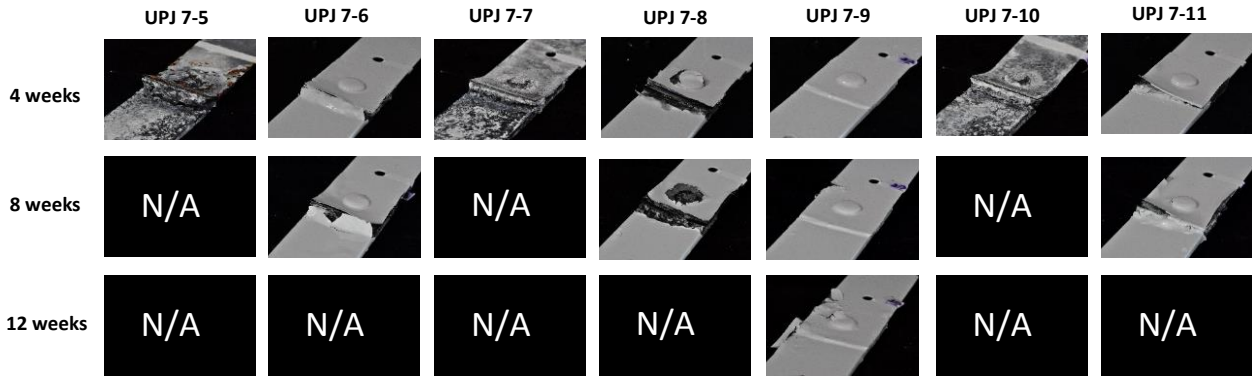

Figure 84: Typical corrosion progression – lap shear tension samples weeks 4-12

Corrosion test results for cross-tension samples were similar to those of the lap-shear tension samples and are shown below in Figures 85 and 86. In this case, the UPJ7-9 configuration was still performing well even after 12-wks of exposure with no observed paint peeling or other signs of corrosion damage.

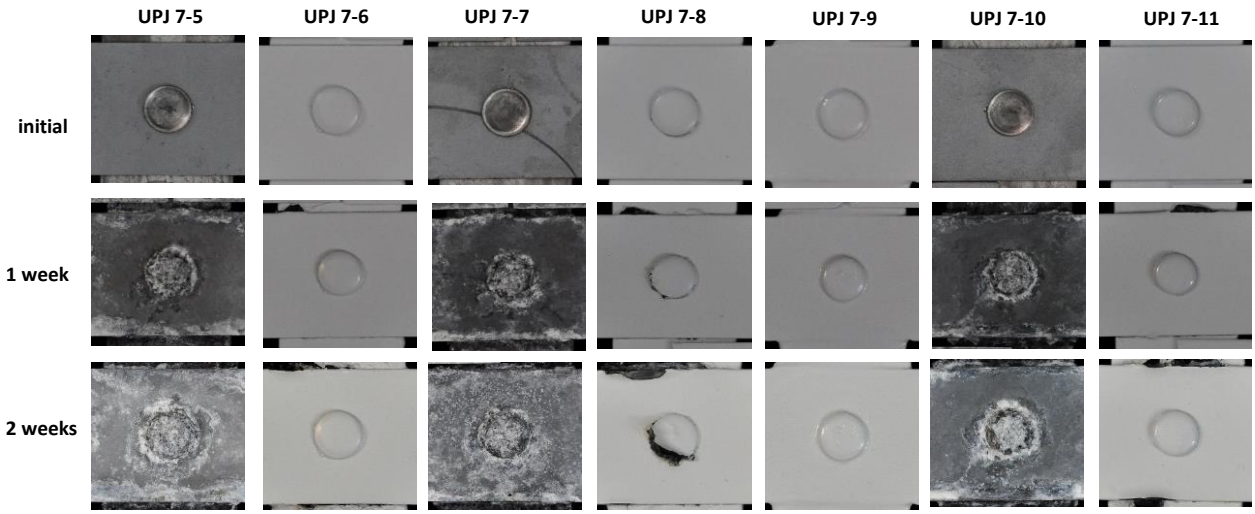

Figure 85: Typical corrosion progression – cross tension samples through 2 weeks

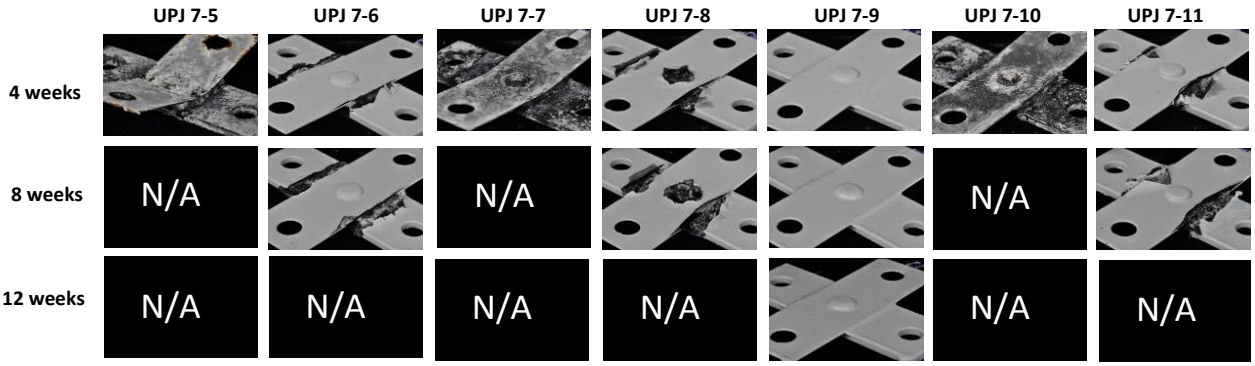

Figure 86: Typical corrosion progression – cross-tension samples weeks 4-12

OVAL BOSS UPJ PROCESS DEVELOPMENT AND PERFORMANCE EVALUATION

To support joint requirements for narrow flange applications, oval boss UPJ joints were developed.

Oval Boss UPJ Joint Development and Evaluation

A schematic of the typical oval boss UPJ protrusion and electrode is shown in Figure 87 while Figure 88(a) and (b) show two steps in the oval boss forming simulation, and Figure 88(c) shows an outline of the shape of the deformed head overlaid to the original boss shape and the clearance hole shape. Unlike the round boss joints, where the final head shape closely matches the clearance hole shape, albeit with a larger diameter intended to provide a consistent overlap, the deformed oval boss UPJ head shape is considerably different from the original boss and clearance hole shape as the head expands significantly more across the width than across the length. Since the primary purpose of the oval joint variation is to allow for use of the UPJ joint on narrow flanges, this change in profile is not desirable. However, a great deal of experimentation and some simulation indicate that it may be unavoidable. Nevertheless, even with this width expansion, the oval boss joint does allow for significantly narrower flanges than round boss joints while maintaining or increasing joint strength.

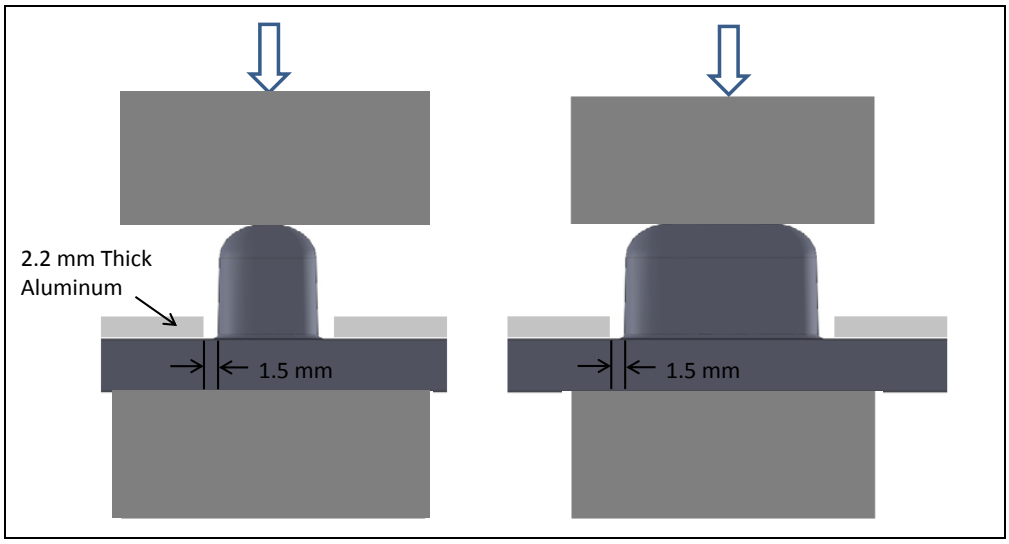

Figure 87: Example oval joint UPJ boss shape shown in longitudinal and transverse direction

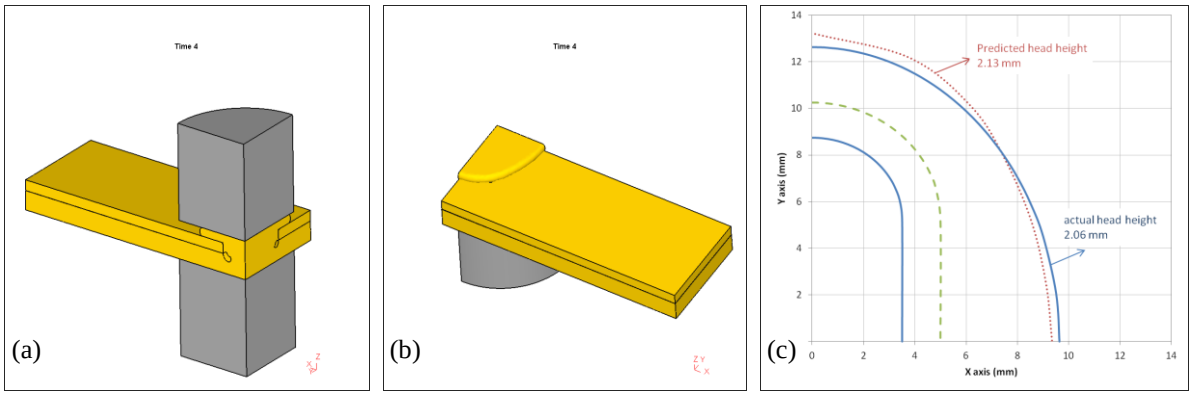

Figure 88: Example oval joint UPJ process simulation (a) and (b), and overlay of formed oval UPJ head to boss shape and clearance hole shape (c).

For this project, the oval boss dimensions were chosen to be 6.0-mm wide by 15.0-mm long. Oval boss electrodes were machined to optimized shapes, and optimized force/current process parameters were developed for oval boss configurations using CAE simulation tools and physical experimentation. Figure 89 shows three oval boss UPJ head formations resulting from increasing temperature and force. The yellow oval superimposed on the formed head shape in the pictures indicates the shape of the clearance hole in the top sheet. It can be seen from these pictures, that as the head formation is squeezed harder to improve the coverage of the head over the clearance hole, the shape of the head veers further away from the original oval proportions and begins to veer closer to the shape of a circle.

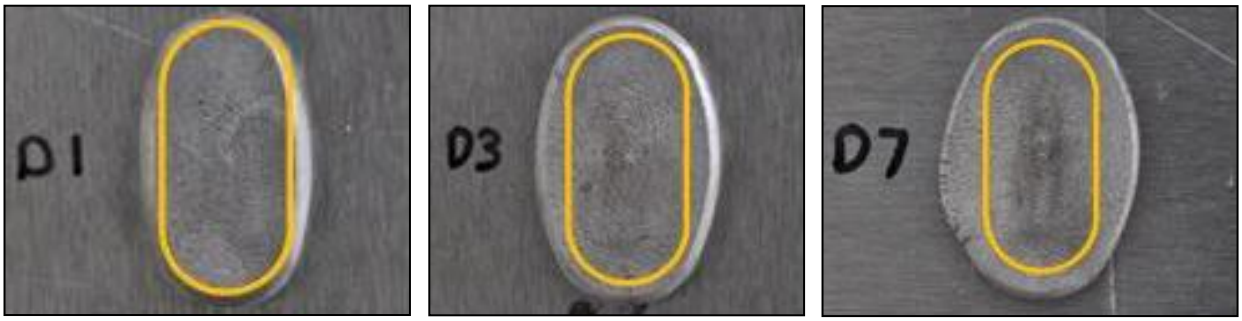

Figure 89: Effect of force and current on head shape and size

Figure 90 shows the results of a study to quantify the effects of electrode contamination resulting from Mg and oxide transference to the electrode surface. For each joint, the top picture shows the top view of the deformed head while the lower picture shows the surface of the electrode. From this study, it appears that the oval boss joints are more sensitive to electrode contamination than the round boss joints, although some issues with the welding equipment (low initial force) during this study may have made the process more sensitive to electrode contamination than usual. In any case, this study clearly shows the importance of maintaining a clean electrode surface for producing consistent crack-free joints.

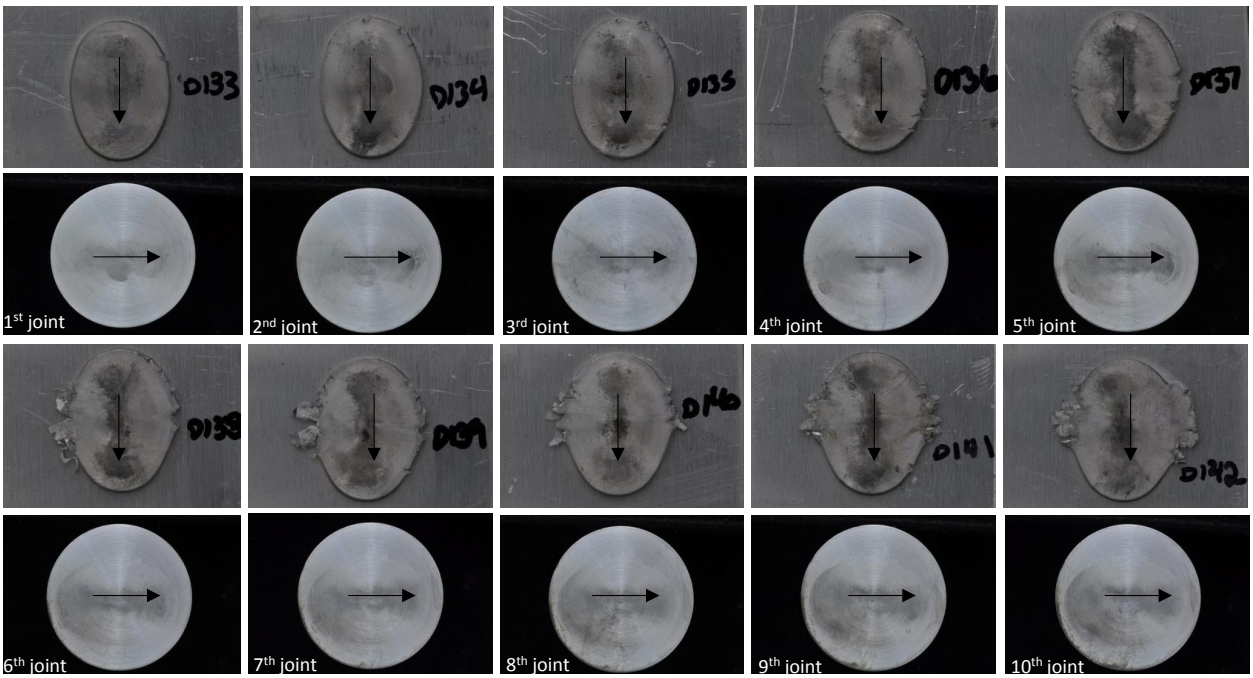

Figure 90: Electrode contamination study for oval boss joints – cool joints – no cleaning

Figure 91 shows the results of a study to quantify the effects of electrode temperature on the ability to produce consistent crack-free joints. In this study, ten joints were produced consecutively without a delay (other than a few seconds for cleaning the oxide from the electrode) to allow the electrode temperature to increase. While there may be some degradation as the temperature of the electrode increases, the effect is clearly not as rapid or pronounced as the effect of electrode contamination. It should be noted that the electrode was quickly cleaned between each joint in order to prevent the effects of electrode contamination from interfering with the study to evaluate effects of temperature, and even though the electrodes

were cleaned very quickly before moving on to the next joint, since the electrode was cleaned with hydrochloric acid, the brief application of acid may have provided enough convective cooling to slightly slow the normal increase in electrode temperature, but not to a significant degree. During this study, the welding equipment was still exhibiting low initial force, which again may have resulted in slightly more sensitivity than would have been observed otherwise.

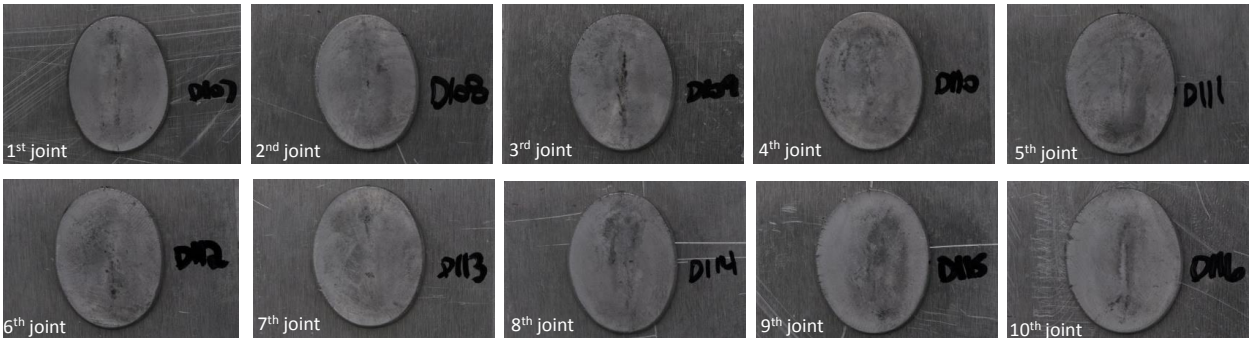

Figure 91: Electrode temperature study – consecutive joining – with cleaning

Mechanical/Structural Testing and Evaluation

To support development and evaluation of oval boss joints, AET produced over 400 joints and completed mechanical/structural evaluation of 220 oval boss UPJ joint configurations. No corrosion testing was conducted for oval boss joints. This is because there was no reason to believe that the corrosion performance of an oval boss in a given material/coating configuration would perform any differently than a round boss joint of the same material/coating configuration.

Table 9 shows material and joint configurations investigated for oval boss UPJ joints. In oval boss joint configurations, an "L" suffix indicates the oval boss is oriented along the longitudinal axis of the casting and a "T" suffix indicates the oval boss is oriented transverse to the longitudinal axis of the casting.

Configuration Number	Boss Orientation on Base Plate	Upper Sheet			Bottom Sheet			Baked Assembly?
		Material	Thickness (mm)	Coating	Material	Thickness (mm)	Coating	
UPJ 1L	longitudinal	Al 6016-T4	1.1	Bare	Mg AM60B	4.0	Bare	No
UPJ 2L	longitudinal	Al 6016-T4	1.1	Pretreated	Mg AM60B	4.0	Pretreated	Yes
UPJ 3L	longitudinal	HSS DP590	2.1	Galvanized	Mg AM60B	4.0	Pretreated	No
UPJ 4L	longitudinal	Al 6016-T4	2.1	Bare	Mg AM60B	4.0	Bare	Yes
UPJ 5L	longitudinal	HSS DP590	2.1	Galvanized	Mg AM60B	4.0	Bare	No
UPJ 6L	longitudinal	Al 6016-T4	2.1	Pretreated	Mg AM60B	4.0	Pretreated	Yes
UPJ 1T	transverse	Al 6016-T4	1.1	Bare	Mg AM60B	4.0	Bare	No
UPJ 2T	transverse	Al 6016-T4	1.1	Pretreated	Mg AM60B	4.0	Pretreated	Yes
UPJ 3T	transverse	HSS DP590	2.1	Galvanized	Mg AM60B	4.0	Pretreated	No
UPJ 4T	transverse	Al 6016-T4	2.1	Bare	Mg AM60B	4.0	Bare	Yes
UPJ 5T	transverse	HSS DP590	2.1	Galvanized	Mg AM60B	4.0	Bare	No
UPJ 6T	transverse	Al 6016-T4	2.1	Pretreated	Mg AM60B	4.0	Pretreated	Yes

Table 9: Oval boss UPJ material and coating configurations

Figure 92 shows several head formations produced on oval boss Mg, Al, and steel top sheets in bare and pre-treated configurations. From these photos, it can be seen that good, crack free head formations were produced in desired material and pre-treatment configurations.

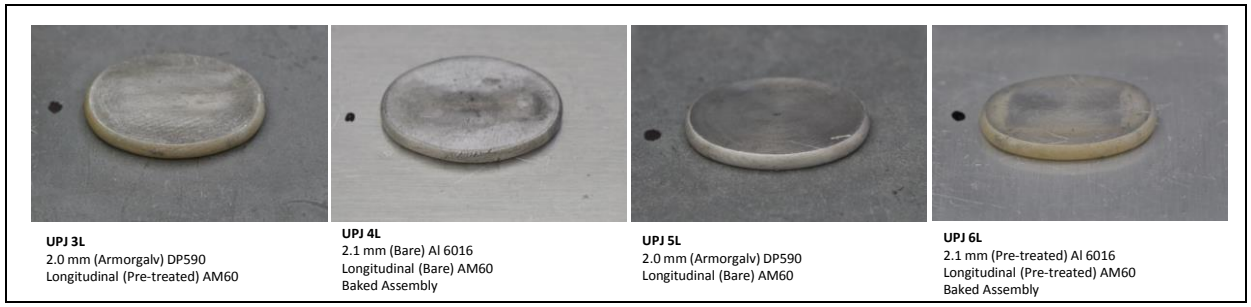

Figure 92: Oval boss UPJ head formations

Figure 93 shows metallurgical cross sections for Mg-Al joints. The sections shown along the top row are cut through the transverse axis (along the longitudinal axis) while the sections along the bottom row are cut through the longitudinal axis (along the transverse axis). These sections illustrate the substantial difference in overlap to clearance hole in the top sheet in longitudinal and transverse directions as a result of the oval joints to tending closer to round as they are deformed.

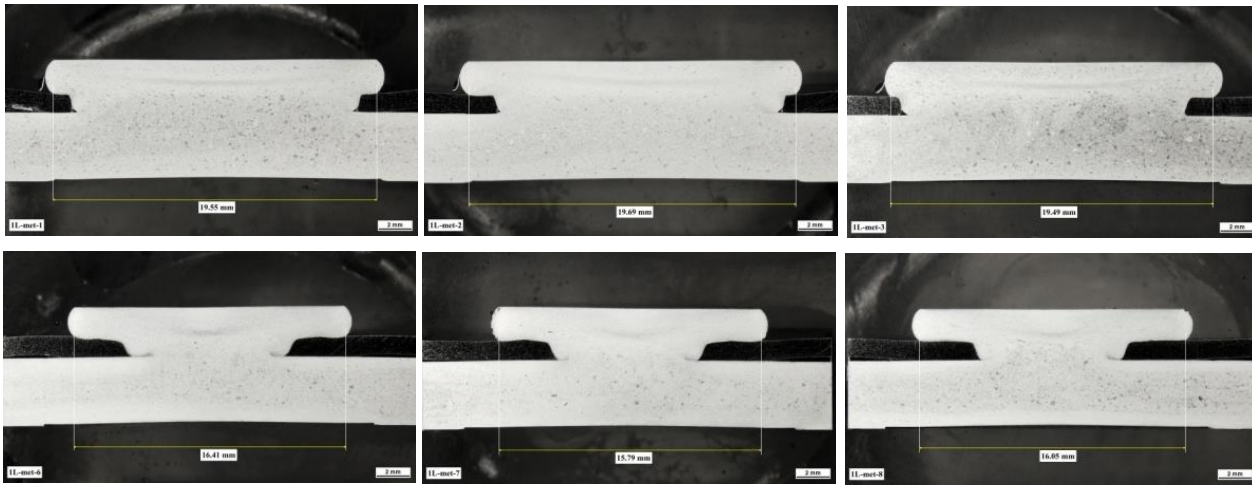

Figure 93: Metallurgical cross-sections of configuration 1L with 1.1 mm Al-6016 top sheet

Figure 94 shows quasi-static ***lap shear*** tension test results for oval boss joints. Figure 95 shows quasi-static ***cross*** tension test results for oval boss joints. The increase in both lap shear and cross tension strength for the 2L and 2 T configurations over the 1L and 1T configurations is a result of the 2L and 2T joints being baked after assembly to simulate the heat treat effect of an automotive paint shop. In all of these configurations (1L, 1T, 2L, and 2T), the upper Al sheet is only 1.1 mm thick, so the failure mode is typically in the top sheet. Since the upper sheet material is Al6016, a material that is bake hardenable, the baking operation after assembly provides a significant increase in strength to the Al material and to the joint.

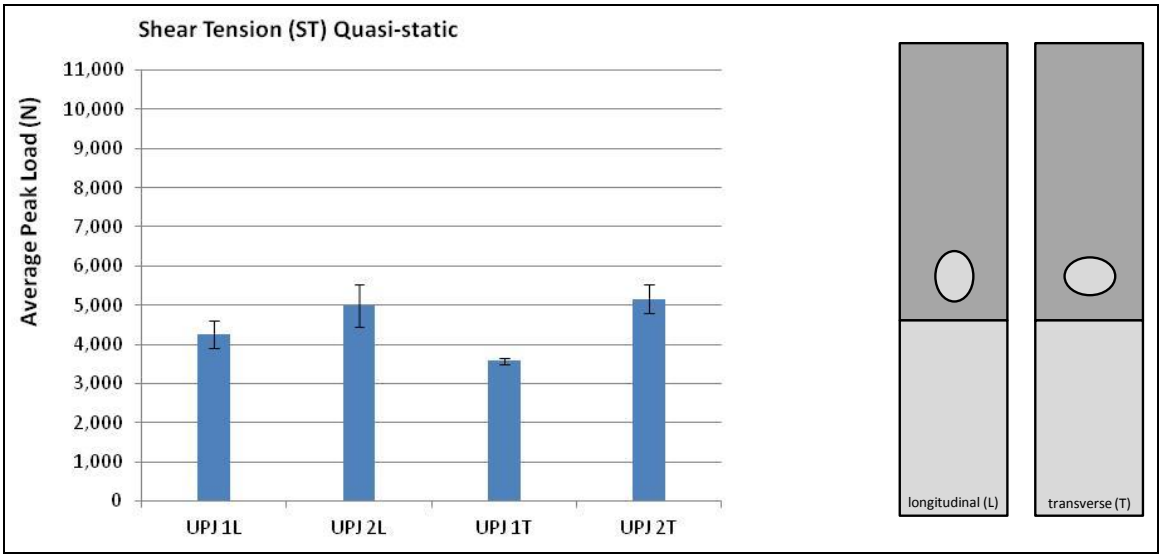

Figure 94: Oval boss UPJ quasi-static lap shear tension test results

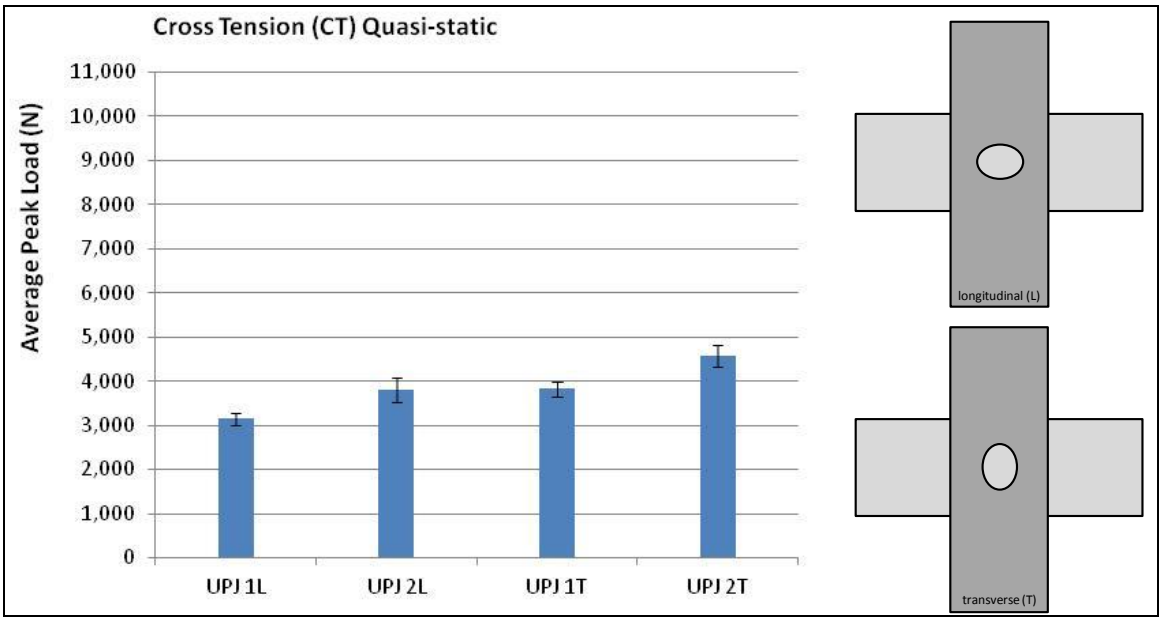

Figure 95: Oval boss UPJ quasi-static cross tension test results

Figure 96 shows quasi-static and impact ***lap shear tension*** and Figure 97 shows quasi-static and impact ***cross tension*** test results for oval boss joints. In the case of all these joints, the upper plate is either steel or Al of 2.0-2.2 mm thickness. This increased thickness and strength of the upper plate results in all joint fractures occurring in the cast base plate, the boss itself, or in a few cases in the head of the boss. In Figure 96, the reason for the reduced lap shear strength for configuration UPJ 4L compared to the other configurations is not readily apparent, while the difference in cross tension strengths (especially for impact) is likely a result of the lower modulus of aluminum compared to steel (UPJ 4T and 6L are both Al while UPJ 3T and 5L are both steel). As identified earlier with round boss joints, the upper plate stiffness has a significant effect on cross tension joint strength even when the actual failure is not in the upper plate.

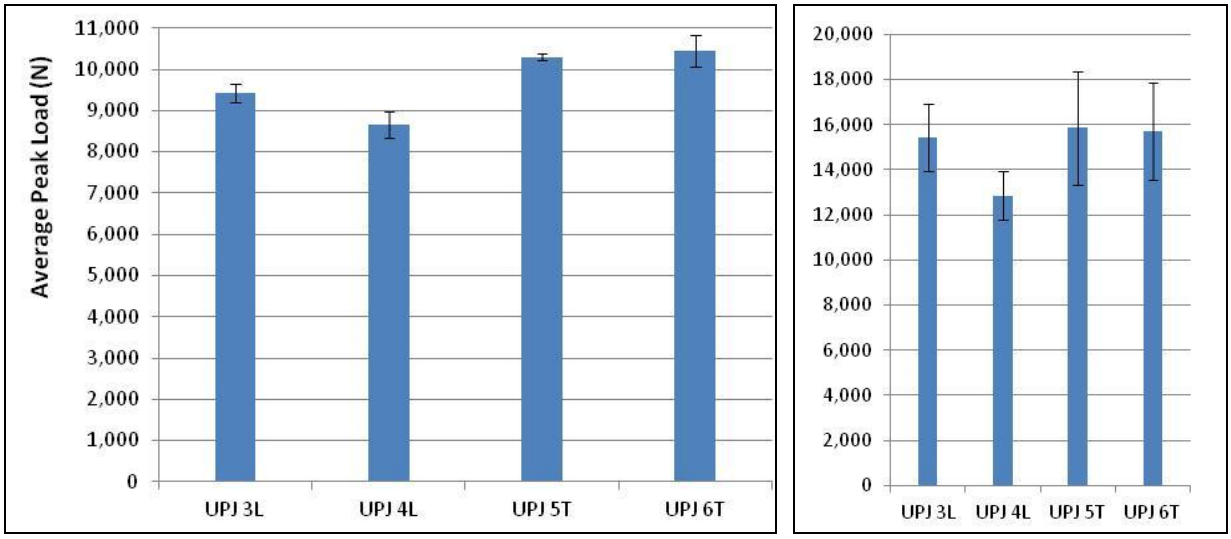

Figure 96: Oval boss UPJ quasi-static and impact lap shear tension test results

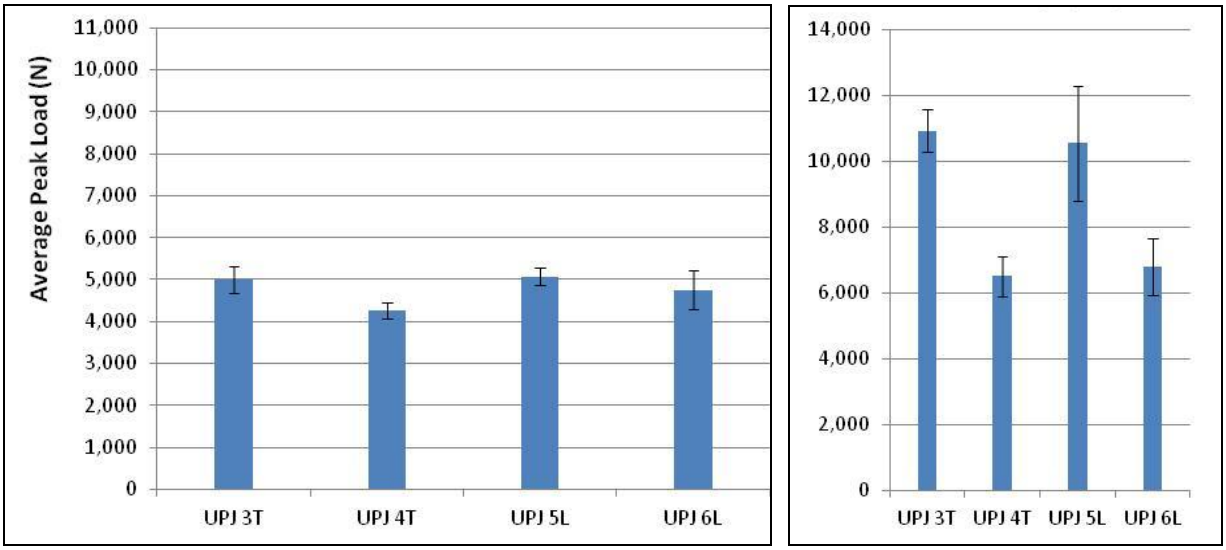

Figure 97: Oval boss UPJ quasi-static and impact cross tension test results

Oval boss to 8.0-mm round boss performance comparisons

Figure 98 shows quasi-static joint performance comparisons between oval boss joints and 8-mm round boss joints. In the case of lap shear tension strength, there are some significant differences in joint strength. It should be noted that the actual shear area of the oval boss joints is ~60% greater than for the round boss joints, which is likely responsible for the difference in lap shear strength. In the case of cross tension testing, the strength of these joints has been previously shown to be highly correlated to the stiffness of the top sheet and the strength of the UPJ head, so the cross sectional area of the boss does not have as great an effect as it does for lap shear tension.

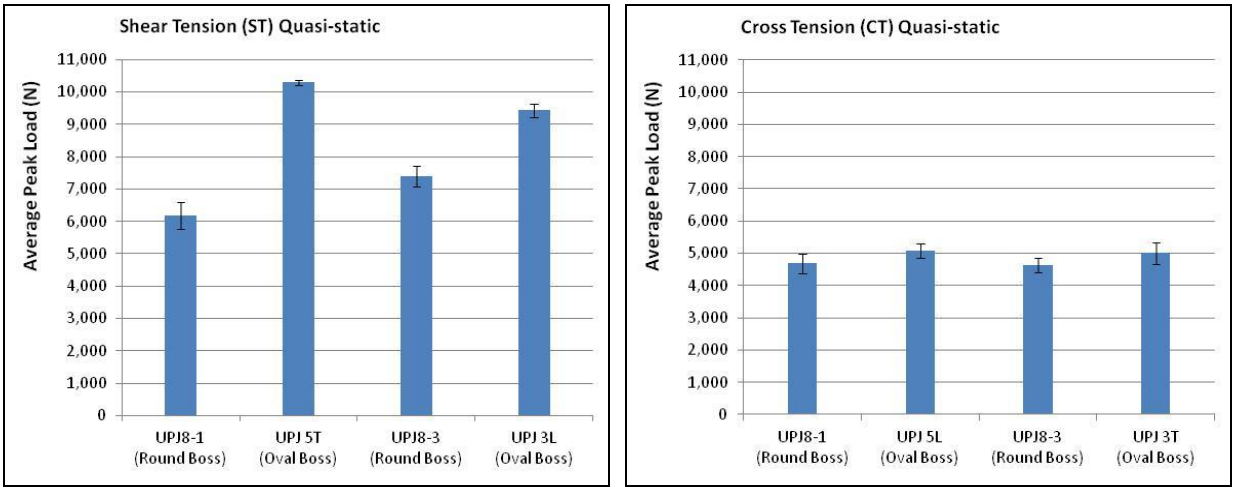

Figure 98: Comparison of oval boss joints (UPJ 5T, 3L, 5L, and 3T) to 8 mm round boss joints (UPJ8-1 and UPJ8-3) in quasi-static lap shear tension (left) and cross tension testing (right)

Figures 99 and 100 show fatigue performance for lap shear tensile testing and cross tension testing, respectively of oval boss joints with comparison to 8 mm round boss UPJ joints. Notably, the substantial improvement in lap shear tensile performance of the oval boss joints over the round boss joints in the low cycle fatigue region in Figure 99 is not exhibited in the high cycle region, except for the UPJ 5T configuration, which exhibits a substantial improvement in high cycle fatigue performance over both the UPJ 3L and UPJ8-1 configurations. In Figure 100, while both oval boss joints exhibit improved low cycle fatigue performance over the round boss joints, this improvement is not exhibited at all in the high cycle region. It should be noted that for these joint configurations, the upper sheet is between 2.0 and 2.2 mm thick Al and all joint failures occur in the cast Mg base plate or at the base of the boss.

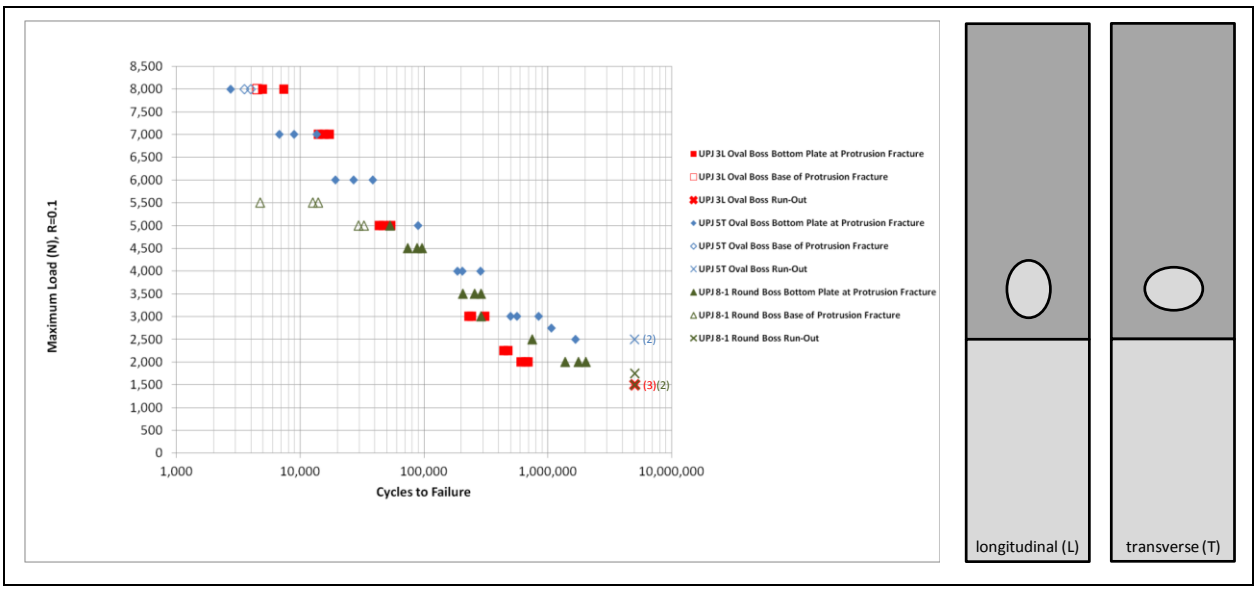

Figure 99: Comparison of lap shear tensile fatigue performance for oval boss UPJ joints (UPJ 3L and 5T) to 8 mm round boss UPJ joints (UPJ8-1)

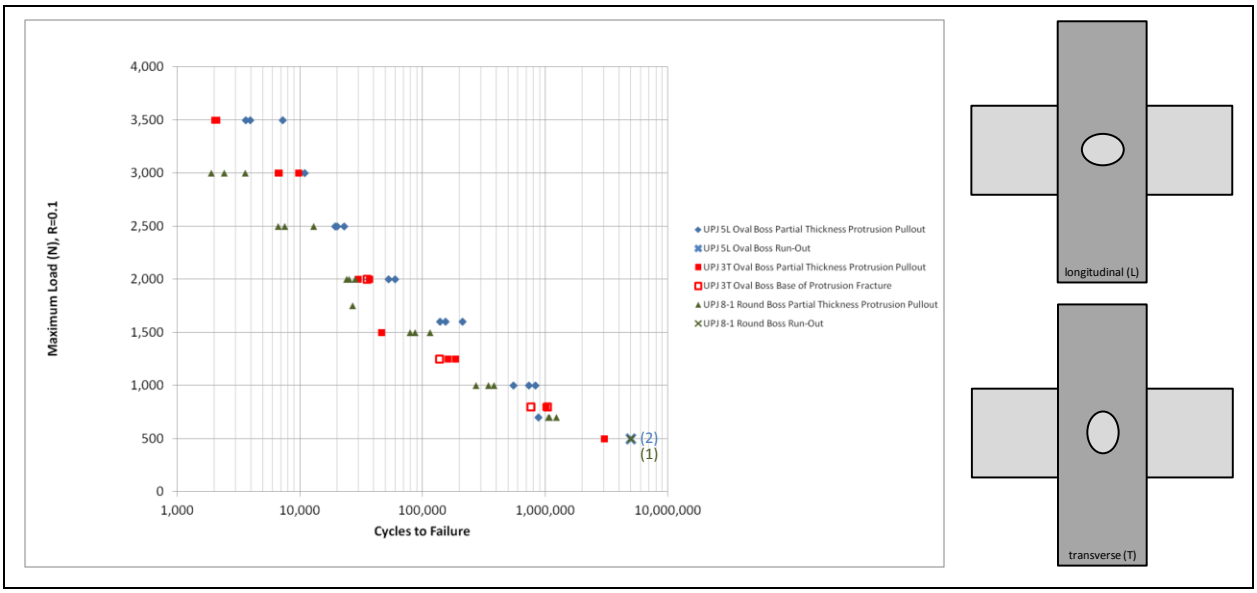

Figure 100: Comparison of cross tension fatigue performance for oval boss UPJ joints (UPJ 3L and 5T) to 8 mm round boss UPJ joints (UPJ8-1)

ROUND BOSS UCR PROCESS DEVELOPMENT AND PERFORMANCE EVALUATION

In order to provide a joining process for applications where neither parent material is a die-casting, a process variant of UPJ known as upset cast riveting (UCR) was developed. This process utilizes a die-cast Mg rivet that is formed using the same process as UPJ and protrudes through clearance holes in both joined materials instead of only one. The rivet is die-cast with a head on one end, so that only the other end is required to be formed, although there is still a relatively small amount of deformation that occurs in the formed head as well.

8.0-mm Round Boss UCR Joint Development and Evaluation

8.0-mm round boss UCR joint electrode geometry and force/current application were optimized using CAE simulation tools and physical experimentation. After evaluating over 20 unique rivet and electrode concepts, the ultimate rivet and electrode geometry wound up being very similar to the optimized UPJ boss and electrode geometry. Figure 101 shows a simulated comparison of one the final optimized UCR rivet and electrode geometry configurations to one of the similar final optimized UPJ boss and electrode geometry configurations with similar current and force rate applications. The formation and temperature profiles are very similar but with slightly higher temperatures in the UCR simulation compared to the UPJ simulation. This is likely a result of increased heat transfer from the boss to the large mass of cast base plate material in the UPJ process compared the relatively small mass of the UCR rivet head.

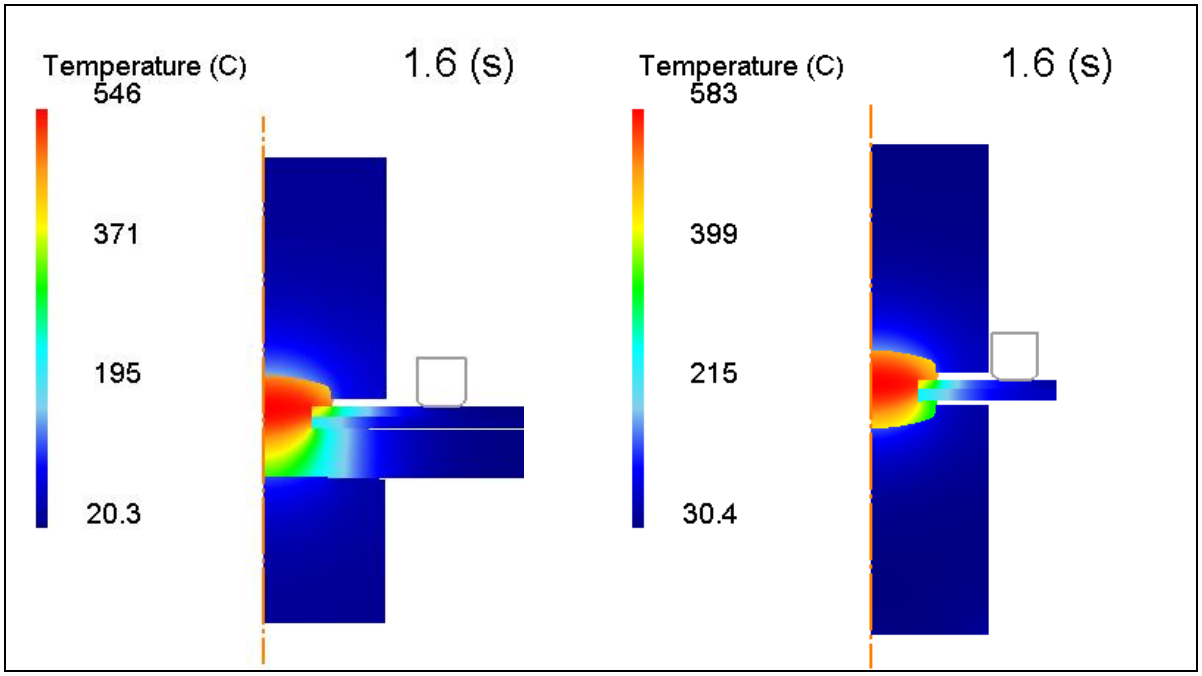

Figure 101: Comparison of UCR process simulation (right) to UPJ simulation (left) for similar electrode design and process parameters

8-mm diameter round boss UCR rivets were produced and electrodes were machined to optimized shapes based on results of the simulations and physical experimentation. The rivets were die cast from Mg AM60B material. The final rivet shape is shown in Figure 102.

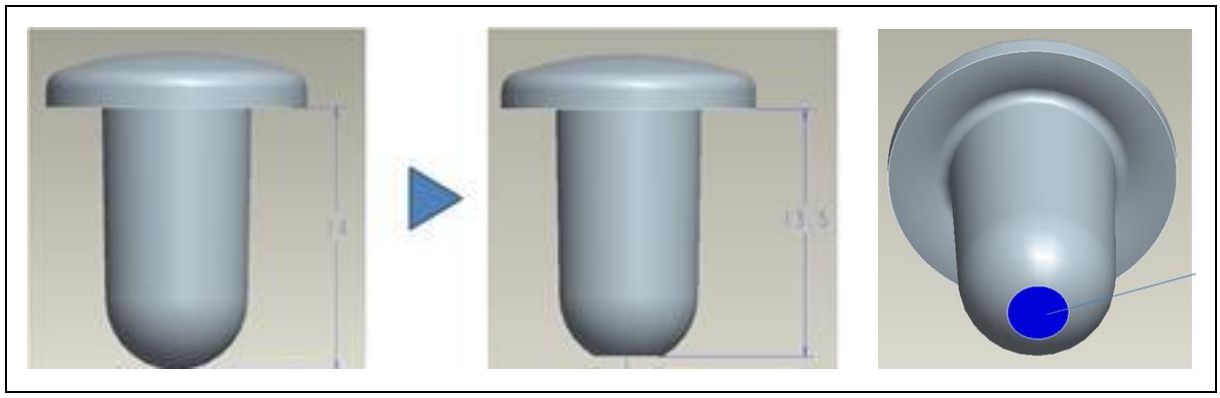

Figure 102: Final design of die-cast UCR rivet

AET produced over 384 round boss UCR assemblies to support pre-corrosion structural/mechanical testing and evaluation of 180 assemblies, and initiated and completed accelerated corrosion evaluation of 204 assemblies. Based on corrosion test results with steel coupons and the ASTM G85-A2 corrosion schedule reported in previous quarterly reports, the length of accelerated corrosion exposure was reduced for these Al to steel joints in order to ensure that samples could be tested at the end of the exposure.

Figure 103 shows the head form and metallographic cross section of an optimized bare (no pre-treatment) UCR joint for joining a 1.0 mm DP590 top sheet to a 1.3 mm Al6016 bottom sheet. Even though the ge-

ometries and current and load rate profiles are very similar to the 8-mm round boss UPJ joints, the UCR joints appear to be more robust with respect to cracking during the forming process. The reason for this is not completely clear, although the casting quality of the UCR rivets appears to be significantly better (less porosity) than that of the UPJ bosses. This may be at least partly responsible for the more robust forming behavior. Additionally, the improved heat transfer observed in Figure 104 may be beneficial as well.

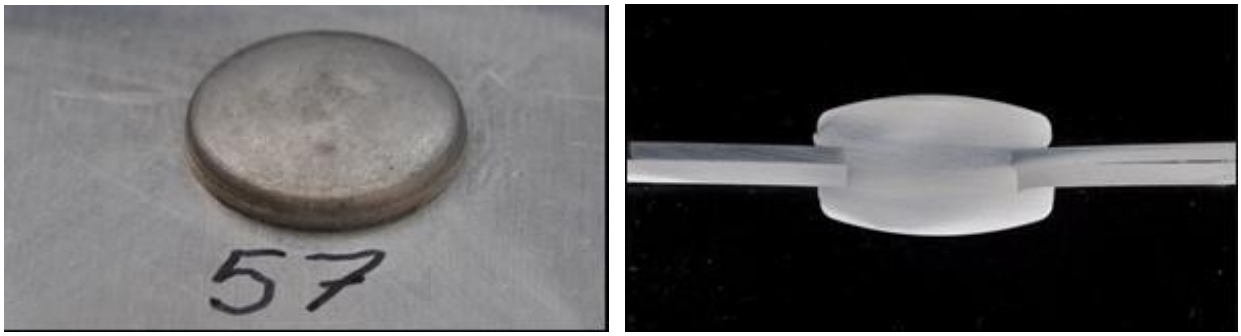

Figure 103: UCR head formation and metallographic cross section produced from optimized parameters

All round boss UCR material/coating configurations discussed in this report are defined in Table 10.

Configuration Number	Upper Sheet			Bottom Sheet			Assembly Coating Configuration
	Material	Thickness (mm)	Coating	Material	Thickness (mm)	Coating	
UCR1	DP590	1.0	Bare	Al 6016-T4	1.3	Bare	Uncoated
UCR2	DP590	1.0	Galvanized	Al 6016-T4	1.3	Bare	Uncoated
UCR3	DP590	1.0	Galvanized	Al 6016-T4	1.3	Pretreated	Uncoated
UCR4	DP590	1.0	Galvanized, e-coat, sealed	Al 6016-T4	1.3	Pretreated	Coated
UCR5	DP590	1.4	Bare	Al 6016-T4	1.3	Bare	Uncoated
UCR6	DP590	1.4	Galvanized	Al 6016-T4	1.3	Bare	Uncoated
UCR7	DP590	1.4	Galvanized	Al 6016-T4	1.3	Pretreated	Uncoated
UCR8	DP590	1.4	Galvanized, e-coat, sealed	Al 6016-T4	1.3	Pretreated	Coated

Table 10: Round boss UCR material and coating configurations

Figures 104 and 105 show the head form and metallographic cross section of UCR1, UCR2, UCR5, and UCR6. Clearly all four of these configurations can be produced with good quality head formations even when the holes in the test coupons are misaligned as is evident in several of the sections shown in Figure 105.

Figure 104: Round boss UCR formed heads for material/coating configurations UCR1, UCR2, UCR5, and UCR6

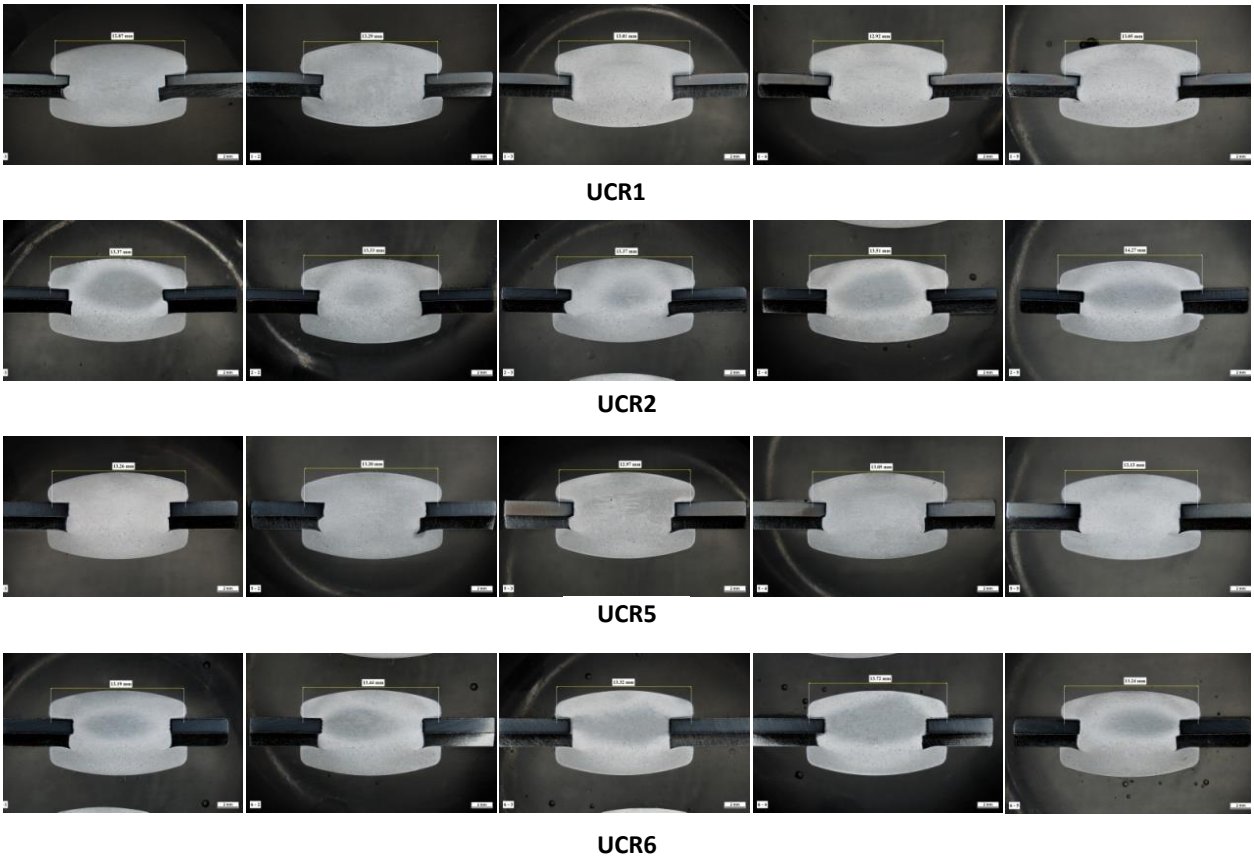

Figure 105: Round boss UCR metallographic cross sections for material/coating configurations UCR1, UCR2, UCR5, and UCR6

Initial (pre-corrosion) Mechanical/Structural Testing and Evaluation

Figure 106 shows the initial (pre-corrosion) lap shear and cross tension test performance of UCR1, and UCR2 (left) and UCR5, and UCR6 (right). In both graphs, the red bars indicate lap shear performance while the blue bars indicate cross-tension performance. The results are quite interesting in that the lap shear tension results for UCR5 and UCR6 are slightly lower than those for UCR1 and UCR2 despite the fact that UCR5 and UCR6 incorporate a thicker 1.4 mm thick steel plate compared to a 1.0 mm thick steel plate on UCR1 and UCR2. In both cases, the attaching plate is 1.3 mm thick aluminum 6016. It is also interesting to note the vastly different load/displacement curves for the two different situations in Figure 107, where the results for UCR5 and UCR6 show dramatically higher level of deformation before failure.

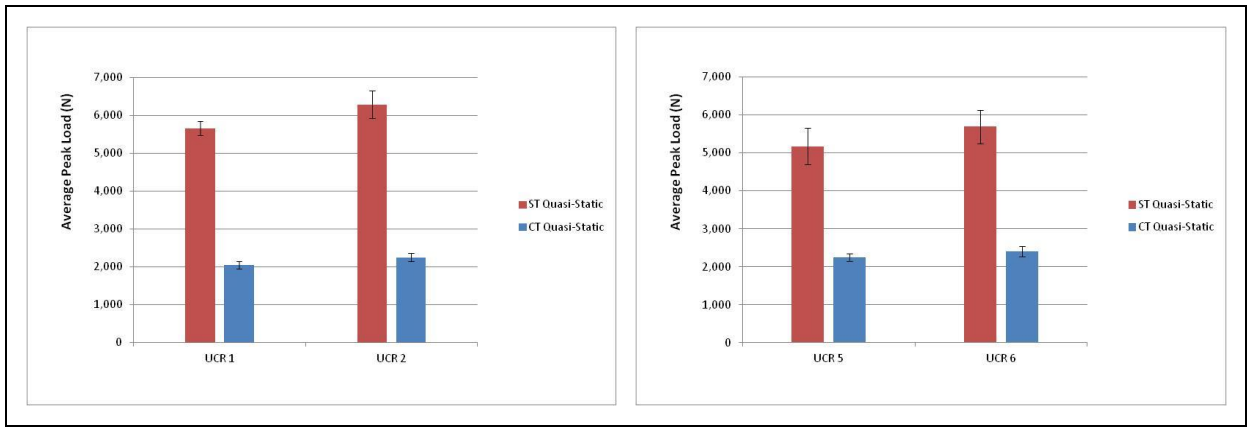

Figure 106: Round boss UCR initial (pre-corrosion) quasi-static lap shear and cross tension test results

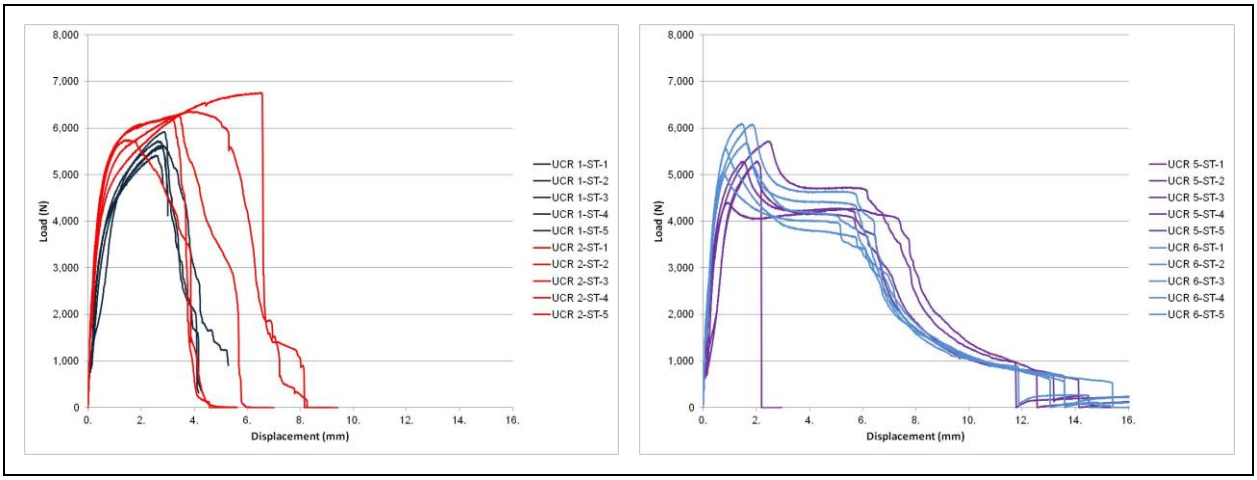

Figure 107: Round boss UCR initial (pre-corrosion) quasi-static lap shear tensile test load/displacement curves. UCR1 and UCR2 are shown on the left while UCR5 and UCR6 are shown on the right

A review of the lap shear tension failure modes shown in Figures 108 and 109 provides a little more insight as it can be seen that in UCR5 and UCR6, the aluminum panel is being pulled to complete failure whereas in UCR1 and UCR2, the aluminum panel is exhibiting substantial deformation, but the ultimate failure is typically in the rivet. Looking more closely at Figure 109, it can be observed that the thinner steel plate in UCR2 is bending slightly, resulting in more of a peel loading mechanism than is observed in UCR6 where the thicker steel plate is comparatively rigid and forces more of the load into the aluminum plate in a direct shear loading action.

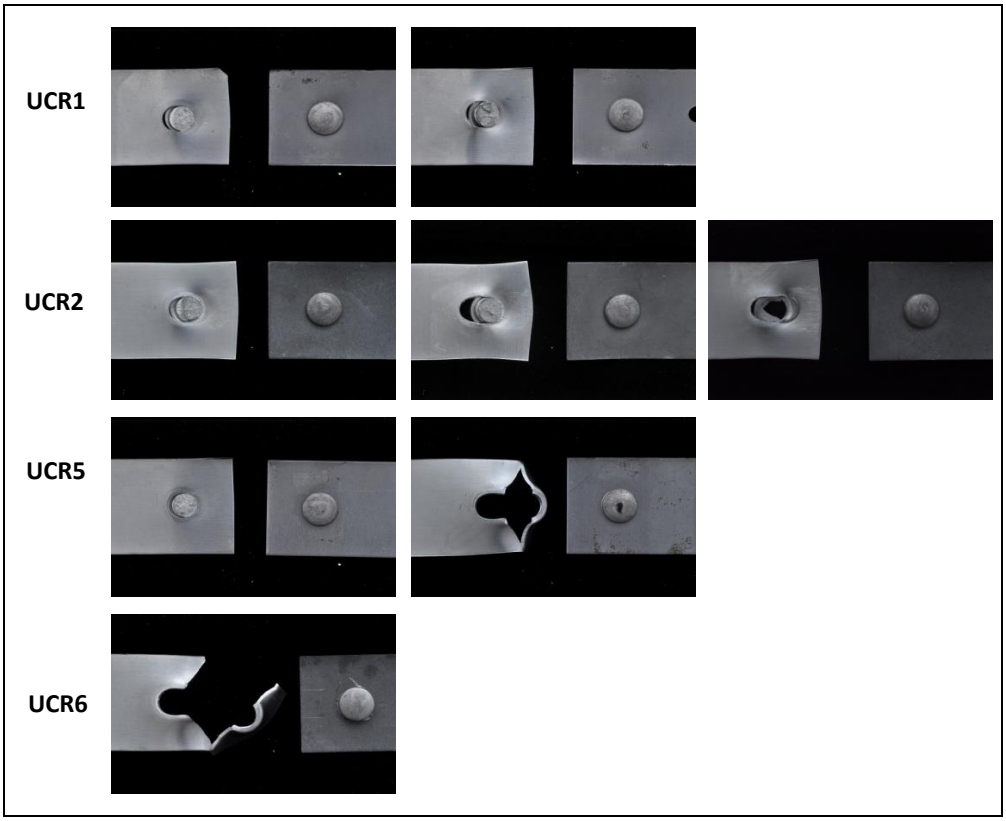

Figure 108: Round boss UCR lap shear tension tests failure modes

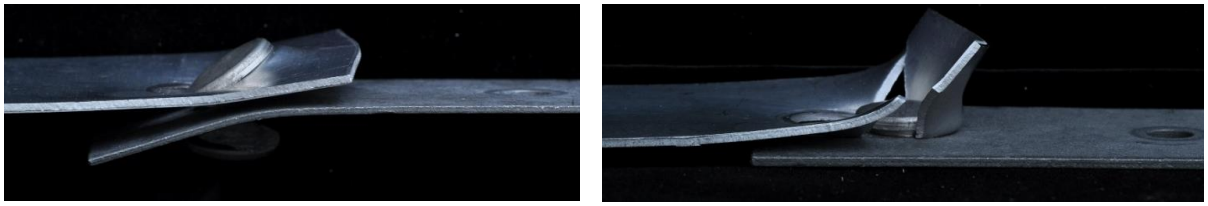

Figure 109: Round boss UCR lap shear tension test failure mode direct comparison of UCR2 (left) and UCR6 (right)

No similarly unexpected results were observed in the cross-tension test results, and a review of the failure modes shown in Figure 110, verifies that the failure mode is the same for all tested UCR samples with the rivet being pulled in two.

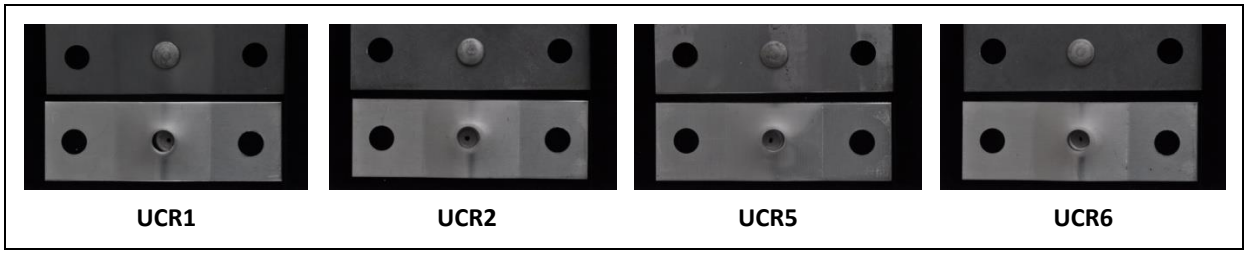

Figure 110: Round boss UCR cross tension test failure modes

Quasi-static lap-shear and cross tension results for all UCR joints are shown in Figure 111 prior to accelerated corrosion testing. All of these configurations incorporate a 1.3 mm thick 6016 alloy coupon joined to either a 1.0 mm thick (UCR 1-4) or 1.4 mm thick (UCR 5-8) DP590 HSS coupon. The UCR 5-8 configurations with the 1.4 mm thick steel plate displayed slightly lower lap-shear tension strengths than the UCR 1-4 with the 1.0 mm thick steel plate. As discussed previously, this was likely a result of different failure modes affecting the lap-shear strength in the aluminum coupon as shown in Figure 109. Not surprisingly, the UCR4 and UCR8 configurations displayed the highest lap shear strength due to the strengthening of the Al6016 alloy during the paint bake process.

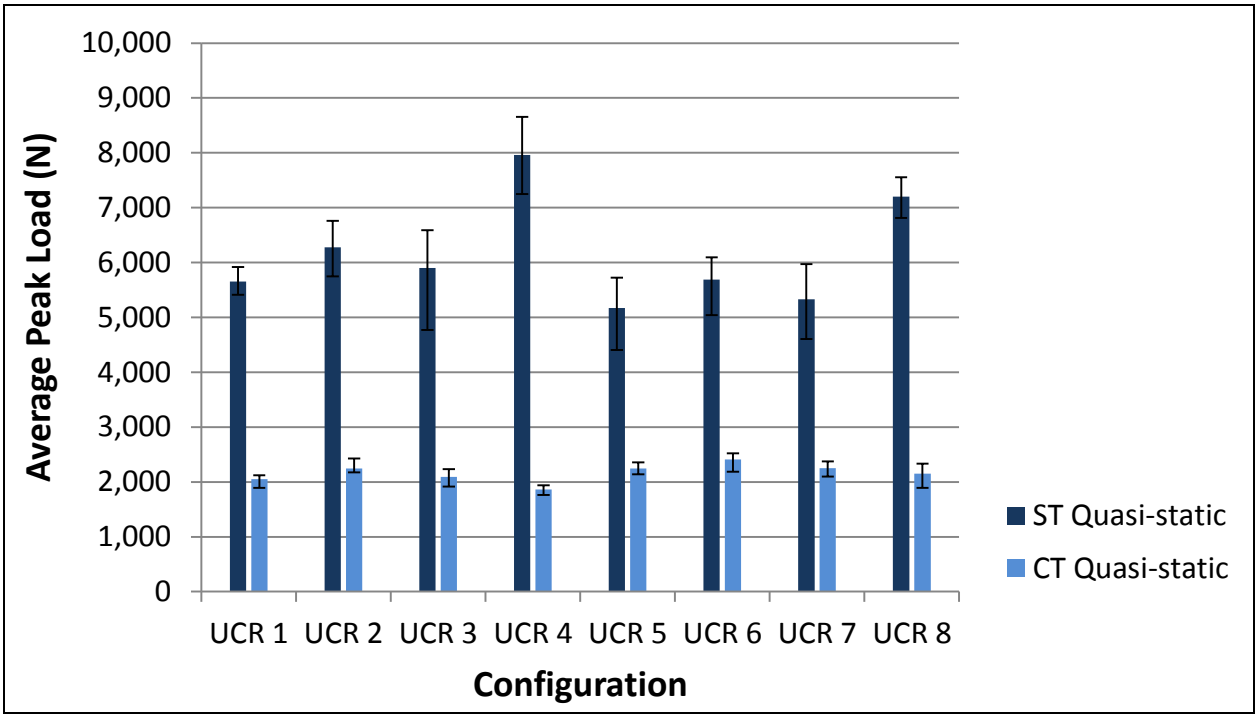

Figure 111: UCR quasi-static lap-shear tension (ST) and cross-tension (CT) test results prior to corrosion exposure

The ***impact lap shear tension*** and ***cross tension*** results for UCR4 and UCR8 are shown in Figure 112 prior to accelerated corrosion exposure.

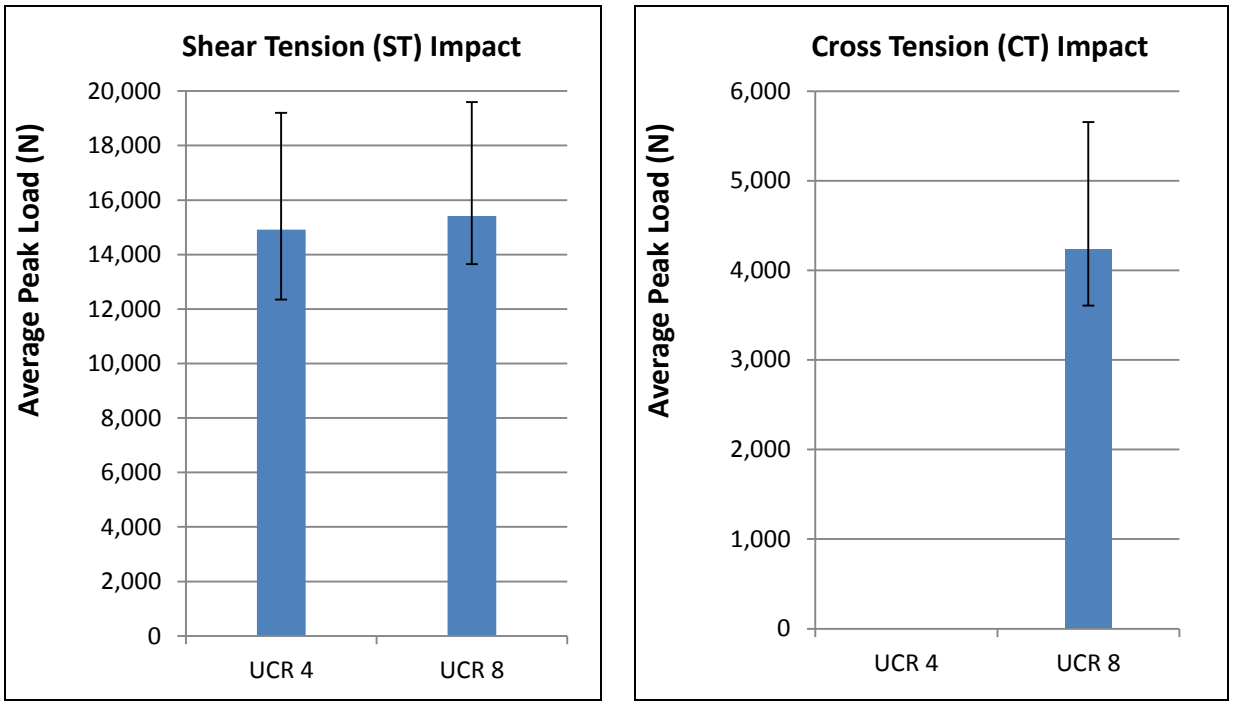

Figure 112: UCR impact lap-shear tension (ST, left) and cross-tension (CT, right) test results prior to corrosion exposure

Lap-shear tension fatigue results prior to corrosion are shown in Figure 113. Results are generally consistent with previously reported results for UPJ lap-shear tension fatigue testing although the high cycle fatigue results are higher since the actual base materials are steel and aluminum and only the rivet is magnesium. In previous UPJ lap-shear fatigue testing, many of the high cycle fatigue failures had occurred in the magnesium die-cast plate.

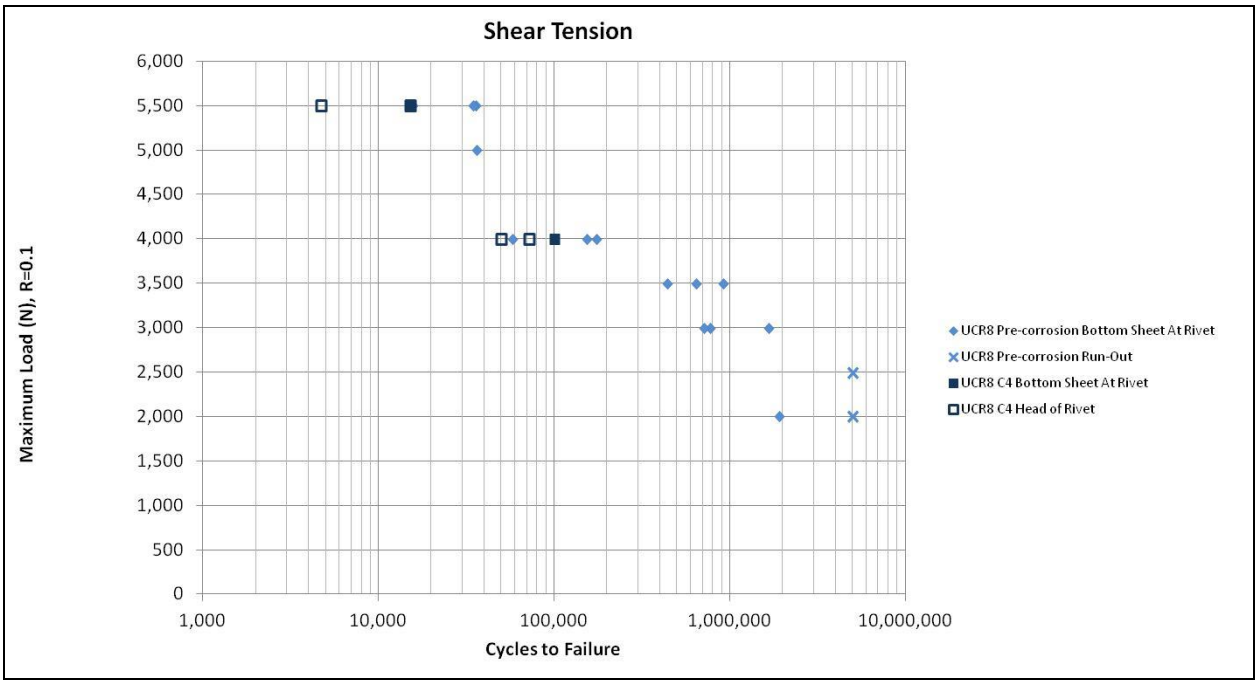

Figure 113: UCR8 lap-shear tension fatigue test results prior to corrosion exposure

Cross tension fatigue results are shown in Figure 114. Again, results are generally consistent with previously reported results for UPJ cross tension fatigue testing.

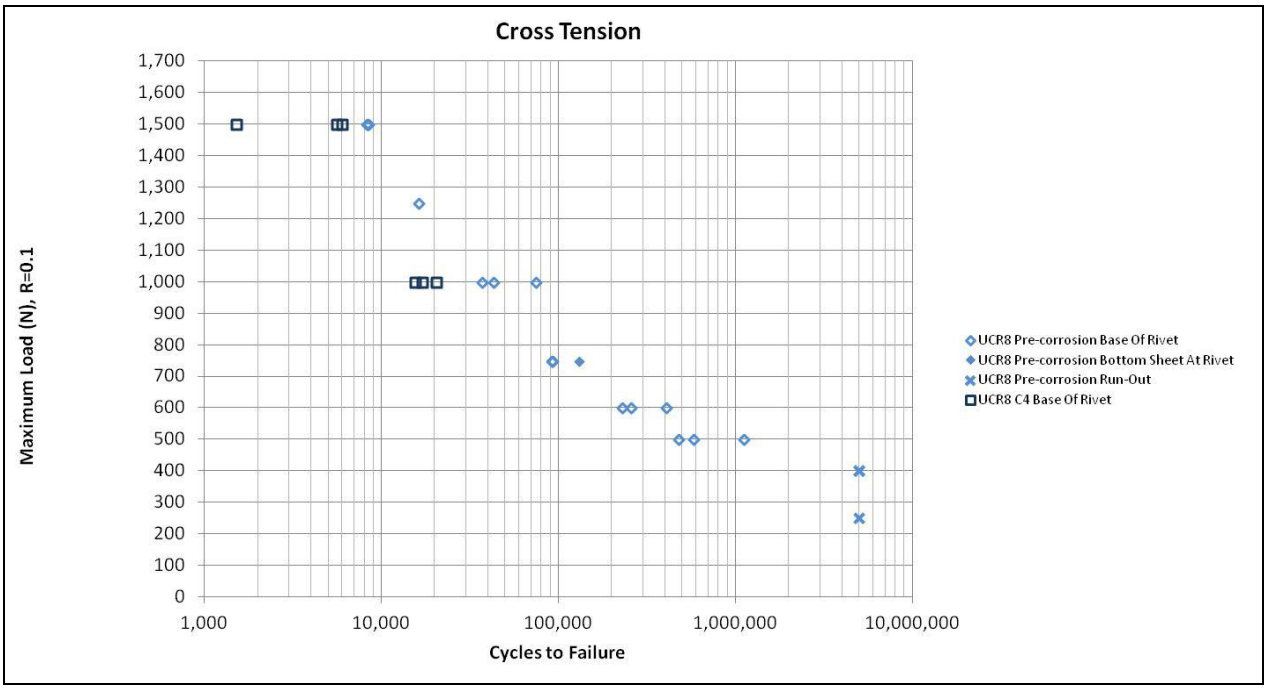

Figure 114: UCR8 cross-tension fatigue test results prior to corrosion exposure

Corrosion Testing and Evaluation

Because earlier evaluation of Mg to steel round boss UPJ assemblies had demonstrated that these joints would not pass the full 12-wk test with the current coating configurations, the test protocol for the UCR Al to steel joints with Mg rivets was reduced to only 6 weeks and the samples were evaluated on a weekly basis instead of a bi-weekly basis. All configurations except for the e-coated assemblies with sealed edges (UCR4, 8) were tested at one week as well. Over 200 round boss UCR assemblies were subjected to the ASTM G85-A2 (Acidified Salt Fog Testing) schedule. While all of UCR configurations 1-8 were tested, this report only discusses UCR configurations 1-4 since the coatings for configurations 5-8 are the same as those for 1-4, only the thickness of the steel coupon is different.

Figures 115-117 show the results of accelerated corrosion exposure for UCR1 over two weeks of exposure. The lap-shear tension samples are shown on the left while the cross-tension samples are shown on the right. Figures 115 and 116 (a) show the steel side of the joint while figures 115 and 116 (b) show the Al side of the joint. Note, there is very little corrosion damage to the rivet head on the Al side, while the steel side shows substantial corrosion degradation.

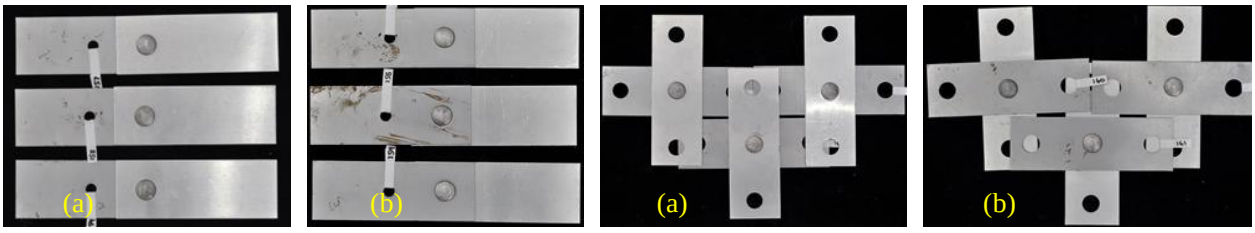

Figure 115: UCR1 corrosion test samples prior to corrosion exposure

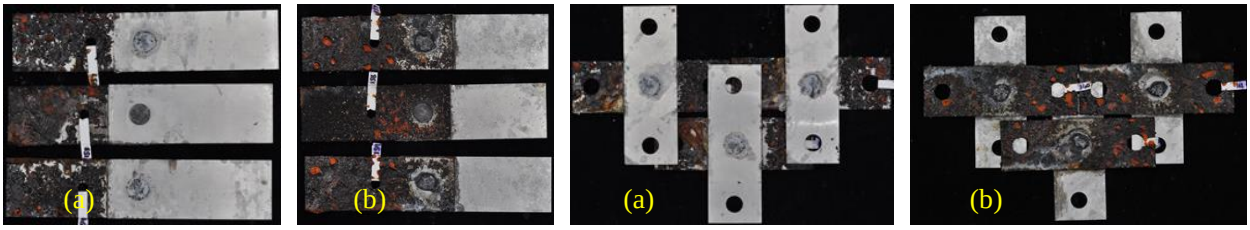

Figure 116: UCR1 corrosion test samples after 1-wk of corrosion exposure

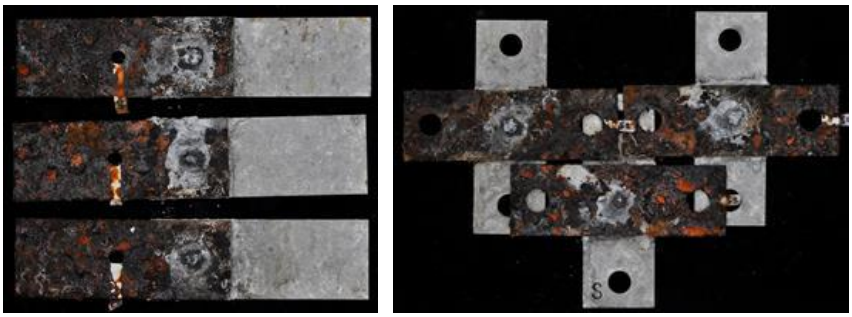

Figure 117: UCR1 corrosion test samples after 2-wks of corrosion exposure

Figures 118-120 show the results of accelerated corrosion exposure for UCR2 over two weeks of exposure. The lap-shear tension samples are shown on the left while the cross-tension samples are shown on the right. Figures 118 and 119 (a) show the steel side of the joint while figures 118 and 119 (b) show the Al side of the joint. Again, there is very little corrosion damage to the rivet head on the Al side, while the steel side shows substantial corrosion degradation.

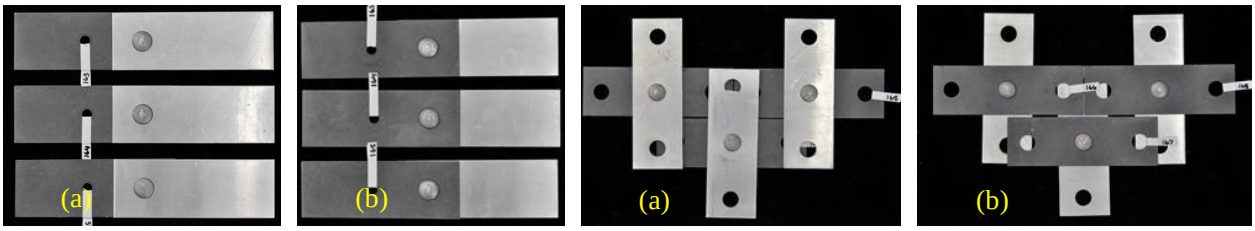

Figure 118: UCR2 corrosion test samples prior to corrosion exposure

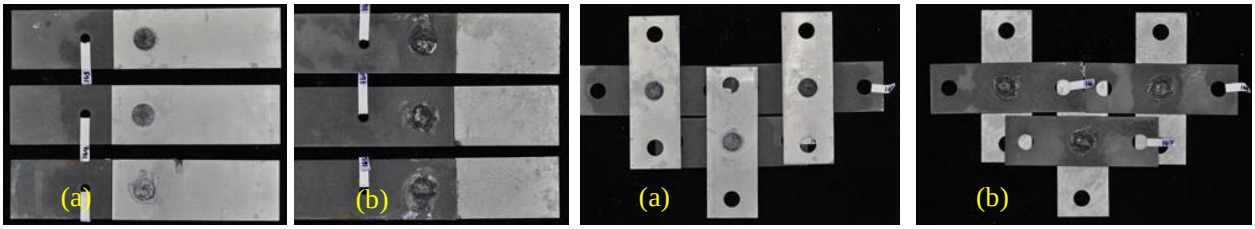

Figure 119: UCR2 corrosion test samples after 1-wk of corrosion exposure

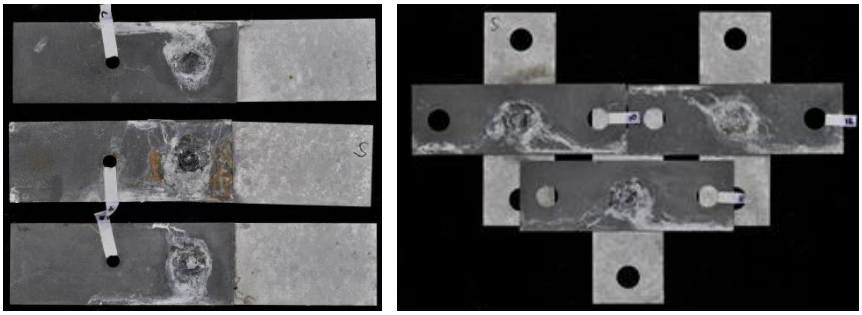

Figure 120: UCR2 corrosion test samples after 2-wks of corrosion exposure

Figures 121-123 show the results of accelerated corrosion exposure for UCR3 over two weeks of exposure. The lap-shear tension samples are shown on the left while the cross-tension samples are shown on the right. Figures 121 and 122 (a) show the steel side of the joint while figures 121 and 122 (b) show the Al side of the joint. Again, there is very little corrosion damage to the rivet head on the Al side, while the steel side shows substantial corrosion degradation.

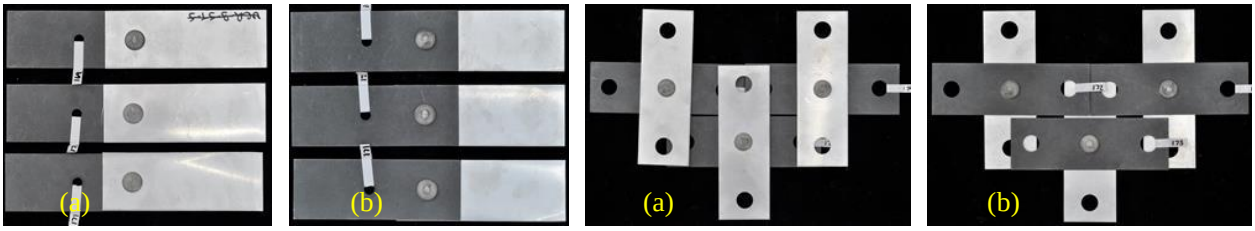

Figure 121: UCR3 corrosion test samples prior to corrosion exposure

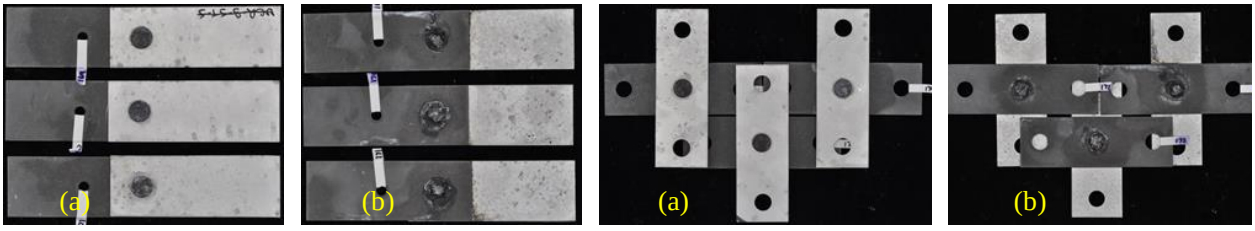

Figure 122: UCR3 corrosion test samples after 1-wk of corrosion exposure

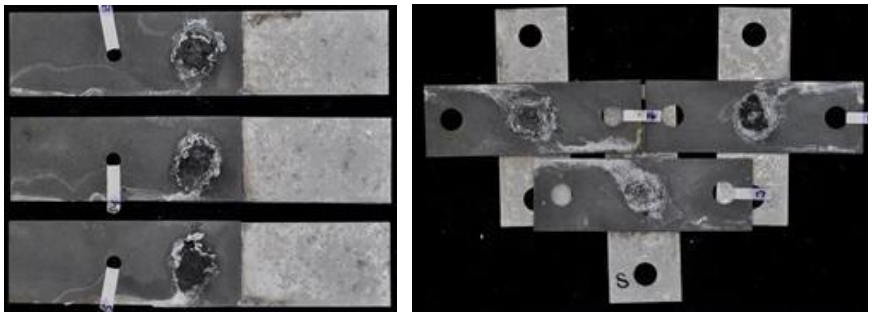

Figure 123: UCR3 corrosion test samples after 2-wks of corrosion exposure

Figures 124-126 show the results of accelerated corrosion exposure for UCR4 over six weeks of exposure. The lap-shear tension samples are shown on the left while the cross-tension samples are shown on the right. Figures 124-126 (a) show the steel side of the joint while figures 124-126 (b) show the Al side of the joint. Again, there is very little corrosion damage to the rivet head on the Al side, while the steel side shows substantial corrosion degradation.

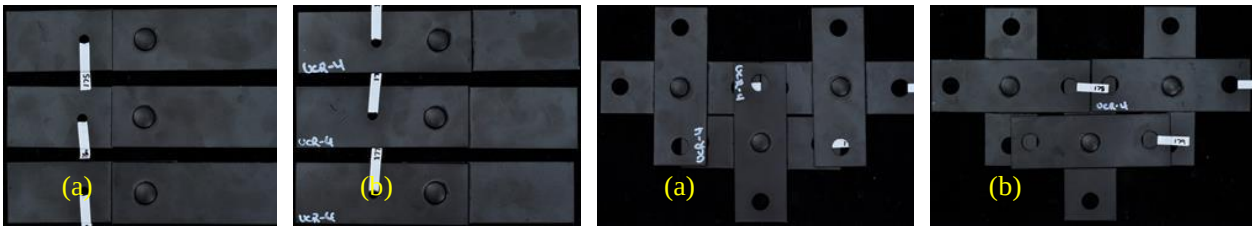

Figure 124: UCR4 corrosion test samples prior to corrosion exposure

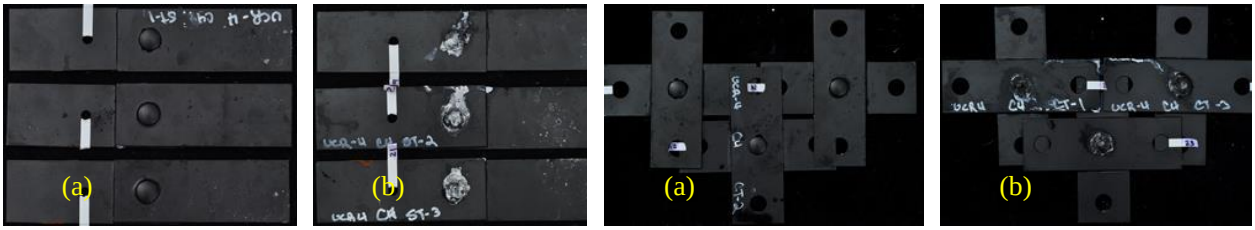

Figure 125: UCR4 corrosion test samples after 3-wks of corrosion exposure

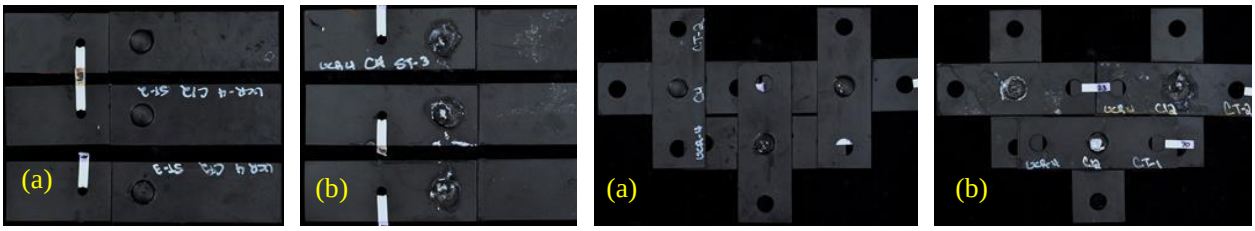

Figure 126: UCR4 corrosion test samples after 6-wks of corrosion exposure

Figure 127 shows close-up views of the actual joint for UCR configurations 1-4 prior to corrosion exposure and at 1, 2, 4, and 6-wks of exposure. In all these views, the rivet head on the steel side is shown. Clearly, when joining Al to steel with a Mg rivet, it is imperative to provide a substantial coating on the steel, as well as sealing around the head and between the panels, and coating the assembly afterward as well, as was done for UCR4. It should be noted that although UCR4 displayed dramatically improved performance over UCR configurations 1-3, that 6-wks is still only about half of the desired longevity in this corrosive environment, so improved coating processes (especially for the steel) are required for joining of Al to steel with a Mg rivet.

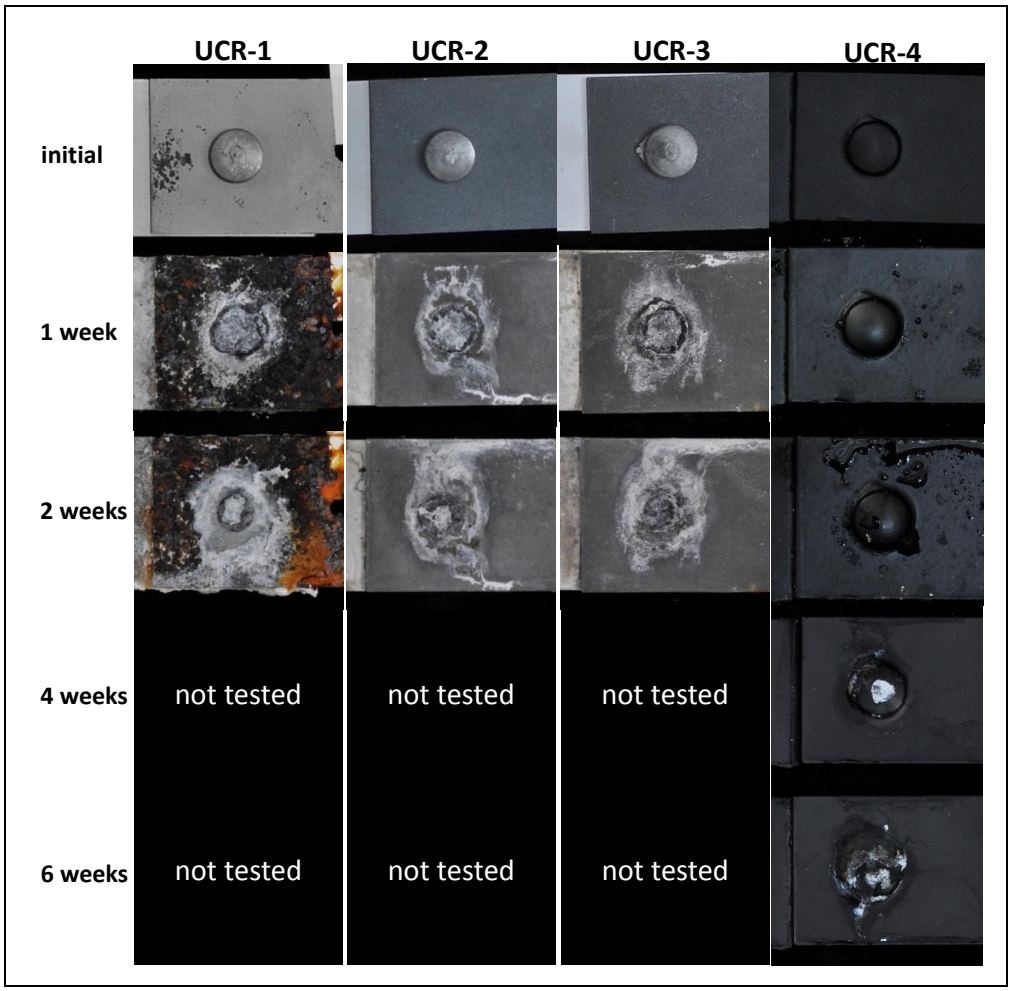

Figure 127: UCR joint configurations before and after ASTM G85-A2 accelerated corrosion exposure

Post Corrosion Mechanical/Structural Testing and Evaluation

Quasi-static lap-shear tension results for all UCR joints are shown in Figure 128 prior to accelerated corrosion exposure, and at 1-wk, 2-wks, 4-wks, and 6-wks of exposure. All of these configurations incorporate a 1.3 mm thick 6016 alloy coupon joined to either a 1.0 mm thick (UCR 1-4) or 1.4 mm thick (UCR 5-8) DP590 coupon. Similar to the previously evaluated round boss UPJ Mg to steel assemblies, with the exception of UCR4 and UCR8 (the e-coated samples with sealed edges), all of the samples displayed a dramatic drop in strength over only two weeks of exposure. UCR4 and UCR8, however both maintained good joint strength levels even after 6-wks of exposure. Failure modes are shown in Figure 129.

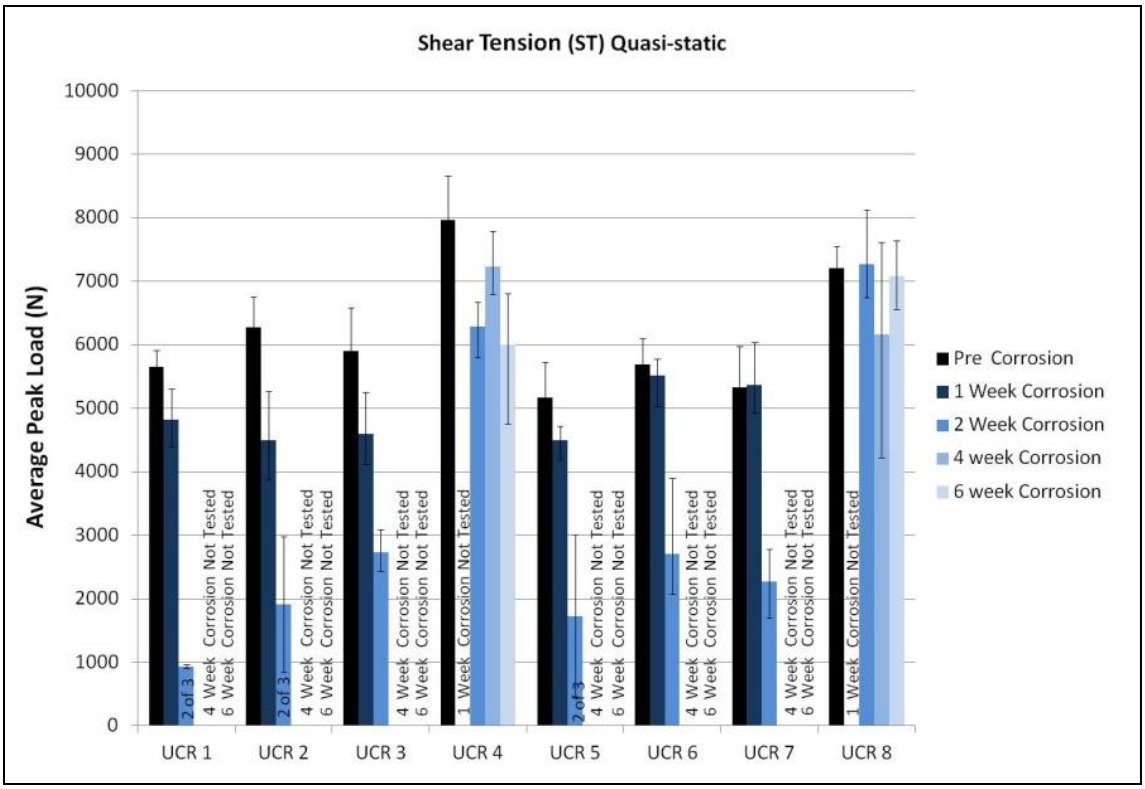

Figure 128: UCR quasi-static lap-shear tension (ST) test results prior to corrosion testing and at 1-wk, 2-wks, 4-wks, and 6-wks of accelerated corrosion exposure

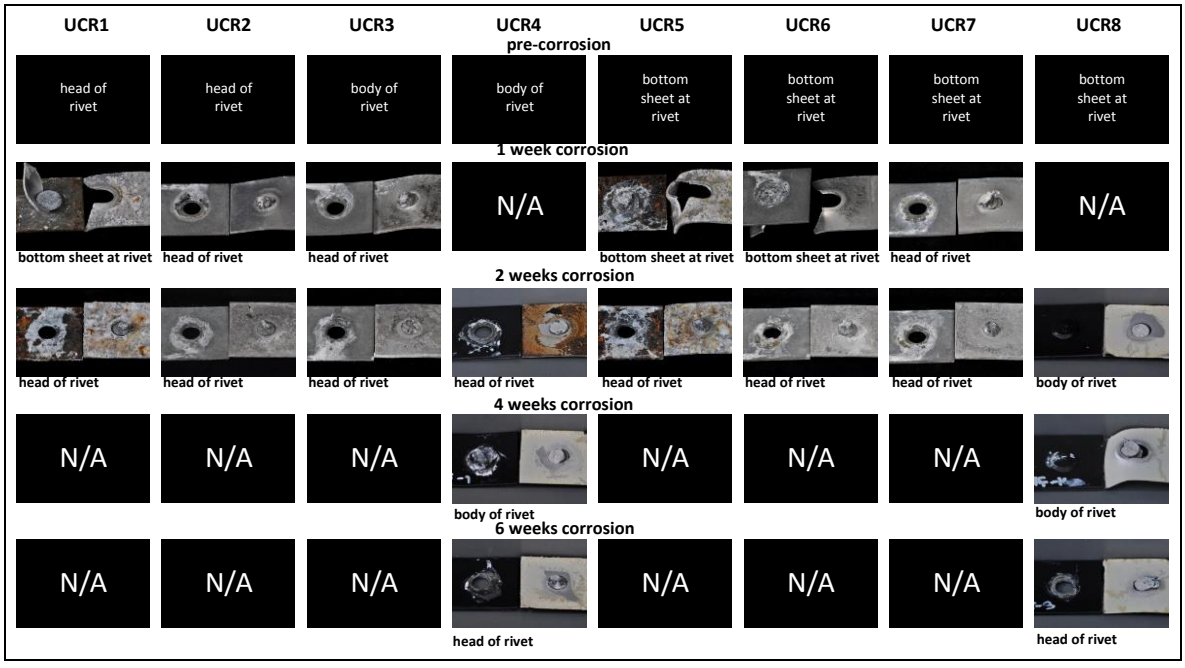

Figure 129: UCR quasi-static lap-shear tension (ST) test assembly failure modes prior to corrosion testing and at 1-wk, 2-wks, 4-wks, and 6-wks of accelerated corrosion exposure

Quasi-static cross tension results for all UCR joints are shown in Figure 130 prior to accelerated corrosion exposure, and at 1-wk, 2-wks, 4-wks, and 6-wks of exposure. Similar to the lap-shear tension testing described above, with the exception of UCR4 and UCR8, all of the samples displayed a dramatic drop in strength over only two weeks of exposure. UCR4 and UCR8, however both maintained good joint strength levels even after 6-wks of exposure. Post-corrosion failure modes are shown in Figure 131. All pre-corrosion samples failed at the base of the rivet.

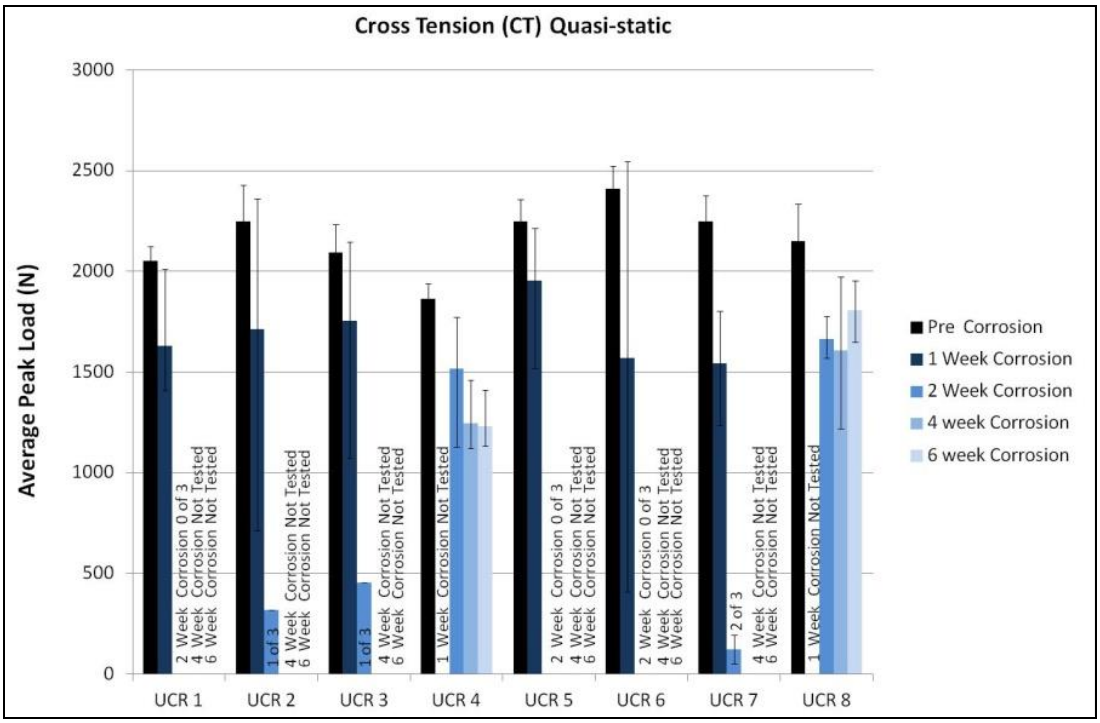

Figure 130: UCR quasi-static cross tension (CT) test results prior to corrosion testing and at 1-wk, 2-wks, 4-wks, and 6-wks of accelerated corrosion exposure

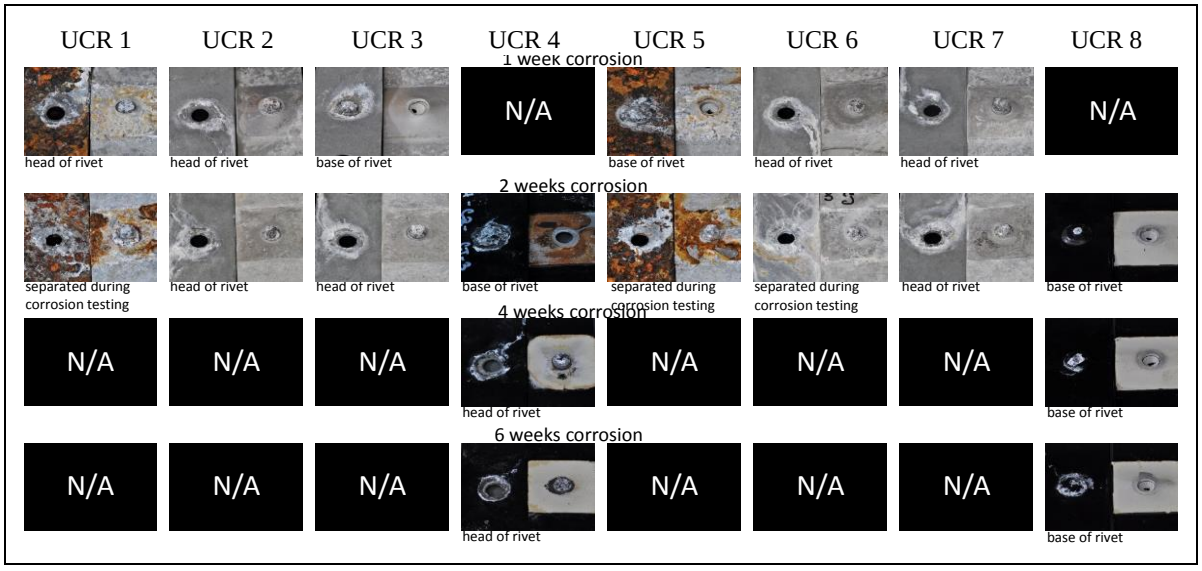

Figure 131: UCR quasi-static cross tension (CT) test assembly failure modes at 1-wk, 2-wks, 4-wks, and 6-wks of accelerated corrosion exposure

Impact lap shear tension results and failure modes for UCR4 and UCR8 prior to corrosion and at 1-wk, 2-wks, 4-wks, and 6-wks of accelerated corrosion exposure are shown in Figures 132 and 133 while ***cross tension impact*** results and failure modes are shown in Figures 134 and 135.

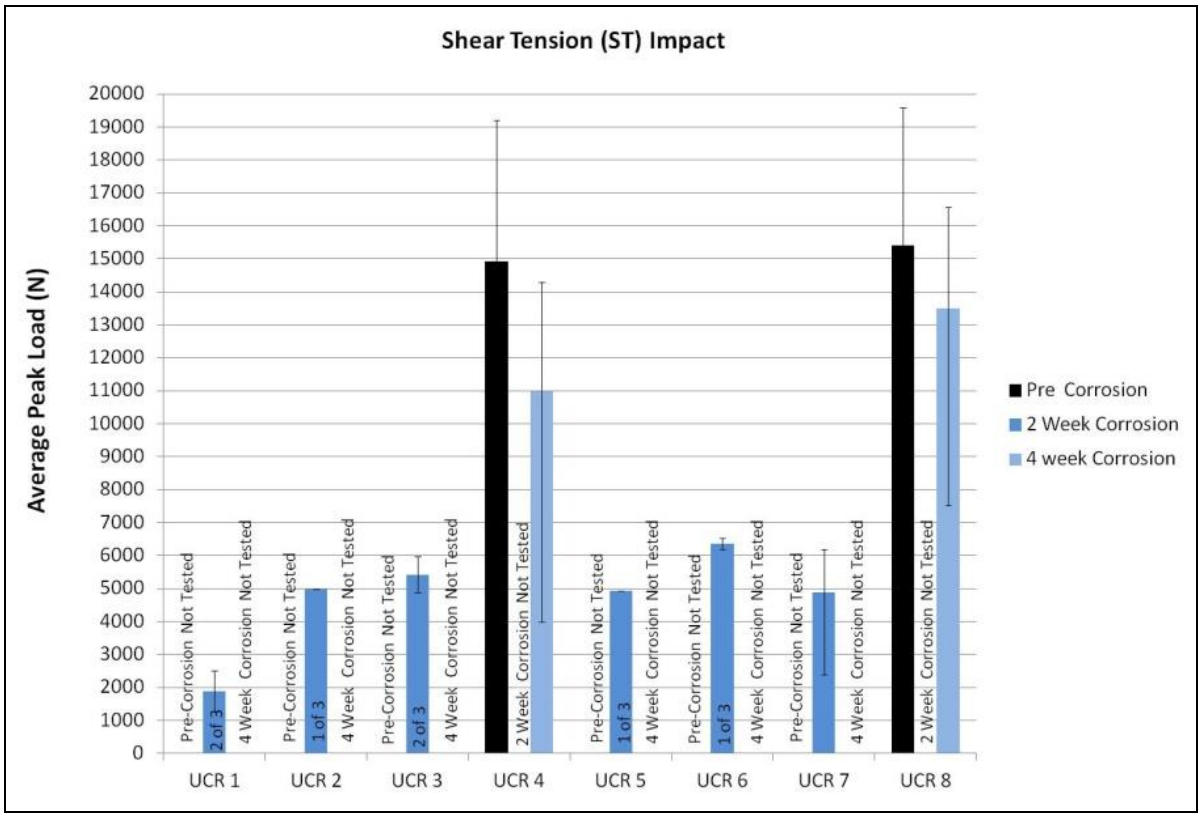

Figure 132: UCR impact lap-shear tension (ST) test results prior to corrosion testing and at 1-wk, 2-wks, 4-wks, and 6-wks of accelerated corrosion exposure

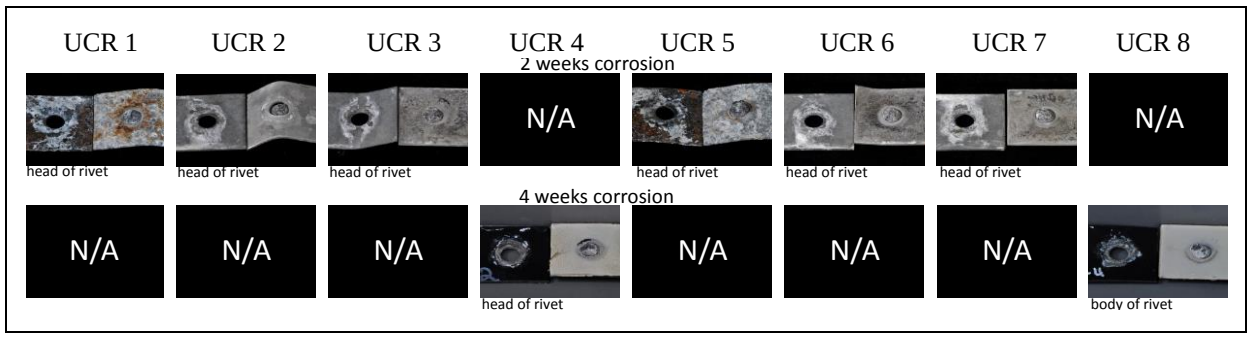

Figure 133: UCR impact lap shear tension (ST) test assembly failure modes at 2-wks and 4-wks of accelerated corrosion exposure

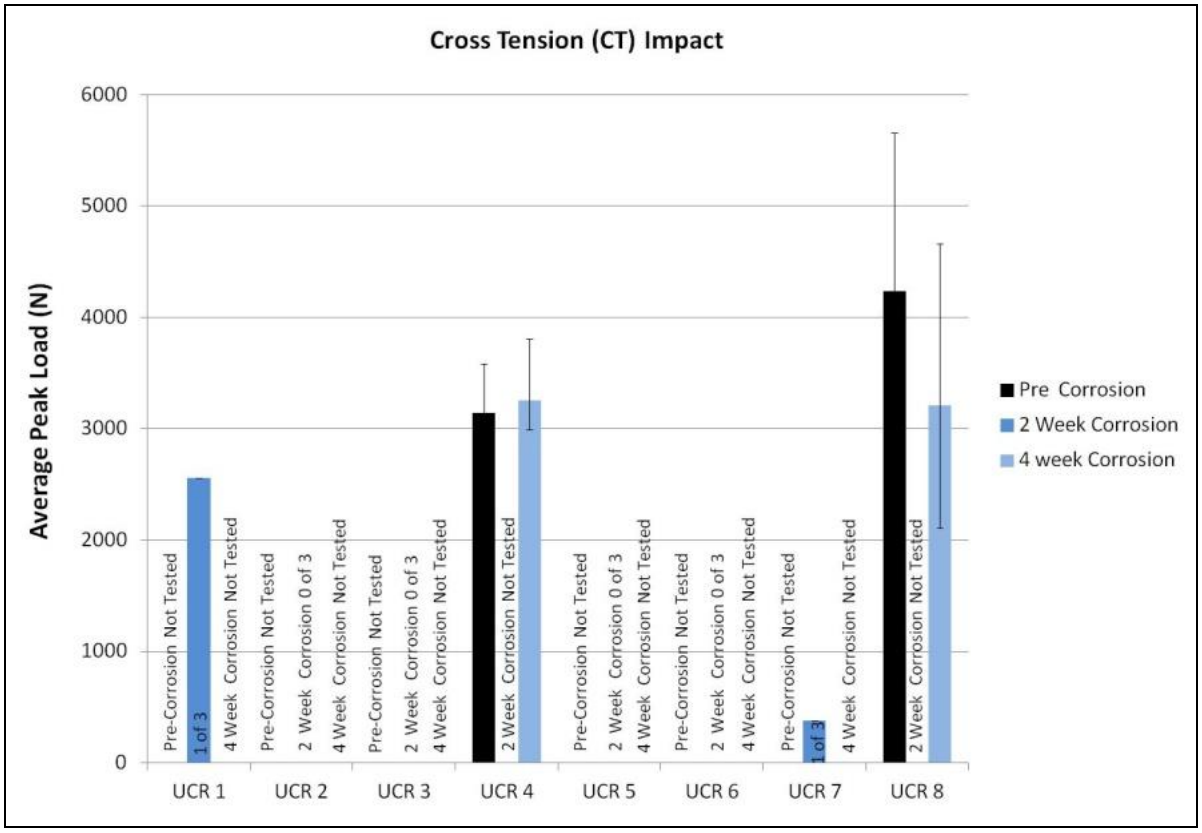

Figure 134: UCR impact cross tension (CT) test results prior to corrosion testing and at 1-wk, 2-wks, 4-wks, and 6-wks of accelerated corrosion exposure

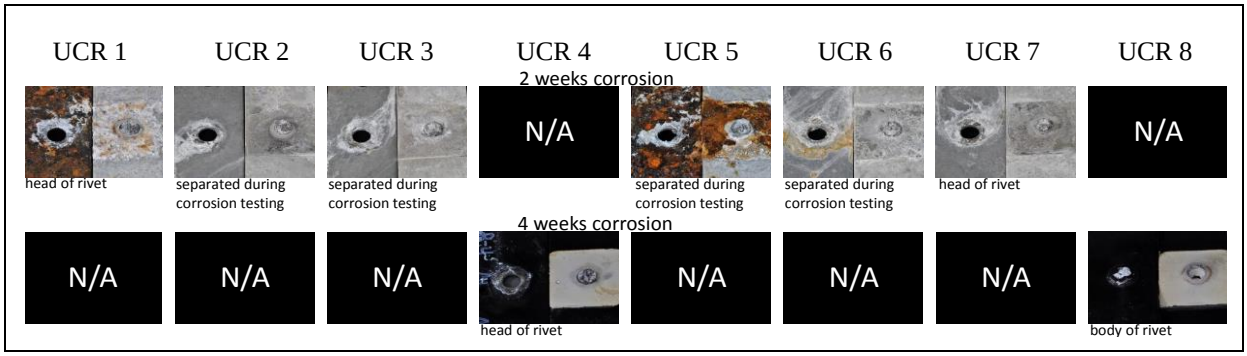

Figure 135: UCR impact cross tension (CT) test assembly failure modes at 2-wks and 4-wks of accelerated corrosion exposure

Lap-shear tension fatigue results prior to corrosion and after 4-wks of corrosion exposure are shown in Figure 136. Results are generally consistent with previously reported results for UPJ lap-shear tension fatigue testing although the high cycle fatigue results are higher since the actual base materials are steel and aluminum and only the rivet is magnesium. In previous UPJ lap-shear fatigue testing, many of the high cycle fatigue failures had occurred in the die cast magnesium plate.

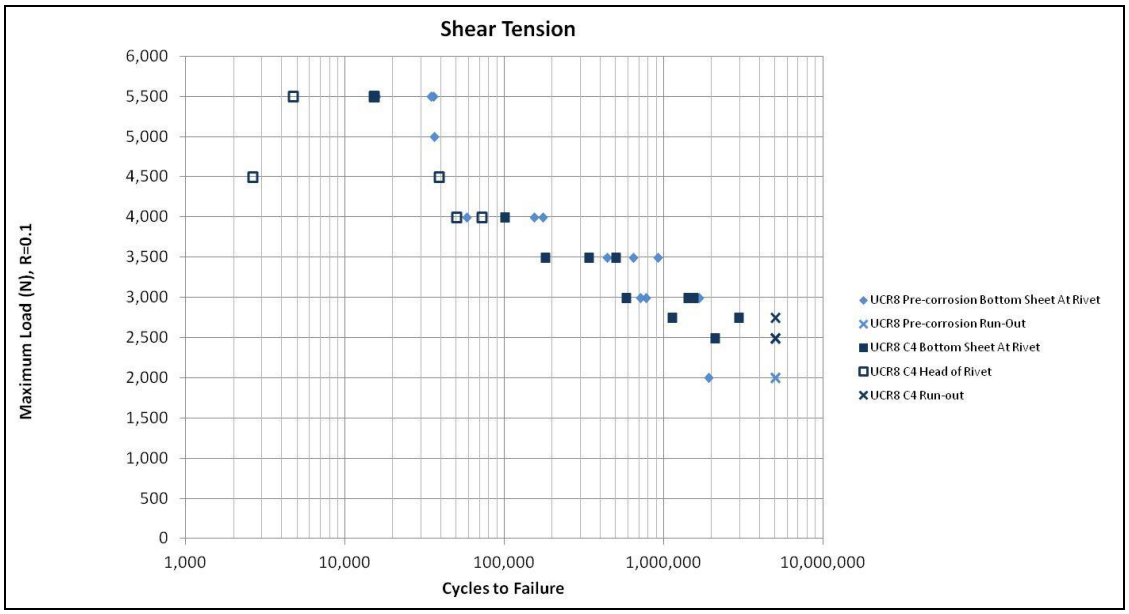

Figure 136: Comparison of UCR8 lap-shear tension fatigue test results prior to corrosion exposure and at 4-wks exposure

Failure modes for UCR8 lap shear tension testing are shown in Figure 137 where it can be seen that all of the pre-corrosion samples (top photos) failed in the parent material of the lower 1.3 mm aluminum sheet. However, while some of the post-corrosion samples (bottom photos) failed in the aluminum parent material, others failed in the actual rivet head.

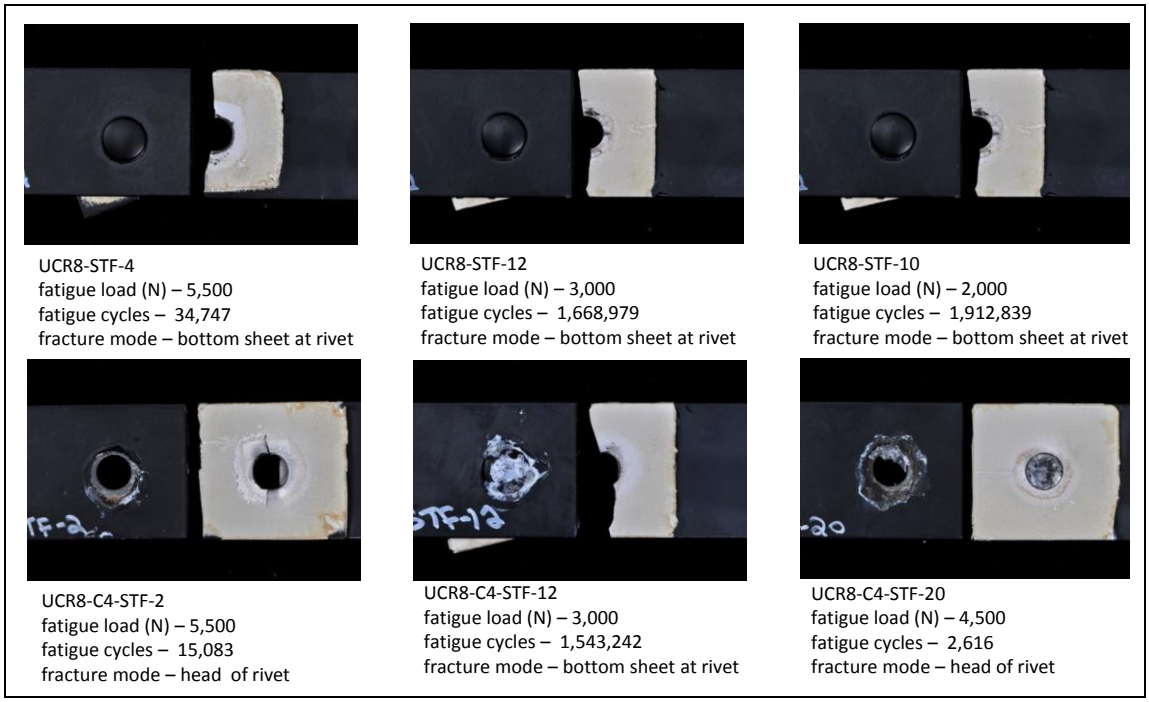

Figure 137: UCR fatigue lap shear tension (ST) test assembly failure mode at 4-wks of accelerated corrosion exposure (typical failure in bottom sheet parent material)

Cross tension fatigue results are shown in Figure 138. Again, results are generally consistent with previously reported results for UPJ cross tension fatigue testing with the exception that there is not a dramatic increase in post-corrosion high cycle fatigue vs. pre-corrosion high cycle fatigue. As can be seen in Figure 139, all of the samples failed at the base of the rivet.

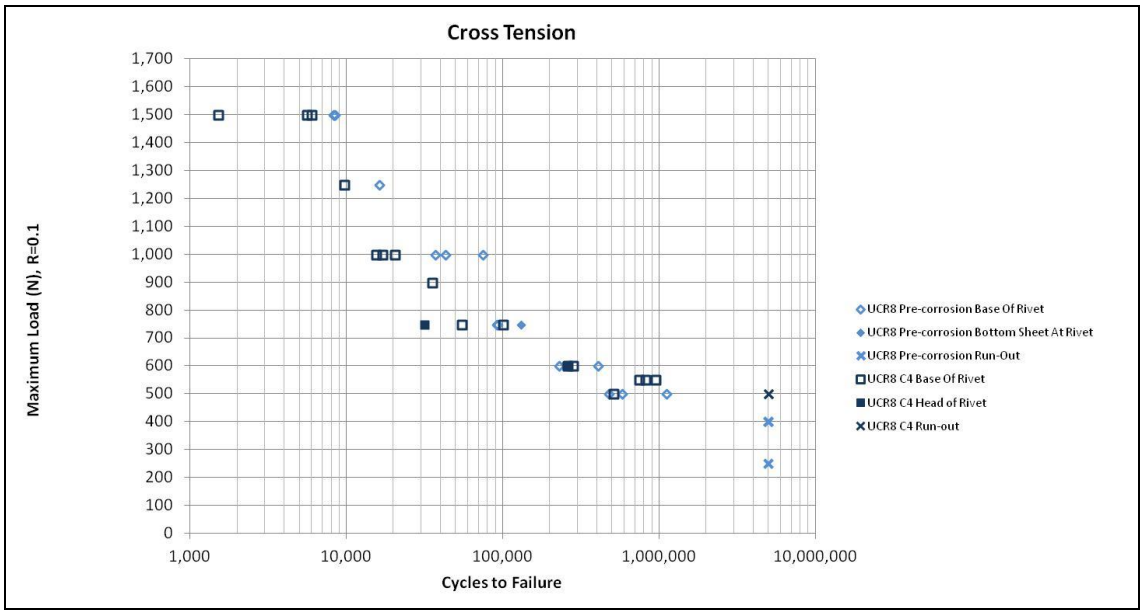

Figure 138: Comparison of UCR8 cross-tension fatigue test results prior to corrosion exposure and at 4-wks of exposure

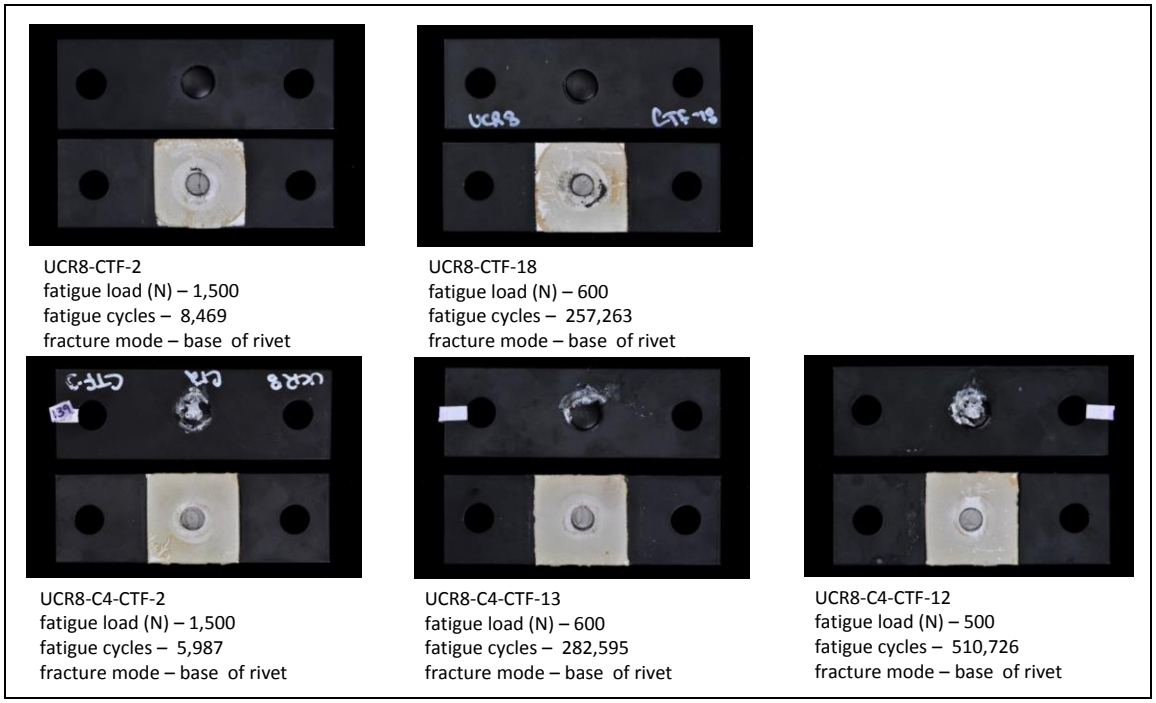

Figure 139: UCR fatigue cross tension (CT) test assembly failure mode at 4-wks of accelerated corrosion exposure (typical failure at base of rivet)

CONCLUSIONS

- All three initially proposed process variants (round boss UPJ, oval boss UPJ, and round boss UCR) were successfully produced and evaluated with different dissimilar metal joints and different coating configurations. All three process variants showed promising results for specific types of commercial applications.
- In general, round boss UPJ showed improved performance over the benchmark SPR process in joining MgAM60B to Al6013.
    - Quasi-static results were substantially higher with lap shear tension results ~35-40% higher and cross tension results ~160-170% higher. Similarly, impact lap shear tension results were ~47% higher and impact cross tension results were ~150% higher. Low cycle fatigue results were substantially higher while high cycle fatigue results were only minimally higher.
        - It should be noted that most of the quasi-static and impact performance improvement is likely a result of the joint geometry since the protrusion is larger in diameter than the comparable SPR rivet and has a large head formation locking the two materials together.
        - The high cycle fatigue results seem to be related more to the fatigue strength of the Mg sample than the actual joint strength
    - However, this particular dissimilar metal joint combination posed a substantial galvanic corrosion challenge for both joining processes due to the high level of copper in the Al6013 alloy.
        - Bare MgAM60B to Bare Al6013 – Substantial corrosion was observed on both Mg and Al coupons with both processes, and additional fracturing of the steel rivets as a result of hydrogen embrittlement was observed with the SPR process.
        - Pretreated MgAM60B to Pretreated Al6013 with powder-coat applied after assembly – A substantial number of steel rivet fractures were observed as a result of hydrogen embrittlement with the SPR process. Very few separations were observed with the UPJ process.
        - Pretreated MgAM60B to powder-coated Al6013 – Few separations were observed in SPR, no separations were observed in UPJ.
        - Pretreated MgAM60B to powder-coated Al6013 with powder-coat applied after assembly – No separations were observed in samples produced by either process.
- Substantial galvanic corrosion challenges were observed in joining MgAM60B to DP590 high strength steel with the UPJ process.
    - This particular dissimilar metal join combination was not considered feasible with SPR and therefore was not evaluated with SPR.
    - New Zn-Mg-Al steel pretreatment processes seemed to reduce galvanic corrosion effect of steel coupons on Mg compared to conventional galvanizing. However, some differences were observed between products from different suppliers even when comparing the same level of surface density.
    - Even with the new steel treatments, it was necessary to apply adhesive between the two dissimilar metals, seal the edges, and completely paint the assembly, not just powder-coat prime, in order to get acceptable corrosion performance over 12-wks of accelerated exposure.
- Dramatically reduced galvanic corrosion degradation was observed in MgAM60B to Al6016 UPJ joints compared to MgAM60B to Al6013 as a result of reduced copper content in the aluminum.
    - This particular dissimilar metal join combination was not considered feasible with SPR and therefore was not evaluated with SPR.

  - Even bare MgAM60B to bare Al6016 joints survived 12-wks of accelerated corrosion exposure with no structural joint separations.
  - Nevertheless, substantial blistering and peeling of the powder-coat on coated assemblies indicate that, in joints where cosmetic appearance is critical, more effort will be required to isolate the dissimilar metals. Possibly, the addition of adhesive application between the dissimilar metals, as well as sealing the edges, and a full paint process can resolve this issue.

- Oval boss joints were successfully produced on MgAM60B to Al6013 coupons.
  - This joint type can be used on narrower flanges than round boss joints while still exhibiting great strength as a result of cross sectional area through the protrusion.
    - Joint strength was substantially higher than for 8.0-mm round boss UPJ joints with the actual percentage increase depending on whether the load was applied longitudinally to the oval protrusion or transverse to the oval protrusion.
  - However, the finished joint width is not quite as narrow as would be expected from the initial protrusion because the oval protrusion tends to become more round as the head is formed.
  - No corrosion evaluation was conducted on this joint configuration as there was no reason to believe the corrosion results of an oval shaped boss would be any different than a round boss for the same material and coating configurations.

- Round boss UCR joints were produced on Al6016 to DP590 high strength steel coupons.
  - Joint process parameters were very similar to those of UPJ with the same protrusion height and diameter.
  - Joint quality seemed to be even better than standard UPJ joints. This could be a result of improved heat transfer due to the smaller size of the rivet compared to an entire cast test coupon, or could be a result of better casting quality since these parts were cast directly instead of being cast as a protrusion on a flat plate.
  - As expected, galvanic corrosion was a severe challenge on these joints with three dissimilar metals. These tests were conducted before the evaluation of alternative Zn-Mg-Al steel coatings, so it is not known if the new Zn-Mg-Al steel coatings (as well as adhesive application and sealed edges) would have resulted in the same level of corrosion performance seen on the updated UPJ MgAM60B to DP590 steel samples.

- Key processing findings
  - Cracking during the head forming operation is difficult to predict with computer simulations unless a large number of samples are produced with different parameters in order to develop correlation. There was not sufficient time in this project to do this.
  - Initial electrode temperature may play a role in head formation quality with some increased cracking observed with increasing initial electrode temperatures.
  - Electrode cleanliness plays a substantial role in head formation quality with dramatically increased propensity for cracking observed with increased level of oxidation on the electrode.

PRODUCTS

PRESENTATIONS

Logan, S. D., 2016, "Evaluating the Upset Protrusion Joining (UPJ) Method to Join Magnesium Castings to Dissimilar Metals," *3rd Global Lightweight Vehicle Manufacturing Summit*, Detroit, Michigan, February 24, 2016.

Logan, S.D., 2015, "Evaluating the Upset Protrusion Joining (UPJ) Method to Join Magnesium Castings to Dissimilar Metals", *Global Automotive Lightweight Materials Detroit Conference*, August 19, 2015